Revealing the Interactions of *Clostridioides difficile* Toxin B With Epithelial Receptors

By
Kevin O'Neal Childress

Dissertation
Submitted to the Faculty of the
Graduate School of Vanderbilt University
in partial fulfillment of the requirements
for the degree of

DOCTOR OF PHILOSOPHY
in
Microbe-Host Interactions
May 12, 2023
Nashville, Tennessee

Approved:
Timothy L. Cover, M.D.
Christopher R. Aiken, Ph.D.
John J. Karijolich, Ph.D.
Ethan Lee, M.D, Ph.D.
D. Borden Lacy, Ph.D.

I dedicate this thesis to my hard-working parents,
Christopher & Sun ok Childress,
who sacrificed so much of their lives for the
sake of their children.
We miss you, Dad!

Acknowledgements

First, I would like to thank my mentor, Dr. Borden Lacy, for her unwavering support, guidance, and patience throughout my time in graduate school. Through all the highs and lows of my graduate school career, she was always there for me and kept me focused. She challenged me to explore tough questions, never give up, and always pushed my creativity. I can only hope to one day be as good a mentor as Borden has been for me. I know I have become a better scientist because of you.

I would also like to thank all the past and current members of the Lacy Laboratory, as well as Dr. Benjamin Spiller, who have all been like a family to me. I am grateful to Dr. Ramya Chandrasekaran and Dr. Michelle LaFrance for mentoring me in the lab and encouraging me to join. I am also grateful to Dr. Melissa Farrow, for not only the beer but also the comradery. Melissa, thank you for letting me bother you whenever I had an idea or question. Melissa was there for me when I needed it the most and challenged me more than other members of the lab. I appreciate you for letting me be a part of your life over soccer, a happy hour, or over the holidays with your family. Melissa, you are truly one-of-a-kind. I would also like to thank my former bench buddies Drs. Dave Anderson, Michael Sheedlo, and Jaime Jensen, for their technical expertise and for helping me with experiments. It was a joy working closely with you all and watching you become great scientists. I would like to also thank my new bench buddy Dr. Chris Peritore-Galve. It is not always the case where I can instantly click with someone, but you have been a great friend to me in the short time you have been here, and I know you will reach your dreams one day. I would also like to say thank you to Dr. Nick Markham, M.D., Ph.D, who is now an amazing professor here at Vanderbilt! Your knowledge and expertise in tissue sectioning, staining, and organoid culturing have helped me develop ideas and made me a better scientist. I would also like to thank my fellow graduate students still in the lab, including the newly minted Ph.D. Dr. Sarah Bernard, as well as Kateryna Nabokhotna and Audrey Thomas, for their friendships, guidance, and conversations. I would also like to thank all the past and present research assistants I had the pleasure to be around, including Anna Smith, Rubén Cano, KayCei Moton-Melancon, Matthew Hensen, McKenzie King, and Stacey Seeback. You all provided the lab with personality, joy, and reagents, so it has been a pleasure working with you all. Thank you as well to Dr. Heather Kroh, for always letting me bother you with protein questions and kindness, and Dr. Shannon Kordus for your jokes, memes, and expertise on bacteria and electron microscopy. I also cannot forget to thank our lab manager J Shupe, who joined our lab after

arriving from the same town I grew up! J is essentially an encyclopedia of knowledge, a great colleague, and a great person to have a conversation with.

I would like to thank my collaborators. At Vanderbilt University, I thank Dr. Matthew Tyska, for his guidance, reagents, and expertise on my Nectin-3 project. I would like to also thank your past and current lab members, which include Dr. Colbie Chinowsky, Caroline Cencer, and Julia Pinette. Thank you all for taking the time to teach me about the epithelial brush border and microscopy. You all exposed me to novel concepts and made me a more complete scientist. At Monash University, I thank Dr. Dena Lyras and Dr. Helen Abud. Our collaboration revealed that TcdB perturbs stem cell function independently of Frizzled interactions, a result that appears to be relevant for human diseases such as colon cancer. It was a joy working with your labs.

I want to thank my thesis committee as well, Dr. Timothy Cover, Dr. Chris Aiken, Dr. John Karijolich, and Dr. Ethan Lee. To Tim, thank you for meeting with me and checking up on me throughout the semesters here. It was nice knowing that you cared for my well-being and your encouragement kept me inspired as a scientist. I could also always count on you to show up to a talk to ask questions and I appreciate that. To Chris, I appreciate your mentorship, guidance, and our conversations outside of committee meetings when I was the president of the graduate student association. To John, it was awesome watching you start your lab from scratch and becoming a successful professor. I appreciate our one-on-one conversations and learning about your journey. To Ethan, thank you for your guidance, reagents, and mentorship throughout my committee meetings and presentations on campus.

I would like to thank all my friends and my family that supported me throughout graduate school. Being a first-generation student is a challenging and confusing process for everyone, but I know it was hardest on my mother, Sun ok Childress. I appreciate your constant texts of support and pictures of your home-grown flowers and plants. Your sacrifices for me and my sister have not been for nothing. To my late father, Christopher O'Neal Childress, I know you were so proud of me for making it to graduate school. I know you would have been happy seeing me finish as well. Thank you to my sister, Gena Childress, her partner Justin Thompson, and her son Cage Thompson, for their support from afar as well and for taking care of mom. I would like to thank my grandmother, Betty Childress, as well. You are the strongest woman I know, and I thank you for your support.

I would like to acknowledge my funding from the Molecular Biophysics Training Grant T32GM008320.

Table of Contents

List of Tables

List of Figures

Abbreviations

-/-: knockout
aa: amino acids
ADAM: a disintegrin and metalloprotease
ADP: adenosine diphosphate
APC: adenomatous polyposis coli
APD: autoprocessing domain
BSA: bovine serum albumin
cAMP: cyclic adenosine monophosphate
CDI: *C. difficile* infection
CDT: *C. difficile* transferase
CDTa: CDT enzymatic component
CDTb: CDT binding component
CK1α: casein kinase 1α
CM: conditioned media
CPM: counts per million
CRD: cysteine rich domain
CROPs: combined repetitive oligopeptides
cryo-EM: cryo-electron microscopy
cryo: cryogenic
CS: chondroitin sulfate
CSPG: chondroitin sulfate proteoglycan
CSPG4: chondroitin sulfate proteoglycan 4
D0: day zero
D1: extracellular subdomain 1
D2: extracellular subdomain 2
D3: extracellular subdomain 3
DAB: 3,3'-Diaminobenzidine
DD: delivery domain
ddPCR: digital droplet-PCR
DMEM: Dulbecco's Modified Eagle's medium
DVL: Dishevelled
ECD: extracellular domain
ECM: extracellular matrix
EM: electron microscopy
EMEM: Eagle's Minimum Essential Medium
ERK: extracellular signal-regulated kinase
F-actin: filamentous actin
FAK: focal adhesion kinase
FBS: fetal bovine serum

FGF: fibroblast growth factor
FGFR: fibroblast growth factor receptor
FZD: frizzled
GAG: glycosaminoglycan
GEO: Gene Expression Omnibus
GlcNAc: N-acetyl-glucosamine
GREIN: GEO RNA-seq Experiments Interactive Navigator
GSK3β: glycogen synthase kinase 3β
GTD: glucosyltransferase domain
HI-FCS: heat inactivated fetal calf serum
HI: heart infusion
HMW-MAA: High molecular weight melanoma-associated antigen
HRP: horseradish peroxidase
IACUC: Institutional Animal Care and Use Committee
ID: identifier
IG: immunoglobulin
InsP6: inositol hexakisphosphate
KD: dissociation constant
LB: Luria Broth
LCTs: large clostridial toxins
LEF: lymphoid enhancer factor family
LGR: laminin G-type region
LRP: low-density lipoprotein receptor-related protein
MAPK: mitogen-activated protein kinase
MCSP: melanoma cell surface proteoglycan
MEM: Minimal Essential Medium
MLST: multi locus sequence typing
MMP: matrix metalloproteinase
MST: microscale thermophoresis
MT-MMP: membrane-type MMP
NADP+: Nicotinamide adenine dinucleotide phosphate (oxidized)
NADPH: Nicotinamide adenine dinucleotide phosphate
NAP: The North American pulsed-field gel electrophoresis type
NCBI: National Center for Biotechnology Information
ND: not determined
NDS: normal donkey serum
NG2: neural-glial antigen 2
NGS: normal goat serum
NOX: NADPH oxidase
OCT: optimal cutting temperature

PAR-3: protein partitioning defective-3
PBS: Phosphate Buffered Saline
PCC: Pearson correlation coefficient
PDB: protein data bank
PDGF: platelet-derived growth factor
PDGFR: platelet-derived growth factor receptor
PDZ: postsynaptic density-95, discs-large, zonula occludens 1
PG: proteoglycan
PI: propidium iodide
PKCα: protein kinase C alpha
pLDDT: per-residue confidence score
PRR: proline-rich region
PVRL3: poliovirus receptor-like protein 3
qPCR: quantitative PCR
REA: restriction endonuclease analysis
Rho: Ras homologue family member
RT: ribotype
RTK: receptor tyrosine kinases
sc: single-cell
scRNA-seq: single cell RNA-sequencing
SMC: smooth muscle cell
ST: sequence type
TcdA: toxin A
TcdB: toxin B
TCF: T cell factor
Tcnα: alpha-toxin
TcsH: hemorrhagic toxin
TcsL: lethal toxin
TFPI: tissue factor protein inhibitor
TM: transmembrane
TMM: trimmed mean of m-values
TpeL: large cytotoxin
TPSR: Translational Pathology Shared Resource
TY: Tryptone Yeast
Type i: TcdB1-like
Type ii: TcdB7-like
UDP: uradine diphosphate
WB: Western blot
WT: wild-type
ZO-1: zonula occludens-1

Chapter 1

Introduction

Overview of Clostridioides difficile

In 1935, Ivan C. Hall and Elizabeth O'Toole recorded the first description of the obligate anaerobe and Gram-positive bacterium *Clostridioides difficile* (1, 2). The researchers isolated *C. difficile* from the stool of newborn infants and unexpectedly found the bacterium was pathogenic to rabbits and guinea pigs due to the activity of an unknown heat-labile toxin (1). However, as the bacterium was present in the stool of multiple healthy newborns, Hall and O'Toole speculated that *C. difficile* was not likely a concern for human health and simply a component of the collection of microbial organisms we refer to today as the microbiome. This view of *C. difficile* persisted until the late 1970s, when it was determined that *C. difficile* was an etiological cause of pseudomembranous colitis (PMC) (3–5). PMC presents in individuals as severe inflammation along the colonic mucosa with pseudomembranes composed of mucus, necrotic epithelial cells, fibrin, and immune cell infiltrates such as leukocytes and neutrophils (6). The heat-labile toxin inferred by Hall and O'Toole decades prior was associated with the occurrence of PMC and identified as two individual protein toxins, toxin A (TcdA) and toxin B (TcdB) (8–10)(7–9). *C. difficile* infections (CDI) are associated with the use of antibiotics, which can alter the colonic microbiome and increase host susceptibility to *C. difficile* colonization (10–12). Clinical symptoms associated with CDI span from mild and recurrent diarrhea to life-threatening PMC, sepsis, toxic megacolon, and bowel perforation (6, 13–15). The annual healthcare burden of *C. difficile* in the United States of America in modern times are an estimated 223,900 infections and 12,800 deaths per year (16).

The life cycle of *C. difficile* can consist of two unique stages—a metabolically active vegetative cell and a metabolically inactive endospore (17). *C. difficile* transitions between these stages through cellular differentiation pathways called germination and sporulation (17–20). The germination pathway transitions an endospore into a vegetative cell, whereas the sporulation pathway transitions a vegetative cell into an endospore (17, 20). The endospores represent the infectious form of *C. difficile* and are shed from hosts through feces (21, 22). Endospores can persist in the environment for years due to their resistance to heat and common disinfectants used in hospitals (23–25). Importantly, these endospores can

withstand exposure to atmospheric concentrations of oxygen that are lethal to vegetative *C. difficile* (26, 27).

The transmission of *C. difficile* between hosts occurs through the fecal-oral route, although successful infections in humans typically require exposure to risk factors. These risk factors include the use of antibiotics, the use of proton-pump inhibitors, hospitalization, age, and immunodeficiencies (28–32). Exposure to these risk factors alter the gut microbiome's ability to resist colonization to *C. difficile* (12, 33). Ingested endospores will traverse the stomach and will initiate germination in the small intestine upon exposure to primary bile acids (34, 35). In susceptible hosts, vegetative *C. difficile* will colonize the colon and produce TcdA and TcdB (36). The activity of these toxins damages the intestinal mucosa, allowing *C. difficile* to acquire nutrients for growth and reproduction (37, 38). Throughout the infection, a sub-population of *C. difficile* will undergo sporulation to produce endospores that will be shed into the environment (20). For most cases, treatment of CDI involves the administration of vancomycin, an antibiotic that inhibits cell wall biosynthesis (39, 40). Recurrent infections occur in 5-20% of patients, requiring additional administration of vancomycin or the use of experimental treatments such as fecal microbiota transplantation (39, 41). In severe cases of CDI with fulminant colitis, an ileostomy or total colectomy may be performed (39). While most *C. difficile* infections occur in hospitals and long-term care facilities, cases of community-acquired infections associated with farms and unknown causes have been reported (42).

The identification of *C. difficile* as a mediator of pseudomembranous colitis

During the 1970s, researchers were determined to identify the cause of antibiotic-induced PMC; a rapidly spreading disease with reported mortality rates as high as 10% (11, 43–45). In the prior decades, case studies had revealed as many as 1 in 5 postoperative patients on antibiotics experienced symptoms of antibiotic-induced diarrhea that could develop into potentially fatal PMC (46–48). A study reported by Altemeier et *al.* suggested the disease was mediated by *Staphylococcus aureus*, but noted that they could only isolate the pathogen from 53 out of total 155 patients (48). Further evidence linking the disease to bacteria was a report showing that most patients could be cured of disease when given oral vancomycin (49). While the treatment was successful, many researchers were not convinced that *S. aureus* was the cause of PMC (6, 50). Alternative hypotheses predicted that disease was mediated either by an unknown pathogen or by an adverse host reaction to clindamycin, an antibiotic introduced in the 1970s to treat

anaerobic infections that coincided with the rising cases of antibiotic-induced PMC (6, 10, 43, 47, 51). Initial studies testing these hypotheses were performed by screening the stool of diseased patients for pathogens and by conducting longitudinal studies that tracked the use of antibiotics and disease development. From these initial studies, it was found that although pathogens associated with diarrhea could be isolated from some patients with antibiotic-induced PMC, an association with a specific pathogen across a larger cohort of patients could not be found (52, 53). Moreover, while the use of clindamycin could be associated with the development of PMC, a longitudinal study revealed that patients taking ampicillin could also develop the disease (10, 44, 51, 53). Although these data revealed that clindamycin alone was not responsible for mediating disease, it also suggested that a pathogen other than *S. aureus* was responsible for antibiotic-induced PMC.

As researchers had failed to identify a bacterium responsible for mediating PMC, some researchers asked if the disease could be mediated by a virus. In a study performed by Harold E. Larson and colleagues, the researchers attempted to isolate a virus for the stool from a 12-year-old child presenting with the disease (9). While their search for a virus ultimately ended in failure, their characterization of the stool would provide the first evidence that antibiotic-induced PMC was a toxin mediated disease. In their study, Larson and colleagues observed that the patient's stool was capable of inducing a cytopathic, or cell rounding, response on tissue culture cells (**Figure 1-1**) (9). While viruses are also capable of inducing cytopathic effects on cells, their further characterization of the cytopathic factor from the stool suggested it was a protein toxin, not a virus (9). As the disease is associated with the use of antibiotics and bacteria were a known source of protein toxins, Larson et *al.* concluded that a bacterial toxin was responsible for mediating PMC.

Although Larson and colleagues predicted that a bacterium was responsible for producing the toxin, their attempts to isolate a toxin producing bacterium were unsuccessful (9). A series of publications by John G. Bartlett and colleagues would soon establish the role of *C. difficile* and its toxins towards this disease. Their first hints at identifying the pathogen came from the hamster model of antibiotic-induced enterocolitis, a model of spontaneous enterocolitis following antibiotic treatment (54, 55). In their first study, Bartlett and colleagues demonstrated that clindamycin-induced enterocolitis in hamsters could be treated using vancomycin, which suggested that the disease was likely mediated by a bacterium (55). In a follow-up report, Bartlett and colleagues screened stool from similarly diseased hamsters for anaerobic

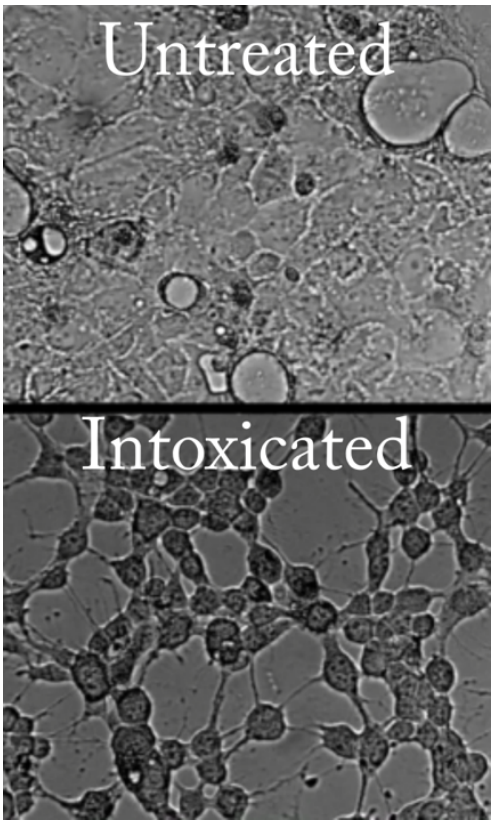

Figure 1-1. An example cytopathic response in 2D-cell cultures.

Caco-2 were intoxicated with 10 pM TcdB and imaged at 20X magnification after 4 hours. Cells treated with TcdB display a cytopathic response. Personal unpublished images acquired on a Cytation 5 imager.

bacteria and isolated a Gram-positive *Clostridium* with striking resemblance to *C. difficile* that alone could mediate disease (56). The *Clostridium* isolate was resistant to clindamycin and produced a toxin in its culture supernatants that was capable of inducing enterocolitis in hamsters as well (56). These data provided a mechanism for antibiotic-induced enterocolitis in hamsters that suggested an antibiotic resistant *Clostridium* was responsible for mediating disease *via* a secreted protein toxin.

Despite the fact that hamsters provided a convenient model for studying antibiotic-induced enterocolitis, it remained unclear if any disease mechanisms in hamsters would translate to disease in humans. For example, as *C. difficile* was not recognized as a human pathogen, the *Clostridium* isolate from Bartlett et *al*. that resembled *C. difficile* could be irrelevant for human disease (3). However, data from Bartlett et *al*. provided insight that the disease mechanism in hamsters may in fact be relevant to human health. Specifically, the researchers found that anti-serum generated against gas gangrene clostridial toxins could neutralize the cytotoxin's activity in hamsters (56, 57). These toxins, produced by various clostridial species, are mediators of clostridial gas gangrene, a potentially lethal infection of soft tissue that was and still remains a human health concern (58–60). These findings from Bartlett et al. allowed researchers to hypothesize that the cytotoxin(s) present in the stool of PMC patients were produced by a *Clostridium* capable causing of gas gangrene. Studies by Larson et *al*. and Rifkin et *al.* tested this hypothesis by treating the stool of PMC patients with anti-serum generated against individual clostridial gas gangrene toxins (61, 62). Collectively, these studies revealed that the cytotoxin(s) present in the stool of PMC patients could be neutralized with anti-serum generated against *Paeniclostridium sordellii* (formerly *Clostridium sordellii*) toxins (61, 62). As a result, Larson, Rifkin, and colleagues concluded that *P. sordellii* was the likely mediator of antibiotic-induced PMC.

Although the discoveries by Larson et al. and Rifkin et al. implied that *P. sordellii* was responsible for mediating antibiotic-induced PMC in humans, *P. sordellii* was not known to cause gastrointestinal disease in humans and was never isolated from the stool of PMC patients (61, 62). At the time, the only study linking *P. sordellii* toxins to colitis was a similarly performed toxin neutralization study in canines (63). Without evidence showing that *P. sordellii* was present in the stool of PMC patients or demonstrating that disease could be mediated by the bacterium, some researchers speculated if the results were a red herring. An alternative explanation considered by Bartlett and colleagues was that the *Clostridium* isolate from their hamster model was responsible for mediating disease in humans. The observation that anti-

serum against *P. sordellii* toxins neutralized the cytotoxin(s) in the stool of PMC patients could be explained by the possibility that the *Clostridium* produces a homologous toxin. Bartlett and colleagues tested this alternative hypothesis by characterizing bacterial isolates isolated from the stool of five patients with antibiotic-induced diarrhea, four of whom presented symptoms of PMC (64). From these stool samples, Bartlett et *al*. isolated twenty-five clostridia, four of which produced a toxin whose activity could be neutralized by anti-serum against gas gangrene toxins (64). Notably, the toxin producing *Clostridium* was only present in the stool samples of patients presenting with PMC (64). The researchers also found that these toxin producing isolates were capable of causing enterocolitis in hamsters (64). Taxonomic characterization performed by Bartlett and colleagues identified the isolates as *C. difficile* (64). From these data, Bartlett et *al*. concluded that antibiotic-induced PMC was mediated by opportunistic *C. difficile* infections and its disease was mediated through a toxin(s) with antigenic features similar to *P. sordellii* toxins (65).

Historical perspectives of *C. difficile* toxins TcdA and TcdB in disease

The discovery of *C. difficile* as the mediator of antibiotic-induced PMC in hamsters and humans was further corroborated by multiple researchers, including Larson and colleagues (5, 66–69). The collective work of these pioneering studies suggested that a heat-labile protein toxin was responsible for disease. However, as researchers began their work to isolate and characterize the toxin, confounding results were reported between studies. These confounding data included differences in molecular weight, the presence and absence of enterotoxic activity *in vivo*, as well as differences in cytotoxic activity *in vitro* (70–72). These differences were soon explained, however, by the finding that independent research groups had unknowingly purified two unique toxins from *C. difficile* supernatants (7, 8, 73–76).

In 1981, reports by Taylor et *al*. and Banno et *al*. revealed that two unique toxins could be isolated from the supernatants of *C. difficile* (7, 76). The names introduced by Taylor et al., toxin A and toxin B, were adopted by the field (7). These names were aptly derived from the order by which the toxins eluted from an anion-exchange column during purification, where TcdA is eluted earlier than TcdB (7). The initial characterization of the toxins in Taylor et al. suggested that TcdA was responsible for mediating disease in animals while TcdB was responsible for mediating the cytopathic response on cells (7). This observation was corroborated by other studies that also showed TcdA injections in animals caused fluid accumulation, edema, and significant injuries to the intestinal mucosa while little to no symptoms could be observed with

TcdB (7, 8, 73, 76). As a result of these observations, TcdA is historically referred to as an enterotoxin while TcdB is historically referred to as a cytotoxin (8).

While many of these early investigations suggested TcdA alone was sufficient for mediating disease, there were reports that suggested otherwise during the context of infection. For example, a vaccine study performed soon after the discovery of the toxins by Tracey Wilkins and colleagues revealed that hamsters could be fully protected from CDI and its disease only when vaccinated against both TcdA and TcdB (77). If a hamster was vaccinated against a single toxin, those hamsters would die and suffer from disease (77). While the data could not reveal a mechanism of how this occurred, it suggested that TcdB contributes to disease during infections. To gain further insight into a potential mechanism, the same research group hypothesized that TcdB could synergize with TcdA during infections to promote disease (78). The researchers tested this hypothesis by treating hamsters intragastrically with non-lethal concentrations of TcdA together with TcdB (78). Their study revealed that the combination of both toxins was lethal to all hamsters and suggested that TcdB does synergize with TcdA to promote disease. As TcdB had not been shown to facilitate injuries to the intestinal epithelium in animals, one mechanism proposed by Wilkens and colleagues was that TcdB would injure tissue outside of the intestines once TcdA injures the intestinal mucosa (6). In support of this model, the researchers would later show that the lethal dose of TcdA and TcdB were essentially identical if administered intraperitoneally or intravenously into mice or infant rhesus monkeys (79, 80). Their proposed mechanism would be supported by most of the *C. difficile* field for decades as to how disease was mediated by TcdA and TcdB.

While the conclusions of Wilkins and colleagues were logical, a clear mechanism of how each toxin contributed to disease was lacking. How did the injection of TcdA into intestinal tissue cause fluid secretion and epithelial damage? Additionally, how does the activity of TcdB contribute to disease? An initial hypothesis was that TcdA mediates diarrhea through mechanisms similar to that of cholera toxin from *Vibrio cholerae* and heat-labile toxin of enterotoxigenic *Escherichia coli* (81). The activity of both of these toxins results in the elevation of cyclic adenosine monophosphate (cAMP) within the cytosol of intoxicated cells (82, 83). The elevated levels of cAMP disrupts ion-transport function which ultimately drives secretory diarrhea during infection (84). However, experiments failed to detect changes in cAMP levels from tissue intoxicated with TcdA (81). If TcdA did not induce disease through the elevation of cAMP, an alternative mechanism considered by some was that disease was mediated through the immune

response. Researchers such as John LaMont and colleagues first considered this hypothesis after observing that rabbit ileal loops injected with TcdA contained massive amounts of neutrophils (85). As neutrophils are known to contain inflammatory cytokines that are capable of causing injury and fluid secretion, LaMont and colleagues speculated that the neutrophils, and not TcdA, would drive the symptoms of disease (85). In support of this hypothesis, the researchers found that TcdA was unable to cause injury to rabbit intestinal explants (85). Therefore, without the involvement of the host immune response, TcdA itself did not appear capable of mediating disease symptoms alone. Moreover, the researchers also demonstrated that TcdA, and not TcdB, could elicit a strong chemotactic response to neutrophils *in vitro* (86, 87). Macrophages, another immune cell population found in *C. difficile* infected tissue, was also found to be stimulated by TcdA (88). Together, these data suggested that TcdA can promote intestinal injury and potentially facilitate diarrhea through the recruitment and activity of immune cells during infection.

As LaMont and colleagues continued to explore the role of these toxins in disease, they would later report that both TcdA and TcdB were capable of altering intestinal epithelial cell barrier function—a property of polarized cells mediated by cell junctions—*in vitro* by disrupting the actin cytoskeleton of cells (89–91). Loss of barrier function in intestinal epithelial cells is believed to promote diarrhea by affecting the ion gradient or solute gradient across a cell (92). Although these observations were from tissue culture cells, LaMont would also make the surprising observation that TcdB was in fact more potent than TcdA on human colonic explants (93). By measuring the permeability and resistance of the epithelium during intoxication with either TcdA or TcdB, the researchers determined that TcdB was approximately 10 times more potent than TcdA (93). Furthermore, both toxins were capable of injuring epithelial cells, an observation that had not been seen in rabbit, mouse, rat, or hamster tissue (7, 8, 73, 76, 78, 93). As the study utilized explant, these observations would be independent of any contributions from neutrophils and macrophages. These observations suggested that TcdB may in fact be more relevant to human disease than previously thought.

The mechanism of disease proposed by Wilkins and colleagues in the late 1980s was modified to incorporate these new observations. By the mid-1990s, both TcdA and TcdB were proposed to contribute to epithelial cell injury, but TcdA would facilitate more injury by recruiting innate immune cells. Although questions remained on how the activity of the toxins mediated diarrhea, the requirement of TcdA for the disease in humans and animals was so far considered essential. This view was challenged in the year 2000

when two studies reported an outbreak of antibiotic-induced PMC in patients infected with *C. difficile* that was TcdA negative and TcdB positive (94, 95). Historically, strains of *C. difficile* producing only TcdB were not thought to cause disease in humans or animals (96, 97). Further characterization of the TcdB produced by this strain of *C. difficile* would demonstrate it was capable of inducing enterotoxic effects and enterocolitis on human intestinal xenographs (98). If disease could be mediated by TcdB alone, as the outbreak of antibiotic-induced PMC suggested, the working model of how the toxins mediate disease was incorrect.

An obvious approach that could establish a mechanism for TcdA and TcdB in disease would be to generate knockouts of each toxin and perform an infection in animals. However, genetic techniques capable of generating a stable gene knockout in *C. difficile* were only developed in the mid-2000s (99, 100). With these new genetic approaches, researchers would soon investigate the role each toxin in disease. In a study reported by Lyras et al., TcdB was determined to be a mediator of lethality in hamsters during CDI (101). Surprisingly, Lyras et al. found that almost all hamsters infected with *C. difficile*Δ*tcdA* (the Greek letter Δ represents genetic disruption) died while mostly all hamsters infected with *C. difficile*Δ*tcdB* survived, suggesting that: (1) TcdA was not required for mediating disease in hamsters, (2) TcdB alone was sufficient for mediating disease in hamsters, and (3) the role of TcdA is unclear in the hamster model of CDI (101). These results disrupted the long-held model of *C. difficile* toxins proposed by Wilkins and colleagues and suggested that the use of recombinant toxins alone cannot predict the role of each toxin.

A year after the publication of the Lyras et al. study, a report by Kuehne et al. determined *C. difficile* expressing either TcdA or TcdB could cause a lethal infection in hamsters and that loss of TcdB only attenuated the disease (102). Importantly, disruption of both toxins failed to cause any disease in the hamsters. While these findings suggested that TcdB likely contributes more to disease than TcdA, it also revealed that the TcdA could contribute to disease in hamsters. It should be noted, however, that differences in institutional animal use regulations allowed the study by Lyras et al. to use animal death as an endpoint while the study by Kuehne et al. could only use humane death as determined by percent weight loss or signs of lethargy (101, 102). Therefore, the differences observed between the two groups could possibly be explained by factors such as how each group measured death, potential differences in genetic approaches used to generate the knockouts, and even differences in intestinal microbiomes between institutions (103, 104).

As the debate continued, Kuehne et al. performed another hamster infection using isogenic knockouts in another strain of *C. difficile*, reporting the same observations and again showed that TcdA was important for mediating disease (105). Dena Lyras and colleagues would go on to do the same as well, but this time also investigating their role in mice in addition to hamsters (106). In this study, Lyras and colleagues also used the same percent weight loss metric for a humane endpoint used in the studies from Kuehne et al. (102, 105, 106). With the modified metric for death, Lyras and colleagues observed that hamsters could indeed suffer severe disease when infected with *C. difficile*Δ*tcdB*, although the time to death was slower than that of a wild-type (WT) infection or *C. difficile*Δ*tcdA* (106). From the mice infections, Lyras and colleagues demonstrated that TcdB, and not TcdA, was essential for mediating multiple metrics of disease (106). Specifically, *C. difficile* expressing only TcdB during infection exhibited greater weight loss, had worse survival, and worse pathologies than *C. difficile* expressing only TcdA (106). Although *C. difficile*Δ*tcdB* could promote some weight loss and pathology, the disease induced by *C. difficile*Δ*tcdA* was nearly identical to that of a WT infection (106). While these data suggest that TcdB alone is capable of mediating all disease symptoms, it should be noted that most *C. difficile* isolates are capable of expressing both TcdA and TcdB (107). As TcdA is likely produced during most cases of CDI, its contributions towards disease should not be ignored (108, 109). Recent studies from Christopher Peritore-Galve of the Lacy Laboratory and others have shown that the enzymatic activities of the toxins synergize with each other to promote diarrhea in mice, suggesting that both toxins are required for severe diarrhea typically observed during CDI (110). With these collective observations, both toxins can possibly facilitate disease by intoxicating the host colonic mucosa and inducing secondary damage by stimulating the production of cytokines from the innate immune system. Although current experimental observations suggests that TcdB is more pathogenic than TcdA, both toxins are likely important for disease progression in hosts.

In addition to TcdA and TcdB, some strains of *C. difficile* can express a third toxin, *C. difficile* transferase (CDT), which is an actin modifying adenosine diphosphate (ADP) ribosyltransferase toxin (CDT) (111). CDT is a binary AB toxin consisting of an enzymatic A component (CDTa) and a binding and translocation component (CDTb) (112). Although the global prevalence of *C. difficile* that express CDT has decreased since the mid-2000s, these strains are associated with greater disease severity and mortality (105, 113, 114). The ADP-ribosyltransferase activity of CDT induces ADP-ribosylation of G-actin in cells, causing a cytopathic response in cell monolayers (112, 115). The toxin, however, is not capable of causing significant injuries or disease on its own during CDI in hamsters or mice (105, 106, 110). These

observations have suggested that CDT likely synergizes with TcdA and TcdB during infection, although the mechanism is currently unknown. In addition to its cytotoxic properties, CDT may enhance *C. difficile* virulence by suppressing cytokine production in eosinophils, leading to altered colonic mucus production and enhanced epithelial disruption during CDI (116–118). Another proposed mechanism of how CDT enhances *C. difficile* virulence is by promoting bacterial adhesion to the epithelium (119, 120). Interestingly, colonic epithelial cells intoxicated with CDT produce multiple septin guided, microtubule-based protrusions that are enriched with fibronectin along their cell edges that are capable of binding *C. difficile in vitro* (119–121). Moreover, these *in vitro* studies have shown that CDT intoxicated cells bind approximately 5-times more *C. difficile* than non-intoxicated cells (119, 120). Although these protrusions have not been observed *in vivo*, these protrusions are predicted to enhance *C. difficile* colonization during the initial stages of infection (119).

An overview of the structure and function of TcdA and TcdB

TcdA (308 kDa) and TcdB (270 kDa) are members of the large clostridial toxins (LCTs), a family of homologous toxins with similar structure and function. Members of the LCTs includes the hemorrhagic (TcsH) and lethal (TcsL) toxins from *P. sordellii*, the large cytotoxin (TpeL) from *C. perfringens*, and the alpha-toxin (Tcnα) from *Clostridium novyi*. These LCTs are multidomain AB toxins, containing a toxic A-component and a receptor binding B-component across a single polypeptide chain (**Figure 1-2A**) (122). The A-component of most LCTs contains a glucosyltransferase domain (GTD) that covalently modifies Ras homologue family member-(Rho) and Ras-family GTPases with a glucose moiety from uridine diphosphate (UDP) glucose (123–128). However, for the two LCTs that can utilize UDP-*N*-acetyl-glucosamine (GlcNAc), TpeL and Tcnα, the domain is instead called the glycosyltransferase domain (128–130). Nonetheless, the GTPases are modified by the GTD on a threonine residue (Thr37 on RhoA, RhoB, and RhoC and Thr35 of Rac1, Cdc42, Ral, and Ras) within their switch I region; a domain involved in GTP and Mg^{2+} binding (**Figure 1-2A**) (123–128, 131). With the glucosylated GTPase now unable to change into an active conformation, it becomes functionally inactive which results in the disruption of the actin cytoskeleton, tight junction instability, cytokine production and apoptotic cell death (125, 131–134). A table of the LCTs and their common substrates and targets are summarized in Table 1-1.

The receptor binding B-component of LCTs contain multiple domains that contribute to receptor

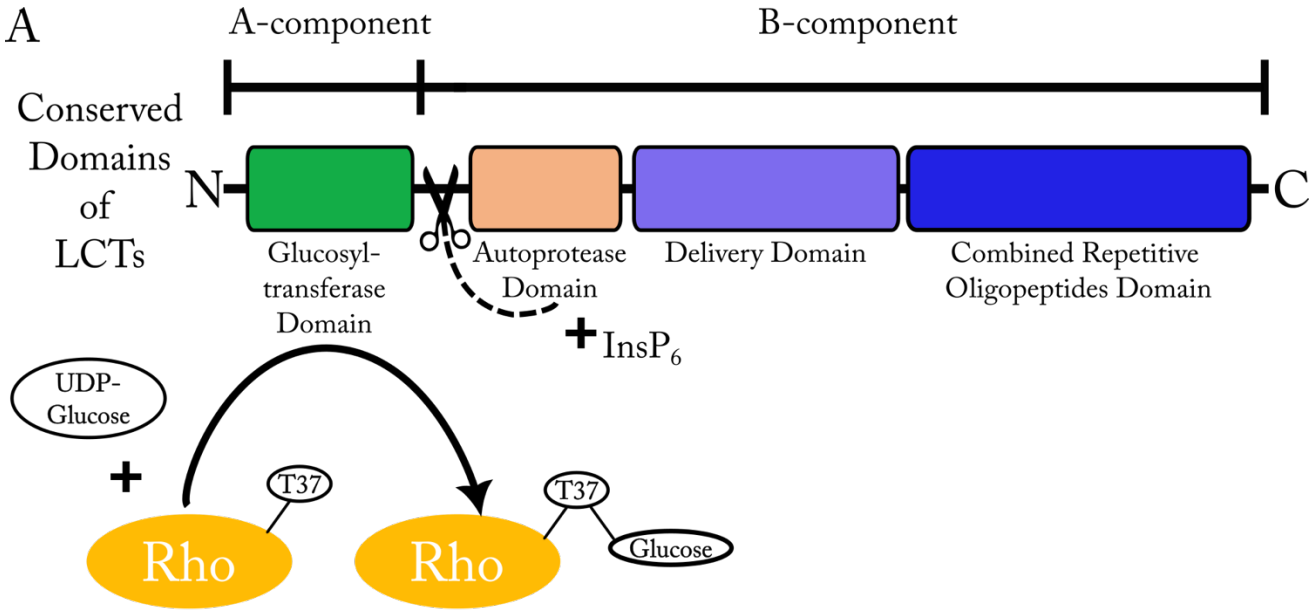
A
A-component
B-component
Conserved Domains of LCTs
N
C
Glucosyl-transferase Domain
Autoprotease Domain
Delivery Domain
Combined Repetitive Oligopeptides Domain
+ InsP6
UDP-Glucose
+
T37
Rho
Rho
T37
Glucose

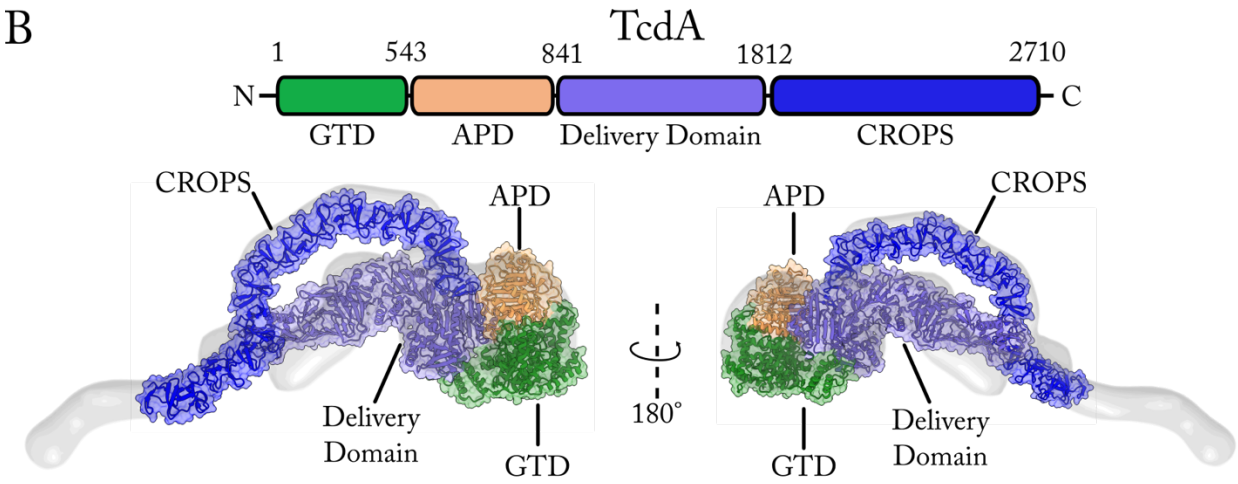
B
TcdA
1
543
841
1812
2710
N
C
GTD
APD
Delivery Domain
CROPS
CROPS
APD
Delivery Domain
GTD
180°
APD
CROPS
GTD
Delivery Domain

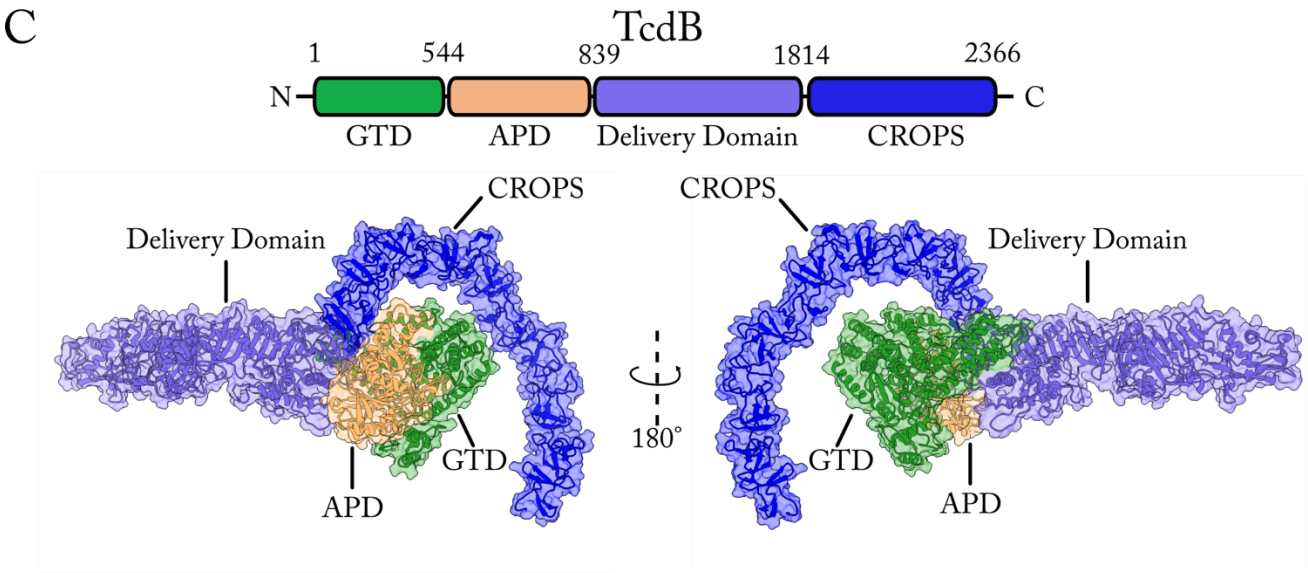
C
TcdB
1
544
839
1814
2366
N
C
GTD
APD
Delivery Domain
CROPS
Delivery Domain
CROPS
GTD
APD
180°
CROPS
Delivery Domain
GTD
APD

Figure 1-2. Common domains of the large clostridial toxins.

A) A cartoon model of conserved domains of large clostridial toxins (LCTs) domains. LCTs are multidomain AB toxins containing a toxic A-component and receptor binding B-component across a single polypeptide. The N-terminal A-component of most LCTs contains a toxic glucosyltransferase domain (GTD). The B-component of LCTs contain an autoprotease domain (APD), a delivery domain, and a combined repetitive oligopeptides (CROPs) domain. In order for LCTs to properly intoxicate cells, the GTD must be released from the B-component. For example, with TcdB, the proteolytic activity of the APD will cleave the GTD from the polypeptide chain between amino acids 543-544 upon binding $InsP_6$. The released GTD will covalently inactivate Rho family GTPases by mono-glucosylating a threonine in the switch I region (Thr-37 of RhoA, Thr-35 of Cdc42, Rac1, Ral, and Ras) of the GTPase.

B) Crystal structures of $TcdA_{1\text{-}1832}$ (Protein Data Bank (PDB) identifier (ID) 4R04) at 3.26 Å resolution and TcdA $CROPs_{1833\text{-}2481}$ (PDB ID 7U1Z) at 3.18 Å resolution docked into an electron density map of the TcdA holotoxin from Pruitt et *al.* (135).

C) Crystal structure of TcdB (PDB ID 6OQ5) at pH 5.2 and 3.87 Å resolution

binding, pore-formation, and autoprocessing of the GTD from the polypeptide chain. These domains are called the autoprotease domain (APD), the delivery domain, and the combined repetitive oligopeptides (CROPs) domain—TpeL lacks the CROPs domain (**Figure 1-2A**) (135–138). The APD is classically considered to be a cysteine protease whose primary function is to facilitate the release of the GTD into the cytosol of cells (139, 140). Its autoprocessing activity is activated upon binding inositol hexakisphosphate ($InsP_6$), a compound enriched in the cytosol, resulting in the proteolytic cleavage of the GTD from the polypeptide chain (139–142). Although initial experiments had suggested that the APD is a cysteine protease, the proteolytic activity is dependent on a zinc ion bound to the cysteine in the active site of the APD (139, 143, 144). This observation suggests that the APD could be a zinc protease instead of a cysteine protease. The delivery domain is the pore-forming domain that facilitates the delivery of the APD and GTD into the cytosol of cells (137, 145). Although the exact mechanism of how pore-formation and translocation is unknown, the process is dependent on pH-dependent conformational changes that occur within the endosome (137, 145).

The final domain of the B-component is the CROPs domain. Before the identification of CROPs-independent receptors for TcdA and TcdB, the CROPs domain was considered to be the sole receptor binding domain of each toxin and a regulator of the APD (146, 147). The CROPs domain is a rigid structure that can adopt multiple conformations as evident in the crystal structures of TcdA and TcdB (**Figure 1-2B & C**) (135, 143, 148, 149). These conformational changes may be dependent on the pH, where more acidic pH causes the CROPs domain to adopt the conformation observed in the TcdB crystal structure (135, 148–151). In TcdB, these conformational changes have been suggested to regulate receptor interactions, however, the significance of these conformational changes for other LCTs remain unknown (151). Moreover, the CROPs domain of TcdA and TcdB have been shown to bind a variety of glycans, which may increase the diversity of cells the toxins can target during an infection (152).

As my thesis investigated the role of TcdB interactions with receptors, the remaining sections of this chapter are dedicated to TcdB.

Table 1-1 A summary of the large clostridial toxin family

Organism	Toxin	Molecular Weight	Targets	Substrate	Ref
Clostridioides difficile	TcdA	308 kDa	Rho, Rac, Cdc42, Rap	UDP-Glu	(123, 138)
Clostridioides difficile	TcdB	270 kDa	Rho, Rac, Cdc42	UDP-Glu	(124, 125)
Paeniclostridium sordellii	TcsH	300 kDa	Rho, Rac, Cdc42	UDP-Glu	(126)
Paeniclostridium sordellii	TcsL	270 kDa	Rac, Ras, Ral, Rap	UDP-Glu	(126, 127, 153)
Clostridium perfringens	TpeL	191 kDa	Rac, Ras, Ral, Rap	UDP-Glu, UDP-GlcNAc	(128)
Clostridium novyi	Tcnα	250 kDa	Rho, Rac, Cdc42	UDP-GlcNAc	(129)

Mechanism of action for TcdB

A model for TcdB intoxication of cells can be summarized through the following steps: (1) receptor binding on the cell surface and (2) clathrin-mediated endocytosis, (3) acidification of the endosome, resulting in (4) pore-formation and translocation of the APD and GTD across the endosomal membrane into the cell cytosol, (5) autoprocessing and release of the GTD from the holotoxin and (6) glucosylation of Rho-family GTPases (**Figure 1-3A**). Four classes of protein receptors have been identified for TcdB, which include chondroitin sulfate proteoglycan 4 (CSPG4), Frizzled (FZD) 1, FZD2, FZD7, Nectin-3, and tissue factor pathway inhibitor (TFPI) (154–158). Each receptor was identified from genetic screens and loss of each receptor attenuates TcdB cytotoxicity or its cell rounding kinetics (154–158). The interactions between these receptors and TcdB are only predicted to result in clathrin mediated endocytosis of TcdB (154–158). Some recent reports even suggest that three of these receptors, CSPG4, Nectin-3, and FZD proteins, are not endocytosed in the presence of TcdB (159). Without a clear mechanism and understanding of their contributions to intoxication, the importance of TcdB interactions with these receptors on cells and tissue remains unknown.

Crystal structures and cryogenic (cryo)- electron microscopy (EM) structures have been determined for TcdB with CSPG4, FZD, and TFPI (**Figure 1-3B**) (148, 157, 160, 161). These co-structures have revealed the binding interfaces between TcdB and receptors can occur within at a conserved interface in the delivery domain—as in the case for FZDs and TFPI (**Figure 1-3Bi**)—and at an interface containing the delivery domain, APD, and CROPS domain—as in the case for CSPG4 (**Figure 1-3Bii**) (157, 160, 161). These structures will be discussed in more detail in later sections.

TcdB variants

One explanation as to why TcdB is capable of interacting with multiple receptors may be explained by the existence of TcdB variants (107, 162, 163). While researchers were aware of various infectious *C. difficile* strains and TcdB variants since the mid 1990s, most had predicted these variants were associated with increased virulence (164–168). The most notable of these TcdB variants was produced by the epidemic *C. difficile* PCR ribotype (RT) 027 that emerged in North America and Western Europe in the early to mid 2000s (114, 169–171). Due to the use of multiple classification techniques for *C. difficile* isolates, this strain may also be referred to as North American pulsed-field gel electrophoresis type (NAP) 1 or restriction endonuclease analysis (REA) group BI (170–172). The full name of these epidemic strains are

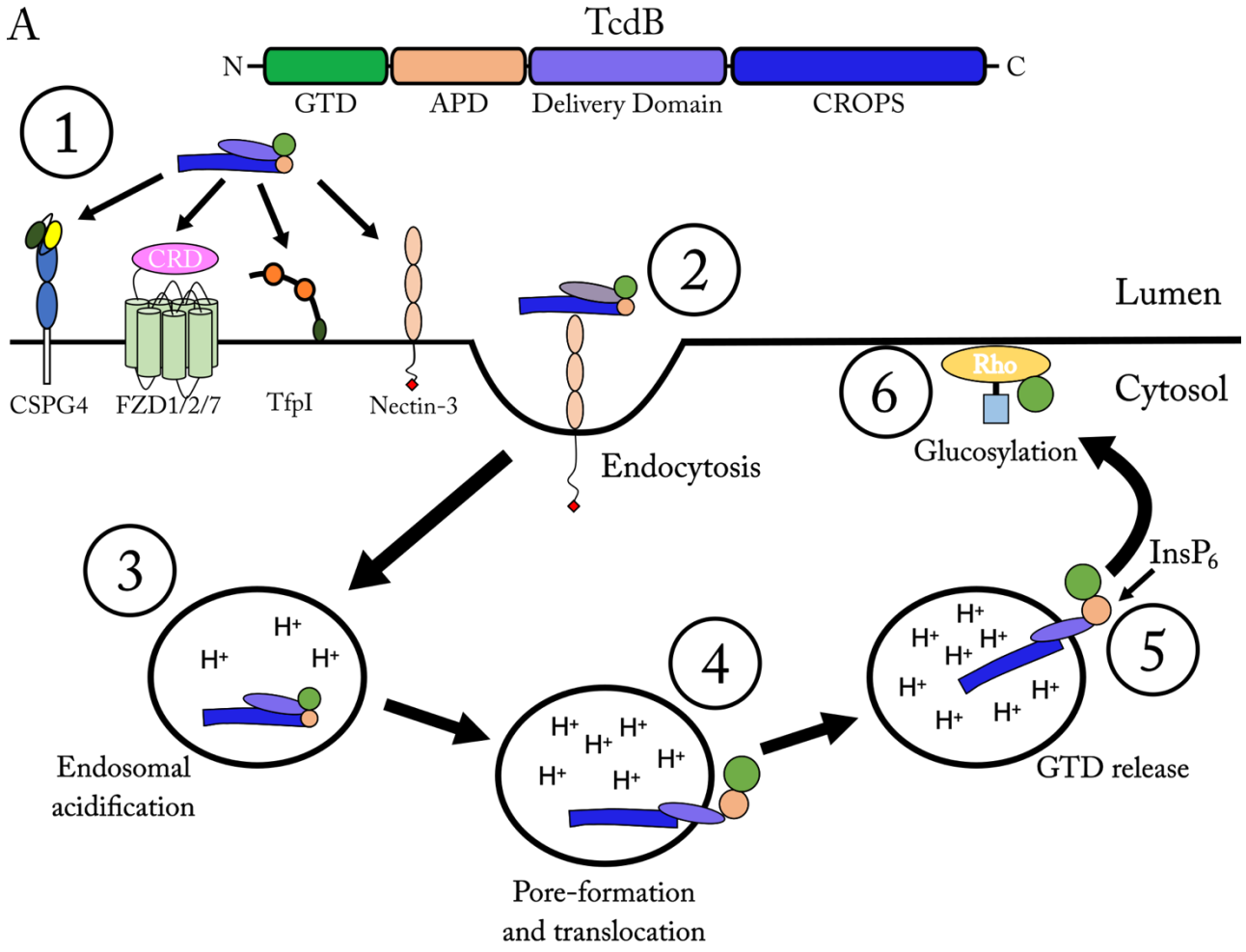
A
TcdB
N
C
GTD
APD
Delivery Domain
CROPS
1
CRD
CSPG4
FZD1/2/7
TfpI
Nectin-3
2
Lumen
Cytosol
Endocytosis
6
Rho
Glucosylation
InsP6
3
H+
Endosomal
acidification
4
Pore-formation
and translocation
5
GTD release

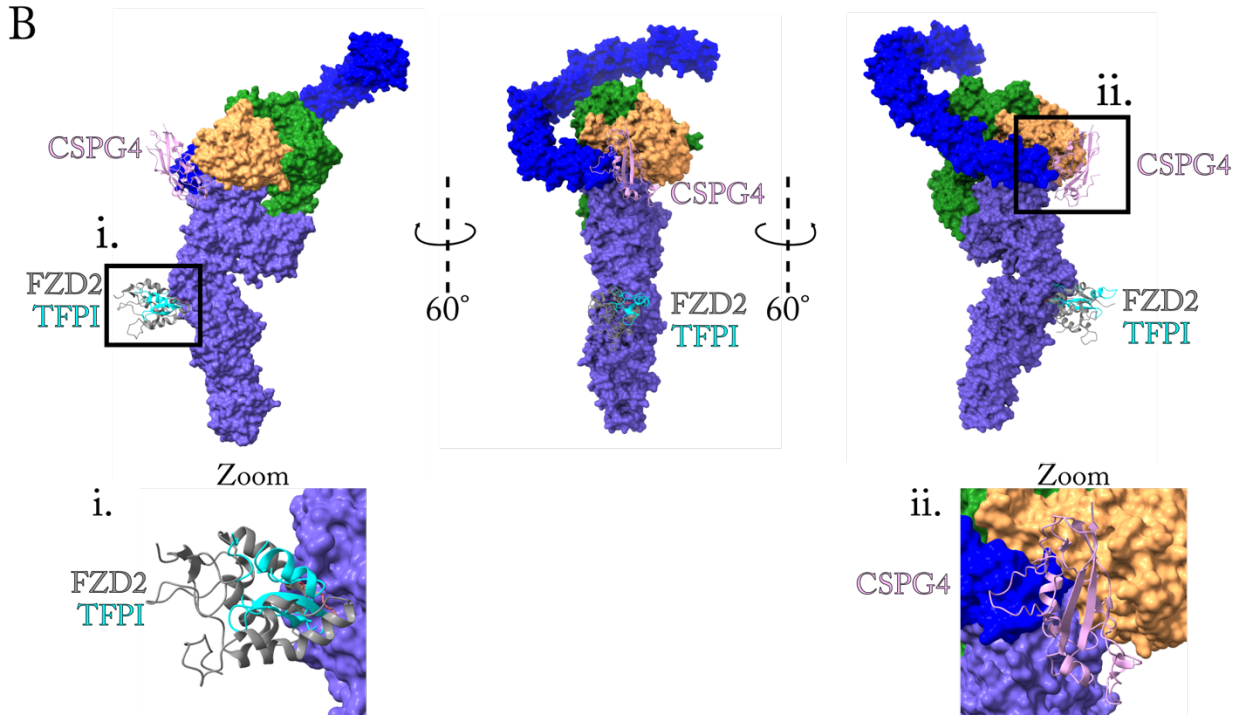
B
CSPG4
i.
FZD2
TFPI
60°
CSPG4
FZD2
TFPI
60°
ii.
CSPG4
FZD2
TFPI
Zoom
i.
FZD2
TFPI
Zoom
ii.
CSPG4

Figure 1-3. Intoxication mechanism of TcdB and receptor binding sites

A) The intoxication of cells with TcdB begins with receptor binding on the cell surface. Four classes of protein receptors have been identified for TcdB: Chondroitin sulfate proteoglycan 4 (CSPG4), Frizzled (FZD) 1, FZD2, FZD7, tissue factor pathway inhibitor (TFPI), and Nectin-3. (1) Engagement of the toxin with these receptors is predicted to result in (2) clathrin-mediated endocytosis. (3) During endosomal maturation, the pH of the endosome becomes acidic. This is predicted (4) to cause conformational changes of the delivery domain, leading to the pore-formation and translocation of the APD and GTD across the endosomal membrane and in into the cell cytosol. (5) Inositol hexakisphosphate ($InsP_6$), present with the cytosol of the cell, activates the APD, resulting in the autoprocessing and release of the GTD from the holotoxin. (6) The GTD localizes to the cell membrane and glucosylates Rho family GTPases, inhibiting their function. As a result, the GTPases are inactivated, leading to the disruption of the actin cytoskeleton, tight junction instability, cytokine production and cell death through apoptosis.

B) A structure of TcdB (PDB ID 60Q5, 3.87 Å crystal structure) resolution with receptors $CSPG4_{411-458}$ (PDB ID 7ML7, 3.17 Å cryo-EM structure), $FZD2_{35-155}$ (PDB 6C0B, 2.5 Å X-ray crystal structure), and $TFPI_{120-178}$ (PDB ID 7V1N, 3.20 Å cryo-EM structure) docked into their binding sites. TcdB and its domains are represented as a surface mesh and color coded as indicated in panel A. CSPG4 (pink), FZD2 (gray), and TFPI (cyan) are modeled as ribbons. The black boxes indicate the location of zoomed panels. **i)** A zoomed in view showing FZD2 and TFPI occupying the same binding site within the delivery domain. **ii)** A zoomed in view showing that CSPG4 interacts with the delivery domain, APD, CROPs domain.

thus commonly referred to as BI/NAP1/027 (170–172). The epidemic strains, hereafter referred to as RT027, were initially considered hypervirulent as epidemiological studies had suggested they were associated with higher mortality as well as being capable of producing all three toxins, TcdA, TcdB, and CDT (170, 171, 173). However, more recent studies have reported that the RT027 *C. difficile* is not any more virulent than other ribotypes of *C. difficile* (174). Nevertheless, soon after TcdB was shown to mediate disease in animal models of CDI, researchers began asking if mutations present in these TcdB variants could affect its virulence (165–167). Although only ~7.9% of residues in TcdB from RT027 *C. difficile* are changed compared to a historic pre-epidemic strain, TcdB from RT027 was reported to induce a faster cytopathic response on cells and induce stronger pro-inflammatory responses on tissue than the pre-epidemic reference TcdB (165–167, 175). These observations suggest that variations in TcdB can indeed impact its virulence.

While the epidemic of CDI was mediated by *C. difficile* RT027 strains in the 2000s, subsequent studies revealed that other strains of *C. difficile* could also mediate severe disease (114, 174). Furthermore, a more advanced classification approach known as multiple locus sequence typing (MLST) revealed the existence of five TcdB sequence type (ST) clades present in circulating clinical isolates (109, 176). Unfortunately, while sequence typing can be used to classify bacteria when utilized together with MLST, drawing conclusions of function using limited sequence resolution (sequence typing only utilizes a small portion of the gene) or lack of functional information (sequence typing for TcdB utilizes only a small portion of the CROPs domain) is a limitation of the approach (109). Although there was a short period of time where TcdB toxinotyping utilized sequence typing—the method revealed the existence of hundreds of TcdB variants in a total of 5 unique clades during its use—biochemical studies revealed that TcdB interactions with receptors could be CROPs-independent and thus, the method was unable to predict TcdB receptor interactions (107, 154, 156, 157, 162). More recently, toxinotyping of *C. difficile* toxins is based on phylogenetic analysis using the entire sequence of TcdB (107, 162). This approach has revealed the existence of 12 distinct clades of TcdB with varying cytotoxicity in animal models and cell lines (107, 162). TcdB sequences typed with this method are simply annotated as TcdB1-12. As to be discussed later, work performed by myself, colleagues, and other research groups have shown that these differences can be attributed to differences in receptor interaction profiles (163, 177–179). Finally, these phylogenetic analyses have also suggested that recombination and domain shuffling events gave rise to the multiple TcdB variants (107, 162). It has been speculated that these variants may have formed due to selective

pressures from *C. difficile* hosts that could differ in receptor expression (107, 162). As *C. difficile* can infect a variety of hosts, it is possible that TcdB evolved to interact with multiple receptors to ensure it is capable of mediating disease.

CSPG4 and its interactions with TcdB

CSPG4 (240–700 kDa) is a complex transmembrane proteoglycan (PG) with a variety of signaling functions due to its ability to interact with over 40 ligands (180). Alternative names for CSPG4 include neural-glial antigen 2 (NG2), melanoma cell surface proteoglycan (MCSP), and high molecular weight-melanoma associated antigen (HMW-MAA) (181–185). As the multiple names for CSPG4 suggest, the protein was originally identified by independent groups investigating neurons, glial cells, and melanomas (181–185). Since its discovery, the protein has been shown to facilitate multiple functions, including cell migration, proliferation, angiogenesis, neurogenesis, wound healing, and cancer metastasis (186–190). Due to the roles of CSPG4 in cell proliferation, angiogenesis, and cell motility, the protein is commonly found to be upregulated after neoplastic cell transformations, which results in aggressive tumor growth in a variety of cancers (189, 191, 192). Intriguingly, deletion of CSPG4 in mice is not embryonically lethal and mice can develop into adults without any obvious phenotypes (193). However, it has been reported that mice lacking CSPG4 have defective wound healing, a process that stimulates angiogenesis and neuronal outgrowth (186, 194–197). The protein is expressed throughout the human body by fibroblast cells, including telocytes and myofibroblasts in the large intestine, by pericytes along capillaries and by oligodendrocytes associated with neurons (187, 198–202). The protein is *not* expressed by epithelial cells of the intestines, which suggests that the protein is not directly involved in TcdB mediated injuries to epithelial cells during CDI (203).

CSPG4 is predicted to consist of three extracellular subdomains (D1-3), a single transmembrane domain, and a cytoplasmic tail (**Figure 1-4A**) (204–206). The N-terminal D1 subdomain (1-640 amino acids (aa)) contains two laminin G-type regions (LGR)—a structural motif that is predicted to facilitate heparin binding—and a single chondroitin sulfate proteoglycan (CSPG) repeat—a structural motif of chondroitin sulfate proteoglycans (**Figure 1-4B**) (207). In addition to heparin binding, the D1 subdomain has been reported to bind receptor tyrosine kinases (RTKs) such as platelet-derived growth factor receptors (PDGFRs) alpha and beta, fibroblast growth factor receptors (FGFR) 1 and 3, integrins, components of

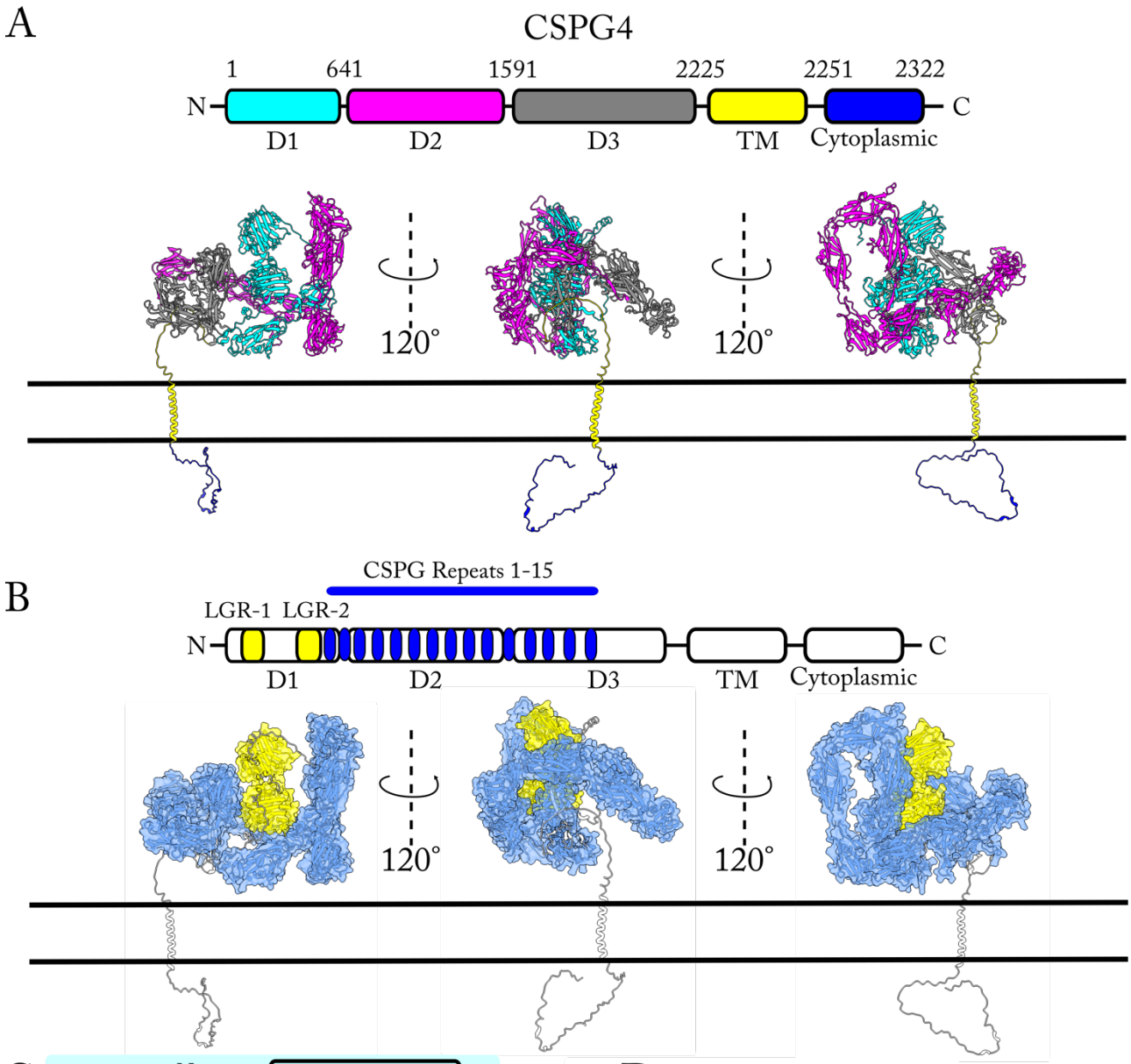
A
CSPG4
1
641
1591
2225
2251
2322
N
C
D1
D2
D3
TM
Cytoplasmic
120°
120°
B
CSPG Repeats 1-15
LGR-1 LGR-2
N
C
D1
D2
D3
TM
Cytoplasmic
120°
120°
C
N
D1
D2
D3
TM
Cytoplasmic
C
RTKs, growth factors, integrins, ECM, TcdB
Collagen Types V and VI, PDGF-AA, FGFs
Galectin-3, β1-integrin, P-selectin
PKCa
ERK1,2
D
Very high (pLDDT >90)
Confident (90 > pLDDT > 70)
Low (70 > pLDDT > 50)
Very low (pLDDT < 50)

Figure 1-4. Predicted structural organization of CSPG4 and ligand interactions.

A) The individual domains of CSPG4 with amino acid positions and the predicted AlphaFold model of CSPG4 (PDB ID AF-Q6UVK1-F1-model_v4) (205, 206). $CSPG4_{2183-2322}$ was rotated from its original orientation to generate the transmembrane and cytoplasmic domains. The color of each domain in the linear cartoon correponds to its color in the AlphaFold model.

B) A cartoon model of CSPG4 highlighting its two laminin G-type repeats (LGR) within the D1 subdomain in yellow and its 15 chondroitin sulfate proteoglycan (CSPG) repeats along D1, D2, and D3 subdomains in blue. The AlphaFold model of CSPG4 is colored to show the locations of each of these motifs.

C) A cartoon model of CSPG4 indicating its subdomains, structural motifs, and example ligands for each subdomain with matched colors from panels A and B. The red X's represent cleavage sites of that result in the release of CSPG4 from the plasma membrane. The cleavage site in D1 is within residues 490-500, while the two cleavage sites in D3 result in the release of the full ectodomain.

D) The AlphaFold CSPG4 model is color-coded by its per-residue confidence score (pLDDT), which scales between 0-100, where 100 is the highest confidence. This indicates a confidence level for the predicted model for CSPG4 is at a per residue level. The TcdB binding site is highlighted in pink and was generated by docking the 3.17 Å cryo-EM model of CSPG4 bound to TcdB (PDB: 7ML7) into the AlphaFold CSPG4 model.

the extracellular matrix (ECM), and TcdB (**Figure 1-4C & D**) (160, 186, 208–212). The D2 subdomain (641-1590 aa) consists of 11 CSPG repeats and three putative glycosylation sites for chains of chondroitin sulfates (CS) (30-60 kDa), a sulfated glycosaminoglycan (GAG) (**Figure 1-4A & B**) (204, 213, 214). Only a single residue, Ser-999 (Ser-995 in humans), has been experimentally demonstrated to be post-translationally modified, however (215). These chains of sulfated GAGs can be of variable length and appear to regulate the distribution of CSPG4 along the cell membrane (215, 216). For example, CSPG4 on the trailing edges of cells apparently lacks CS chains while CSPG4 along filopodia are enriched with CS chains (215, 216). The D2 subdomain interacts with type V and type VI collagens, platelet-derived growth factor (PDGF)-AA, and fibroblast growth factors (FGFs) (**Figure 1-4C**) (193, 208, 217–219). The D3 subdomain (1591-2225 aa) contains four CSPG repeats and can interact with β1-integrins, galectin-3 and potentially P-selectin (**Figure 1-4B & 4C**) (186, 188, 220). While the interactions between β1-integrins, galectin-3 and CSPG4 have been demonstrated biochemically, its interaction with P-selectin has not and is therefore speculated to be facilitated by indirect interactions (180, 186, 188). It is interesting to note that P-selectin can interact with carbohydrates such as CS, sialyl Lewis X, and sialyl Lewis A—both sialyl Lewis X and A antigens are carbohydrates that can interact with TcdA and TcdB at micromolar affinities (152, 188, 221). Finally, the cytoplasmic domain (2251-2322 aa) of CSPG4 contains a proline-rich region (PRR), a postsynaptic density-95, discs-large, zonula occludens 1 (ZO-1) (PDZ) protein domain, and two threonine phosphoacceptor sites for protein kinase C alpha (PKCα) and extracellular signal-regulated kinases (ERK) 1 and 2 (**Figure 1-4B & 4C**) (222–226). While there are no known roles for the PRR domain of CSPG4, PRR domains regulate protein interactions and trafficking in other proteins (223, 226). PDZ domains facilitate interactions with cytosolic scaffold proteins that orchestrate signaling events (222, 227). For CSPG4, the PDZ domain promotes interactions with scaffold proteins GRIP1 and MUPP1 (225).

Similar to integrins, CSPG4 is proposed to facilitate bi-direction inside-out and outside-in signaling (180, 228). Unlike integrins, however, CSPG4 achieves this without any intrinsic signaling activity of its own (229). Instead of signaling on its own, researchers have proposed that CSPG4 serves as an extracellular scaffold for proteins that signal (204, 230). CSPG4 is proposed act by capturing ligands within the ECM using its large and flexible extracellular domain (ECD) and presenting captured ligands to their cognate RTKs or integrins (204, 230). These interactions are predicted to form ternary complexes of CSPG4/ligand/receptors, resulting in sustained and enhanced integrin-regulated focal adhesion kinase

(FAK) signaling, RTK-regulated mitogen-activated protein kinase (MAPK) signaling, and downstream ERK1/2 signaling (186, 193, 208, 219). For RTKs such as PDGFRα, the formation of a ternary complex between these proteins and platelet derived growth factor (PDGF)-AA, a stimulatory ligand of PDGFRα, is likely essential for the function of the RTK (193, 209). In fact, without CSPG4, PDGF-AA is unable to stimulate PDGFRα auto-phosphorylation (193, 209). These and other similar interactions between CSPG4 and growth factors are predicted to be essential for mediating CSPG4-dependent MAPK and ERK1/2 signaling that stimulates proliferative responses within cells (224). Interactions between CSPG4, components of the ECM such as collagen types V and VI are reported to directly stimulate integrins to activate FAK signaling, resulting in cell migration mediated by cytoskeletal rearrangements, cell proliferation, and growth (186, 187, 231). The two cytoplasmic threonine phosphoacceptor sites in CSPG4 for PKCα and ERK1/2 likely influences integrin mediated signaling, as differential phosphorylation of these residues impact cell motility (224). With the various signaling pathways involved in cell migration, growth, and proliferation that CSPG4 can influence, these collective observations may explain why CSPG4 is commonly upregulated in various cancers (186, 189, 191, 192, 209, 224).

Although CSPG4 is expressed as a membrane bound protein, CSPG4 is commonly shed from the plasma membrane into its extracellular environment through the activities of various matrix metalloproteinases (MMPs), membrane-type(MT)-MMPs and a disintegrin and metalloprotease (ADAM)-10 (232–240). Shed forms of CSPG4 can range in sizes, consisting of potentially the entire CSPG4-ECD (240-290 kDa) to smaller forms that only include only the majority of the D1 domain (**Figure 1-4C**) (232–239). CSPG4 shedding has been observed in both diseased and healthy tissue, as well as in tissue culture, suggesting that CSPG4 shedding is a normal process (189, 203, 235, 239). While the role of shed CSPG4 is unknown, CSPG4 is actively shed during injuries to the brain and can be found in the blood of some cancer patients (240, 241). Moreover, shed CSPG4-ECD is capable of stimulating cell migration *via* integrin signaling by binding components of the ECM and integrin-β1 (186, 238). The variable lengths of shed CSPG4 may be dependent on the cell type. For example, while the larger molecular weight forms of shed CSPG4 have been observed in pericytes, a shorter form consisting of only the D1 subdomain have only been observed from macrophages and oligodendrocyte progenitor cells (189). Therefore, while the functional significance of shed CSPG4 remains unclear, these data suggests that the shedding process is regulated.

As a putative entry receptor for TcdB, knockout of CSPG4 on tissue culture cells confers greater protection than loss of Fzd1/2/7 (154, 158). While knockout of CSPG4 impacts cytopathic responses for the majority of TcdB variants, it does not affect cytopathic responses mediated by TcdB4, TcdB6, and TcdB12 (158). Interactions between TcdB and CSPG4 are high affinity (dissociation constant (K_D) ~15.2 nM) and are predicted to result in their endocytosis, although a recent report has suggested this does not occur (155, 159). CSPG4 is expressed by stromal cells that line the epithelium of the intestines and not believed to be expressed by any epithelial cell population (203). Nonetheless, CSPG4 knockout (-/-) mice have reduced pathologies when infected with *C. difficile* expressing TcdB, including reduced epithelial injury and reduced edema (160). In 2021, Rongsheng Jin and colleagues published a cryo-EM structure of $TcdB1_{1\text{-}1967}$ bound to $CSPG4_{30\text{-}764}$ (**Figure 1-3ii**) at 3.17 Å (160). The model revealed that CSPG repeat 1 of CSPG4 (**Figure 1-4D)** binds TcdB at an interface containing the APD, delivery domain, and CROPs domain (**Figure 1-5A**) (160). Across CSPG4, its interaction with TcdB occurs over three sites that encompass a surface area of ~2715 $Å^2$ (**Figure 1-5B**) (160). Site 1 encompasses residues 448-457 of CSPG4 that mediates interactions with residues within 564-621 of the APD using hydrogen bonds, electrostatic interactions, and hydrophobic interactions (**Figure 1-5C**) (160). Site 2 involves residues 466-503 of CSPG4 and CROPs residues 1816-1850 that interact using hydrogen bonds and hydrophobic interactions (**Figure 1-5D**) (160). Finally, site 3 contains residues 457-466 and 527 of CSPG4 and TcdB residues within the APD (573 & 575 aa) and the delivery domain (1754-1812 aa) and interact through electrostatic interactions, hydrogen bonding, and hydrophobic interactions (**Figure 1-5E**) (160). The region of the delivery domain and CROPs domain that CSPG4 interacts with is referred to as the hinge (1792-1834 aa) because it facilitates its flexible dynamics (**Figure 1-3B**) (148). As the residues within the hinge are only accessible to CSPG4 when the CROPs domain is flipped outwards as seen in the structure, it is interesting to speculate that the interactions between CSPG4 will have functional consequences for TcdB by locking the CROPs domain into a single conformation (148, 160).

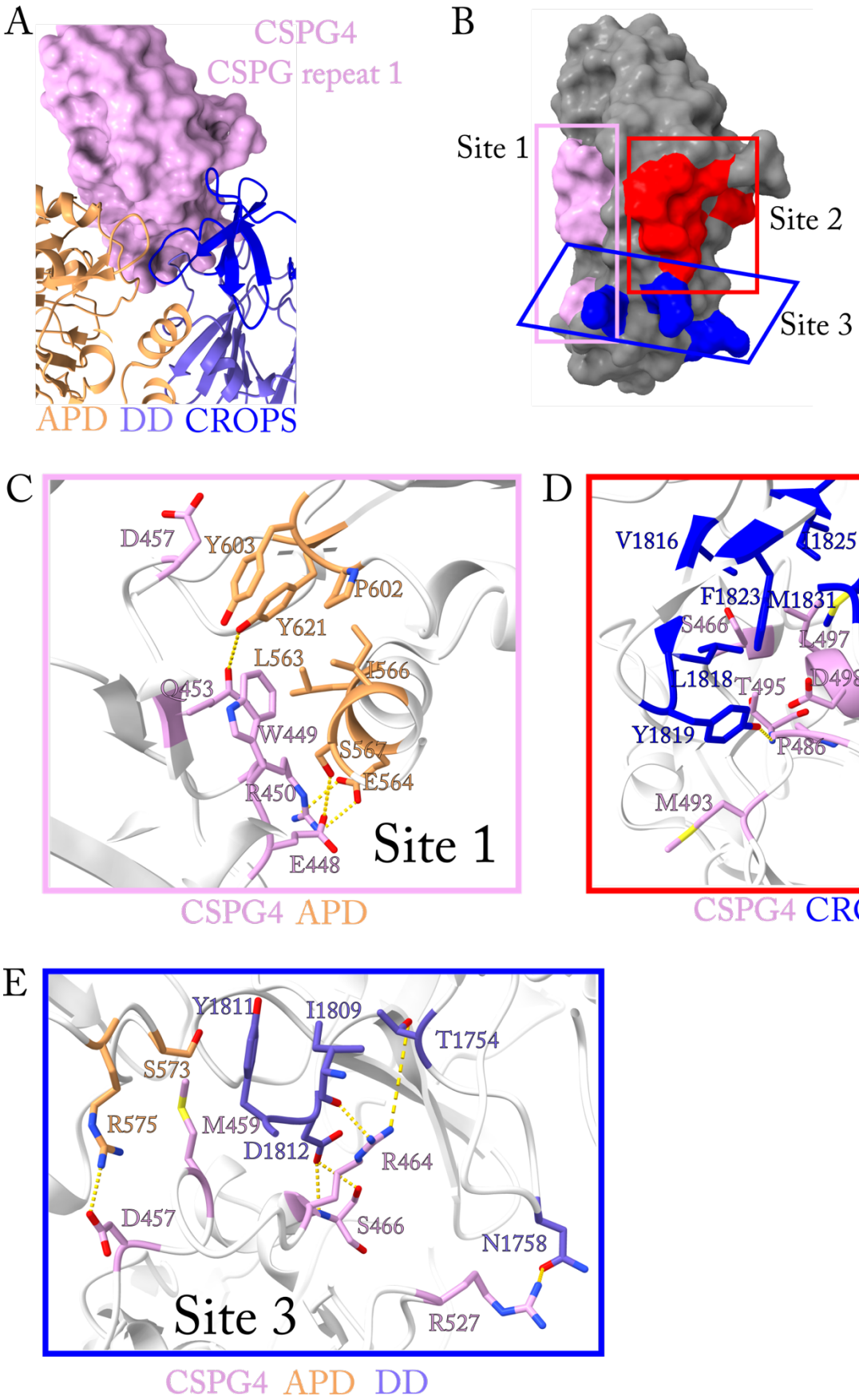
A
CSPG4
CSPG repeat 1
APD DD CROPS
B
Site 1
Site 2
Site 3
C
D457
Y603
P602
Y621
L563
I566
Q453
W449
S567
E564
R450
E448
Site 1
CSPG4 APD
D
V1816
I1825
N1850
F1823
M1831
S466
N501
L497
L1818
T495
D498
K503
Y1819
P486
M493
Site 2
CSPG4 CROPS
E
Y1811
I1809
T1754
S573
R575
M459
D1812
R464
D457
S466
N1758
R527
Site 3
CSPG4 APD DD

Figure 1-5. The structural interface of CSPG4 and TcdB

A) A zoomed in view of the cryo-EM structure TcdB1 and $CSPG4_{411-458}$ (PDB ID 7ML7, 3.17 Å cryo-EM structure, pink) revealing the association of CSPG4 with the APD (orange), the delivery domain (DD) (purple), and CROPs domain (blue). CSPG4 is shown as a surface mesh while the TcdB domains are shown as ribbons.

B) A surface model of $CSPG4_{411-458}$ with highlighted residues that mediate its interactions with TcdB. The matching surface colors and boxes indicate the location of each site used in panels C-E. Site 1 is pink, site 2 is red, and site 3 is blue.

C-E) Zoomed in view of sites 1-3 of the interface between TcdB and CSPG4. Electrostatic interactions and hydrogen bonding are shown as dashed lines. Amino acids implicated or experimentally tested to faciliate these interactions are shown as sticks models. CSPG4 (Pink), APD (orange), DD (purple), CROPs (blue).

FZD and its interactions with TcdB

The FZD proteins are a family of Wnt receptors conserved across the animal kingdom (242–244). They each share a conserved architecture consisting of an extracellular cysteine-rich domain (CRD), a seven-pass transmembrane domain, and a variable cytoplasmic region that contains a KTXXXW motif (243, 245–247). The CRD domain facilitates high affinity interactions with Wnt ligands and the receptor's signaling abilities are mediated by the KTXXXW motif, a PDZ domain (243, 245–251). Interaction between FZD receptors and Wnt ligands leads to the activation of canonical (β-catenin-dependent) or non-canonical (β-catenin-independent) Wnt pathways involved in cell polarity, cell motility, proliferation, as well as promoting stem cell function and maintenance, tissue differentiation, and the regulation of embryonic development (252–259). TcdB1 was shown to bind the conserved CRD domain of Fzd1/2/7. Since FZD1/2/7 have been shown to be expressed by epithelial cells of the colon, the FZD receptors are predicted to facilitate epithelial injuries mediated by TcdB (260–262). In support of this prediction, TcdB injected into the colon of FZD7$^{-/-}$ mice and TcdB FZD binding mutants injected into the colon are partially protected from pathology (154, 161). However, as full protection was not observed in either experiment, these data suggest that TcdB can mediate pathologies independently of FZD interactions.

The TcdB delivery domain interacts with the FZD1/2/7 CRDs with high affinity (**Figure 1-3i**) (K_D=~19-32 nM) (154, 161). The interaction reportedly inhibits canonical Wnt signaling and can potentially cause cell death in colonic stem cells *via* mechanisms independent of TcdB glucosyltransferase activities (154). The canonical Wnt signaling pathway promotes the stabilization and translocation of cytoplasmic β-catenin into the nucleus of cells, inducing the expression of Wnt target genes (**Figure 1-6A**) (263–265). Although β-catenin was originally discovered as an adherens junction protein, nuclear localized β-catenin can facilitate the removal of transcriptional repressors and acts as a transcriptional co-activator of Wnt target genes through associations with T cell factor (TCF)/lymphoid enhancer factor family (LEF) transcription factors (**Figure 1-6A**) (263, 264, 266, 267). In the absence of Wnt stimulation, newly expressed β-catenin will continually associate with the destruction complex, which consists of glycogen synthase kinase 3 (GSK3β), casein kinase 1α (CK1α), axin, and adenomatous polyposis coli (APC), resulting in its phosphorylation, ubiquitination, and subsequent proteasomal degradation (**Figure 1-6A**) (265, 268–271). During canonical Wnt signaling, a single Wnt ligand binds the FZD-CRD and the Wnt

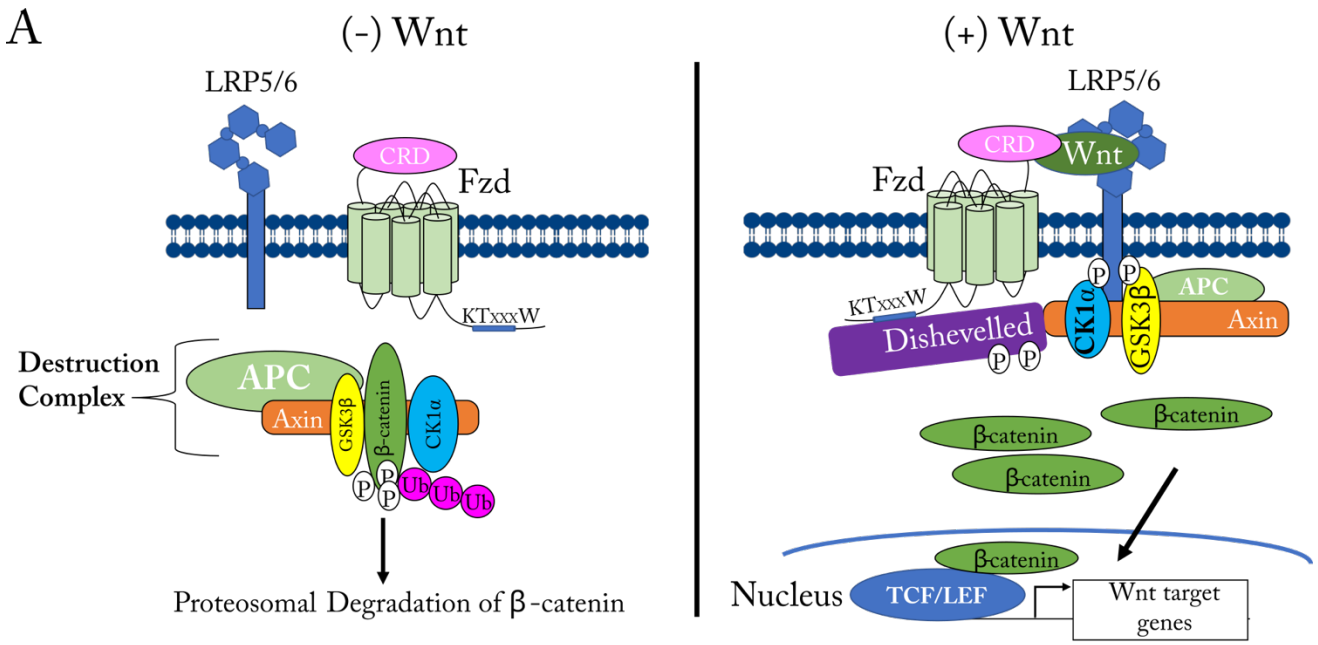
A
(-) Wnt
(+) Wnt
LRP5/6
CRD
Fzd
KTxxxW
Destruction Complex
APC
Axin
GSK3β
β-catenin
CK1α
P
Ub
Proteosomal Degradation of β-catenin
Wnt
Dishevelled
β-catenin
Nucleus
TCF/LEF
Wnt target genes

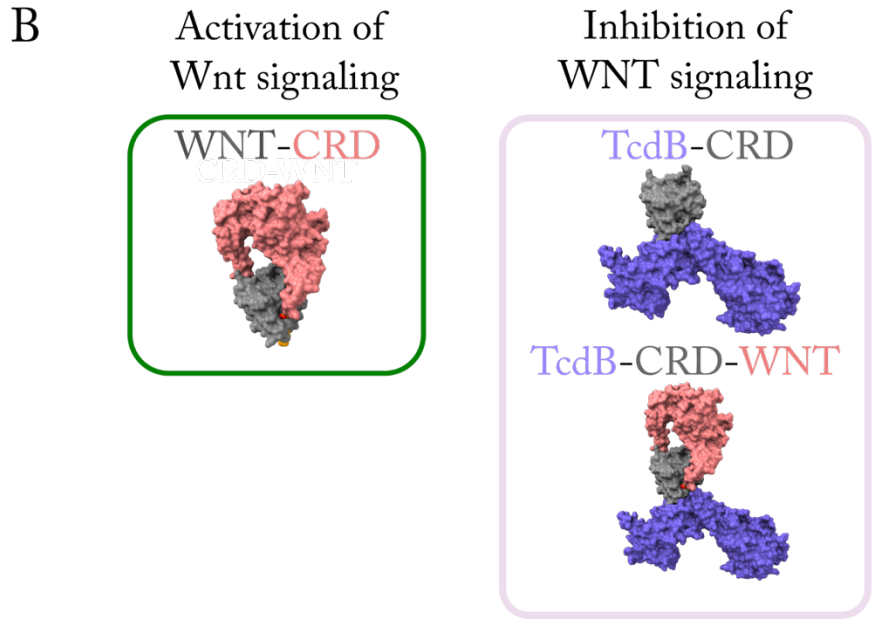
B
Activation of Wnt signaling
Inhibition of WNT signaling
WNT-CRD
TcdB-CRD
TcdB-CRD-WNT

Figure 1-6. Canonical Wnt Signaling is inhibited by TcdB.

A) A cartoon of the canonical Wnt signaling pathway in its inactive (- Wnt) and active (+ Wnt) states. In the absence of signaling, β-catenin associates with the destruction complex, which consists of glycogen synthase kinase 3 (GSK3β), casein kinase 1α (CK1α), axin, and adenomatous polyposis coli (APC). β-catenin associated with the destruction complex are phosphorylated (represented as P) and ubiquitinated (represented is Ub) and will be degraded by the proteosome. Canonical Wnt signaling is facilitated by Wnt binding to the CRD of FZD and lipoprotein receptor-related protein (LRP)-5 LRP6. This interaction promotes the recruitment of Dishevelled to the conserved KTxxxW motif within the PDZ domain of FZD, promoting the phosphorylation of LRP5/6 and the inhibition of the destruction complex. As a result, β-catenin accumulates within the cytosol and is translocated into the nucleus where it promotes Wnt target gene expression by associating with the T cell factor/lymphoid enhancer factor family (TCF)/(LEF) transcription factors.

B) A crystal structure of Wnt-$8_{1\text{-}150}$ (PDB ID 4F0A, 3.25 Å X-ray crystal structure) was docked into the Wnt binding pocket of the CRD of $FZD2_{35\text{-}155}$ (PDB ID 6C0B, 2.5 Å X-ray crystal structure, co-crystal structure of FZD2 and TcdB) to provide an example of how the interactions between the FZD2 and Wnt ligands occur (272). TcdB (PDB ID 4F0A) interactions with the FZD CRD are predicted to inhibit Wnt signaling by either preventing Wnt from binding simply associating with the CRD or by blocking Fzd2-CRD interactions with co-Wnt receptors LRP5/6. The colors of each protein corresponds with the color of the text.

co-receptor low-density lipoprotein receptor-related protein (LRP)-5 or LRP-6 (**Figure 1-6A**) (273–278). The formation of this ternary complex promotes the recruitment of Dishevelled (DVL) to the PDZ domain of FZD, leading to the phosphorylation of LRP5/6 and the recruitment and inhibition of the destruction complex to DVL and LRP5/6 **(Figure 1-6A**) (247, 279–281). Due to the inhibition of the destruction complex, β-catenin will begin to accumulate in the cytosol and will translocate into the nucleus to drive Wnt target gene expression as aforementioned (**Figure 1-6A**) (263–265). TcdB is predicted to disrupt canonical Wnt signaling by preventing Wnt ligands from binding the FZD CRD or by preventing interactions with the co-receptor LRP5/6, however the exact mechanism remains unclear **(Figure 1-6B**) (154, 161, 282). Finally, while TcdB utilizes clathrin-mediated endocytosis to intoxicate cells, there are reports that have shown that FZDs undergo caveolae-mediated endocytosis to mediate canonical Wnt signaling and clathrin-mediated endocytosis for non-canonical Wnt signaling (283–286). As endocytosis of FZD proteins are regulated by their signaling, it is difficult to predict how TcdB interactions with FZDs would stimulate endocytosis.

Nectin-3 and its role in TcdB mediated cytotoxicity

Nectin-3 is a member of the Nectin family (Nectin-1, -2, -3, -4) of adhesion proteins that regulate the formation of cell-to-cell junctions (287). As a component of adherens junctions, Nectins initiate the initial contacts between cells by forming homophilic (weak) and heterophilic (strong) interactions with other Nectin family members (**Figure 1-7A**) (288). The adhesive properties of Nectin-3 are mediated by its three ECDs that each contain immunoglobulin (Ig)-like folds (289) (**Figure 1-7B**). For Nectin-3, the D1 subdomain facilitates homo- and heterophilic interactions with other Nectin molecules *via* its Ig-like folds (**Figure 1-7B**) (289). A non-Nectin protein that can interact with the extracellular domain of Nectin-3 is PDGFRα (290). This interaction can reportedly suppress apoptosis by stabilizing PDGFRα localization to the adherens junction, which results in sustained and robust PDGFRα signaling (290). Nectin-3 is anchored to the plasma membrane through a cytosolic tail that contains an afadin binding motif—a conserved motif in Nectins that allow them to interact with the actin filament (F-actin) binding protein afadin (291, 292). Afadin is an adapter protein for Nectin molecules that allows Nectins to interact with the actin cytoskeleton (291, 292). The cytosolic tail of Nectin-3 can also interact with partitioning defective-3 (PAR-3), a protein that localizes to the tight junctions of cells to regulate cell polarity (293, 294). Genetic deletion of Nectin-3 in mice results in the defective development of the auditory, visual,

A

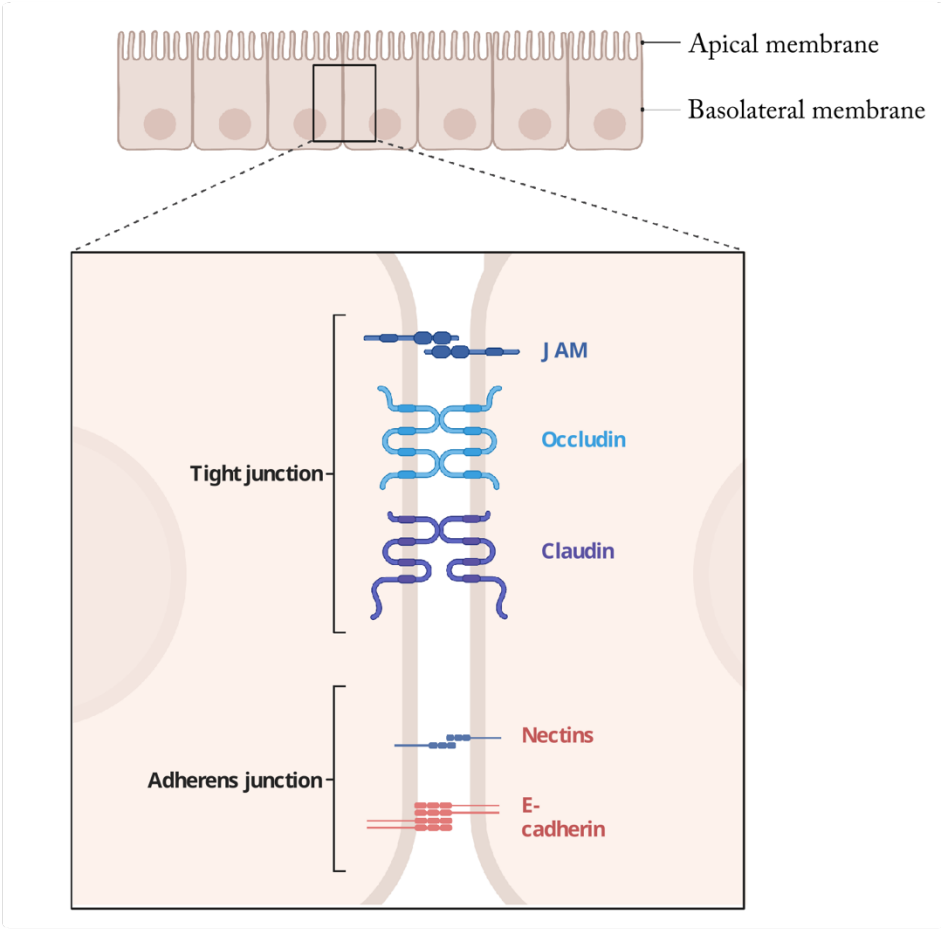
Apical membrane
Basolateral membrane
JAM
Occludin
Tight junction
Claudin
Nectins
Adherens junction
E-
cadherin

B

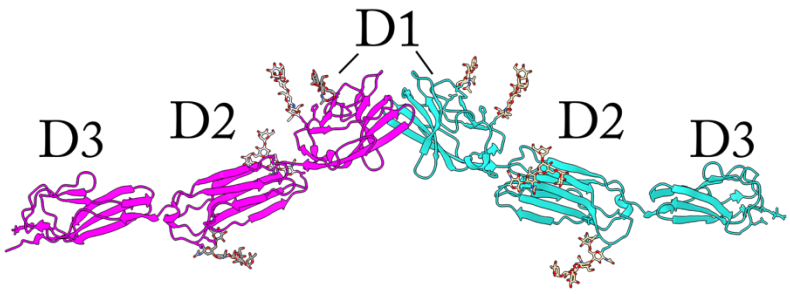
D1
D3
D2
D2
D3

Figure 1-7. Nectin-3 mediates the formation of adherens junctions.

A) A cartoon model of the tight junction and adherens junction. The tight junction is located at the apical membrane and is formed by the junctional proteins JAMs, occludins, and claudins, and ZO-1 (not pictured). The adherens junctions are located below the tight junctions and are formed by Nectins and E-cadherin. The cartoon was made in Biorender.

B) A homophilic dimer of Nectin-3 (PDB ID 4FOM, 3.98 Å resolution, X-ray crystallography) showing the dimerization interface is mediated by the D1 subdomain. Carbohydrates representative of post-translational modifications are shown as sticks. The subdomains are labeled above each Ig-like fold.

and reproductive systems but is not embryonic lethal (295–298). Within the intestines of mice, deletion of Nectin-3 does not cause any apparent defects in its development, structure, or function (299). Nonetheless, Nectin-3 is expressed by epithelial cells of the colon which suggests that Nectin-3 interactions with TcdB may facilitate direct injuries to the colonic mucosa (299).

TcdB has been shown to bind Nectin 3 with high affinity (K_D = 17-53 nM). Knockout of Nectin-3 results in the reduction of TcdB-mediated cytotoxicity but does not affect the cytopathic response (156). The cytotoxic response of TcdB is a necrotic cell death response that is independent of the GTD and APD activities of TcdB but dependent on delivery domain-mediated pore-formation. It results from the over-production of reactive oxygen species from a nicotinamide adenine dinucleotide phosphate (NADPH) oxidase (NOX) complex and is specific to TcdB concentrations greater than or equal to 100 pM (145, 300–302) (Figure 1-8). While cytopathic responses mediated by TcdB will eventually result in apoptosis over a 24-48-hour period, necrotic cell death is a rapid cell death response that can occur within a few hours after exposure to TcdB (300–302). This response has been observed in a variety of conditions, including on human and porcine colonic explants (301, 302). Out of the four classes of TcdB receptors, only Nectin-3 and CSPG4 have been tested and shown to contribute to TcdB-dependent cytotoxic responses on tissue culture cells (155, 156). The role of FZD proteins and TFPI in mediating cytotoxicity are unknown.

Research Objectives

When I joined the Lacy Lab, I was interested in understanding and discovering cellular factors involved in mediating TcdB cytotoxicity and cytopathic responses. Mitch LaFrance, a former graduate student in the Lacy Lab, had identified Nectin-3 as a receptor involved in mediating TcdB cytotoxicity on epithelial cells (156). The only additional receptor for TcdB at the time that was known to mediated cytotoxicity was CSPG4, but its relevance was unclear as the protein was not expected to be expressed by colonic epithelial cells (155, 156, 203). Our model for how TcdB engaged receptors to cause disease was simple: Nectin-3 would mediate epithelial injury and CSPG4 would mediate injuries within the submucosa. Soon after joining the lab, however, another class of receptors was identified for TcdB, the FZD1/2/7 proteins (154). Importantly, knockout of FZD1/2/7 was shown to impact the cytopathic response. As knockout of Nectin-3 impacted the cytotoxic response, one model that we had considered to incorporate this discovery was that TcdB utilizes separate cytotoxic receptors and cytopathic receptors to injure the host. While this

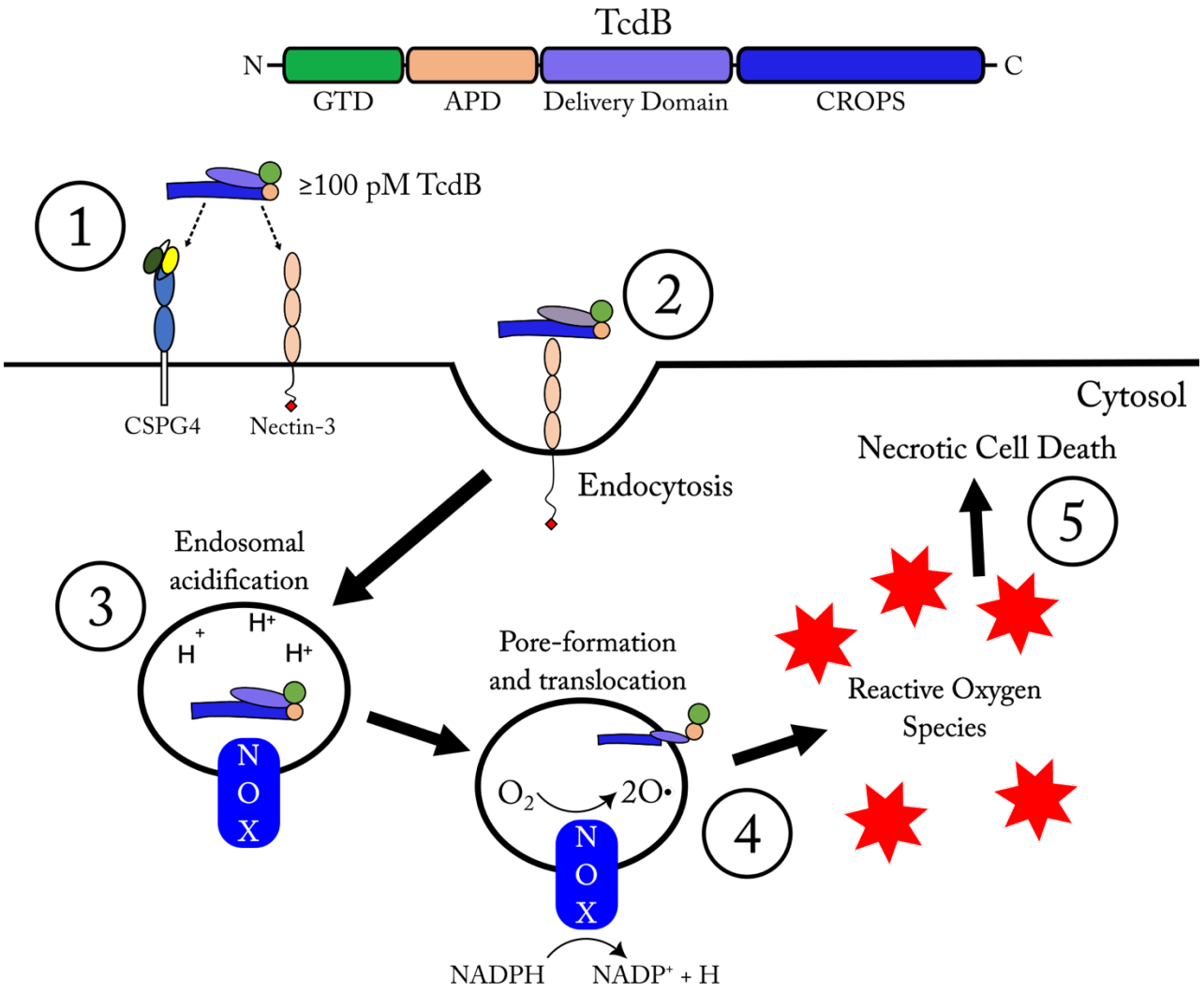

Figure 1-8. TcdB cytotoxicity is mediated by necrotic cell death

TcdB can induce necrotic cell death at concentrations greater than or equal to 100 pM. (1) CSPG4 and Nectin-3 are the two TcdB receptors that have shown to impact TcdB cytotoxicity. Upon binding these receptors, the TcdB is (2) endocytosed through clathrin-mediated endocytosis. (3) Through an unknown mechanism, the nicotinamide adenine dinucleotide phosphate (NADPH) oxidase (NOX) complex, which is made of multiple proteins, is assembled (for simplification, the NOX complex is shown to be within the TcdB endosome, however, this may occur elsewhere). The NOX complex oxidizes NADPH into $NADP^+$ to generate superoxide anion radicals. (4) Pore-formation mediated by the delivery domain of TcdB activates the NOX complex which results in the overproduction of reactive oxygen species that is toxic to the cell and ultimately ends in (5) necrotic cell death.

potential mechanism could still apply, our many attempts to identify TcdB residues involved in Nectin-3 interactions were unsuccessful. However, one day, I decided to compare TcdB sequence variants to facilitate the discovery of potential residues involved in receptor interactions. While this did not yield anything interesting for putative Nectin-3 interactions, I noticed that many residues within the FZD1/2/7-CRD binding domain of TcdB1 were mutated in TcdB2. In Chapter II, I will discuss the importance of these mutations for Fzd interactions, showing that TcdB2 (referred to as $TcdB^{RT027}$ at the time) is unable to inhibit canonical Wnt signaling and that the activities of TcdB2 are identical to that of TcdB1 (referred to as $TcdB^{VPI}$) on host tissue. In Chapter III, I propose novel roles of CSPG4 and Nectin-3 on epithelial cells of the intestines. I show that CSPG4 shed by fibroblasts can potentiate the activity of TcdB on colonic epithelial cells and provide supporting evidence that this process occurs *in vivo* in both humans and mice. I also show that Nectin-3 associates with microvilli on epithelial cells in addition to the cell junctions. By serendipitously discovering a cell line capable of visualizing TcdB, a historically challenging issue, I was also able to determine that both CSPG4 and Nectin-3 interact with TcdB on cells. Mechanistically, I propose that Nectin-3 interactions with TcdB on microvilli and shed CSPG4-ECD interactions with TcdB along cell junctions will facilitate the intoxication of the colonic epithelium. In Chapter IV, I will discuss some final remarks, conclusions, and future directions.

Chapter 2

TcdB From RT027 *Clostridioides difficile* Does Not Use Frizzleds as Receptors

Adapted with permission: Mileto S.J., Jardé T.*, Childress K.O.*, Jensen J.L., Rogers A.P., Kerr G., Hutton M.L., Sheedlo M.J., Bloch S.C., Shupe J.A., Horvay K., Flores T., Engel R., Wilkins S., McMurrick P.J., Lacy D.B., Abud H.E., Lyras D. (2020) Clostridioides difficile infection damages colonic stem cells via TcdB, impairing epithelial repair and recovery from disease. Proceedings of the National Academy of Sciences. DOI: 10.1073/pnas.1915255117* *Co-first authors

Introduction

Gastrointestinal infections often induce epithelial damage that must be repaired for optimal gut function. While intestinal stem cells are critical for this regeneration process, how they are impacted by enteric infections remains poorly defined (303, 304). This chapter is a modification of publication from a collaboration between the Lacy, Lyras, and Abud laboratories published in 2020 in PNAS. The overall goal of this collaboration was to investigate infection-mediated damage to the colonic stem cell compartment and how this affects epithelial repair and recovery from infection. I was particularly interested in the role of FZD receptor interactions with TcdB during CDI. Using the pathogen *Clostridioides difficile,* we show that infection disrupts murine intestinal cellular organization and integrity deep into the epithelium, to expose the otherwise protected stem cell compartment, in a TcdB-mediated process. Exposure and susceptibility of colonic stem cells to intoxication compromises their function during infection, which diminishes their ability to repair the injured epithelium, shown by altered stem cell signaling and a reduction in the growth of colonic organoids from stem cells isolated from infected mice. With the aid of the Lyras and Abud labs, we show using both mouse and human colonic organoids that TcdB from epidemic ribotype 027 strains does not require Frizzled 1/2/7 binding to elicit this dysfunctional stem cell state. Furthermore, I show that Frizzled interactions with TcdB are not required for cytotoxic responses on cells and pathologies in hosts.

Results

Disease outcome during CDI is dictated by toxin titer and depth of colonic epithelium damage

The changing epidemiology of CDI and diversity of strains, coupled with the heightened disease severity associated with ribotype (RT) 027, 017, 126 and 244 *C. difficile* strains, among others, has resulted in more CDI cases involving life-threatening complications and prolonged disease (305–310). Differences in disease severity are seemingly associated with *C. difficile* strains from different clades, however, how genetically diverse *C. difficile* strains affect the host, and particularly the stem cell compartment, during infection is poorly characterized (311, 312). Here, using a mouse model of CDI, we show that three genetically and geographically distinct RT027 strains (M7404, R20291 and DLL3109) and the RT003 strain VPI10463 are capable of inducing severe and devastating colonic damage that penetrates deep into the epithelium, characterized by damage to the base of the colonic crypts, severe inflammation and edema (**Figure 2-1a**). Interestingly, infection with the prototypical *C. difficile* strain 630 (the PaLoc of which has 99% sequence identity to VPI10463 PaLoc) and strain AI35, a naturally occurring $TcdA^{-}TcdB^{+}CDT^{+}$ strain which encodes a variant TcdB, as well as strain JGS6133, a RT078 animal isolate, were unable to induce damage beyond the surface of the colonic epithelium (**Figure 2-1a).** Strains capable of producing increased amounts of toxin during infection were able to induce damage deep into the epithelium. We suggest that higher toxin production during infection damages the epithelium at a rate higher than normal cellular turnover or repair, leading to progressive damage through the mucosa, which can then reach the crypt base. Thus, it appears that the capacity for a strain to induce a collapse in intestinal integrity and expose cells deep within the colonic epithelium is critical to poor disease outcome in CDI.

TcdB mediates severe intestinal damage, disrupting intestinal integrity and exposing stem cells deep within the colonic crypt to intoxication

To gain a better understanding of the deep epithelial damage seen during CDI, we next focused on examining the disruption to tissue integrity over time during CDI. Junctional complexes, including tight-junctions, adherens-junctions, desmosomes and gap-junctions, play an important role in maintaining epithelial integrity, and control the movement of molecules or microorganisms through the epithelial layer (313, 314). Several pathogens, including *Clostridium perfringens* and *Helicobacter pylori*, target intercellular junctions to penetrate deeper into the epithelium and exacerbate disease (314). Previous in vitro work has shown that TcdA and TcdB alter tight-junction permeability, however, toxin-mediated effects on

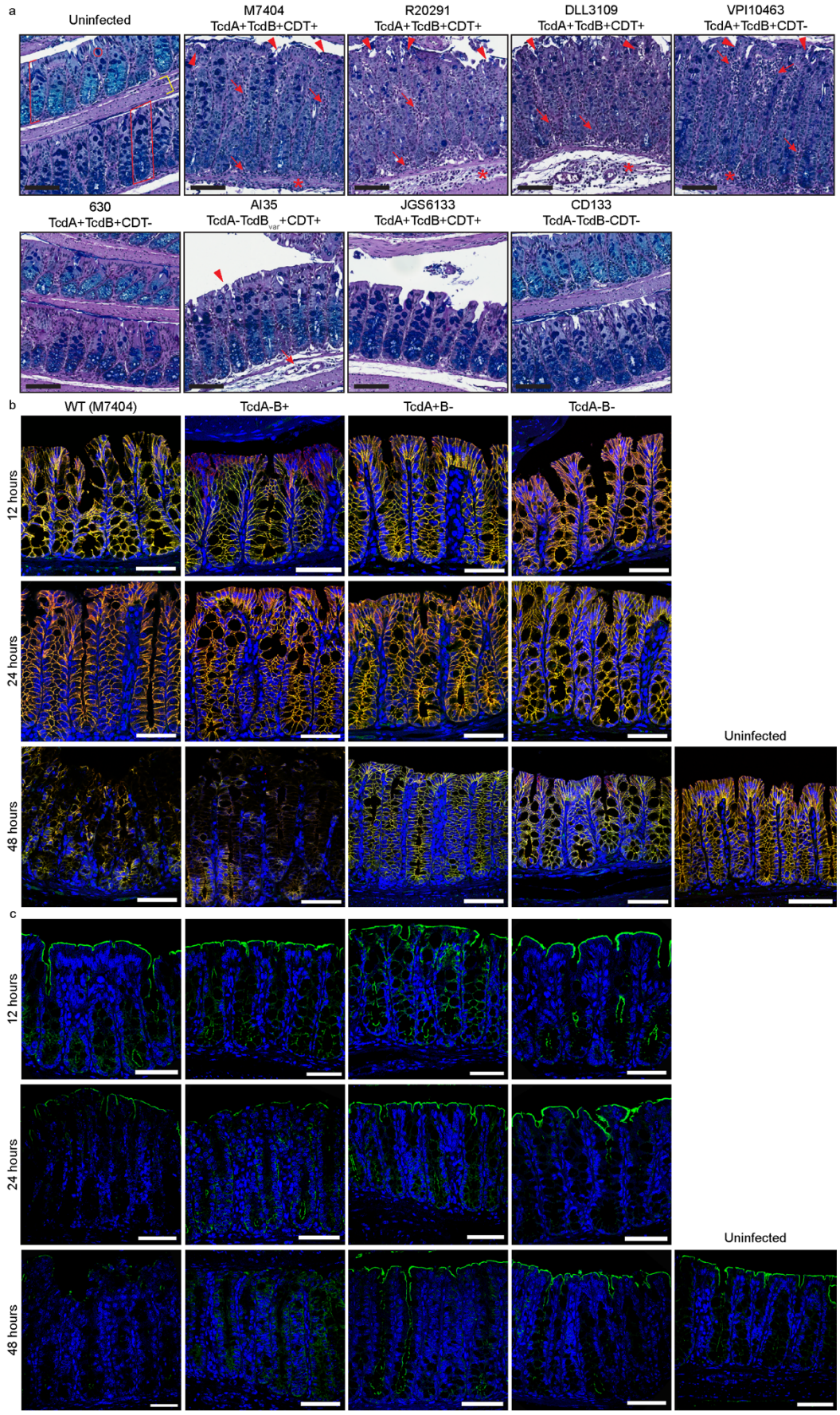
a
Uninfected
M7404
TcdA+TcdB+CDT+
R20291
TcdA+TcdB+CDT+
DLL3109
TcdA+TcdB+CDT+
VPI10463
TcdA+TcdB+CDT-
630
TcdA+TcdB+CDT-
AI35
TcdA-TcdB$_{var}$+CDT+
JGS6133
TcdA+TcdB+CDT+
CD133
TcdA-TcdB-CDT-
b
WT (M7404)
TcdA-B+
TcdA+B-
TcdA-B-
12 hours
24 hours
48 hours
Uninfected
c
12 hours
24 hours
48 hours
Uninfected

Figure 2-1. *C. difficile* induces severe and deep epithelial damage through TcdB alterations in adherens-junction formation and cellular polarity.

a) Mice were infected with a panel of genetically distinct C. difficile isolates and monitored for disease severity and colonic damage through PAS/Alcian blue staining. Representative images of swiss-rolled colonic tissue are shown. The colonic mucosa (red bracket), and more specifically the crypts of Lieberkühn (red box), comprised of colonic epithelial cells and goblet cells (red circle), sit above the submucosa and muscle layers (yellow bracket) of the colon. Arrow=inflammation; Arrowhead=crypt damage/goblet cell loss; Asterisk=edema. n≥5; Scale Bar = 100μm (black). b-c) Colonic tissues were collected at 12, 24 and 48-hours post-infection with M7404 (WT), and the isogenic toxin mutants of this strain; TcdA-B+, TcdA+B-, and TcdA-B- C. difficile or from uninfected mice (48 hours). A representative image of tissues stained for b) β-catenin (Green) and E-cadherin (Red) (Merge=Yellow) or c) Ezrin (Green) is shown, with nuclei stained with DAPI (Blue). n≥5; Scale Bar = 50μm (white).

β-catenin/E-cadherin adherens-junctions have not been reported (89, 315, 316). Cellular polarity is also essential for intestinal integrity. Ezrin, an ERM protein, assists in linking trans-membrane proteins with the actin cytoskeleton and coordinating apical/basolateral receptor localization, among other functions in cytoskeletal stabilization and regulation (317). Ezrin also interacts with Rho-GTPases, which aid in actin cytoskeleton maintenance, and importantly, are the primary targets of TcdA/TcdB (318, 319). Thus, to analyze changes in intestinal integrity during CDI in more detail, mice were infected with either M7404 (WT; RT027), which produces TcdA, TcdB and CDT, or an isogenic mutant strain lacking either TcdA (DLL3045, hereafter $TcdA^{-}B^{+}$), TcdB (DLL3101, hereafter $TcdA^{+}B^{-}$), or TcdA and TcdB (DLL3121, hereafter $TcdA^{-}B^{-}$) and euthanized at either 12, 24 or 48-hours post-infection, to track the progression of intestinal integrity collapse (106). At 12-hours post-infection, β-catenin/E-cadherin interactions and ezrin localization appeared intact and similar to those in uninfected tissues, regardless of the infecting strain (**Figure 2-1b, c**). At 24-hours, β-catenin/E-cadherin immunostaining remained unchanged (**Figure 2-1b**), however, the apical distribution of ezrin in the colon was altered in mice infected with TcdB-producing strains (**Figure 2-1c**). This loss of cellular polarity staining seemingly initiates the collapse in intestinal integrity that begins to expose the deeper regions of the colonic epithelium, since by the 48-hour time point, mice infected with WT or $TcdA^{-}B^{+}$ strains displayed dramatic TcdB-mediated changes to both the adherens-junctions and cellular polarity (**Figure 2-1b, c**). Specifically, β-catenin/E-cadherin staining was severely disrupted, and ezrin was undetectable in tissues from mice infected with TcdB-producing strains suggesting a collapse in adherens-junctions and cellular polarity of differentiated cells within the colonic epithelium, that would otherwise function to protect the stem cell compartment at the base of the crypt from intoxication (**Figure 2-1b, c**). By contrast, β-catenin/E-cadherin and ezrin localization were indistinguishable between uninfected mice and those infected with $TcdA^{+}B^{-}$ or $TcdA^{-}B^{-}$ strains (**Figure 2-1b, c**), suggesting that TcdA and CDT do not play a role in altering the integrity of the intestinal barrier during CDI.

RT027 TcdB induces stem cell damage in a Frizzled independent manner

Since a number of TcdB receptors have previously been identified, we next examined their possible contributions to the disease phenotypes observed within the context of the infected gut. Recent work using purified TcdB together with cell lines and mice has identified FZD1/2/7 as potential TcdB receptors, however the contribution of these interactions to stem cell damage during CDI has not been reported

(154). Under normal conditions, expression of FZD1/2 in the colon is very low or undetectable, with increased expression seen in colonic cancers (320, 321). Importantly, as FZD7 is known to function as a WNT receptor in small-intestinal stem cells, it may function as a TcdB receptor in the colon (262, 322). As such, we wanted to confirm that FZD7 was expressed within the stem cell compartment of the colon. Using qPCR, we confirmed the expression of *Fzd7* in colonic stem cells and immediate daughter cells from LGR5-GFP mice where stem and progenitor cells can be isolated by levels of GFP expression, and showed that *Fzd7* is highly expressed in LGR5^{+} stem cells and decreased in expression in progeny cells, at a similar level to *Lgr5* (Figure 2-2) (259). We also analyzed *Lrp1* and *Pvrl3* (NECTIN-3 hereafter) expression in colonic stem cells and daughter cells from LGR5-GFP mice, both of which are putative TcdB receptors, with expression levels similar to *Lgr5* seen for each receptor, across all cell types (Figure 2-2) (156, 159). Several attempts were also made to detect *Cspg4* expression in both mouse colonic and small intestinal tissues, however, all were unsuccessful, suggesting that CSPG4 (another reported TcdB receptor) is unlikely to act as a TcdB receptor on mouse intestinal epithelial and stem cells since it is not expressed in these tissues (Figure 2-2) (155). Given the loss of stem cell function and reduced capacity to regenerate the colonic epithelium following RT027 TcdB-mediated intestinal assault, I further characterized the underlying mechanism of stem cell damage during CDI, and compared this to VPI10463 TcdB, which was also capable of inducing severe damage deep into the colonic mucosa in our *in vivo* modelling. As FZD7 is a well characterized WNT receptor, I expected that RT027 TcdB binding to FZD proteins on colonic stem cells would be responsible for the observed stem cell dysfunction *in vivo* (262). Strikingly, examination of the key residues for TcdB- FZD2 interaction identified in a crystal structure of the VPI10463 TcdB delivery domain bound to the FZD2-cysteine-rich domain (CRD) revealed that many of the TcdB contact residues are not conserved in the RT027 TcdB sequence from *C. difficile* M7404 (**Figure 2-3a i**), confirming recent observations regarding TcdB sequence variations in binding regions (161, 178). A phylogenic analysis of TcdB from annotated RT027 strains deposited onto the NCBI database revealed a complete clonal conservation of TcdB within RT027 strains, suggesting that these differences exist for all RT027 strains (**Figure 2-4a**).

As these sequence differences may affect the binding affinity of TcdB for FZD, or any of the other reported receptors, Dr. Sheedlo, Dr. Jensen, and I purified TcdB toxins from VPI10463 (TcdB10463) (RT003; previously used to identify and characterize the CSPG4, FZD1/2/7, and NECTIN-3 receptors) and M7404 (TcdB027) and used microscale thermophoresis (MST) to determine the binding affinity of

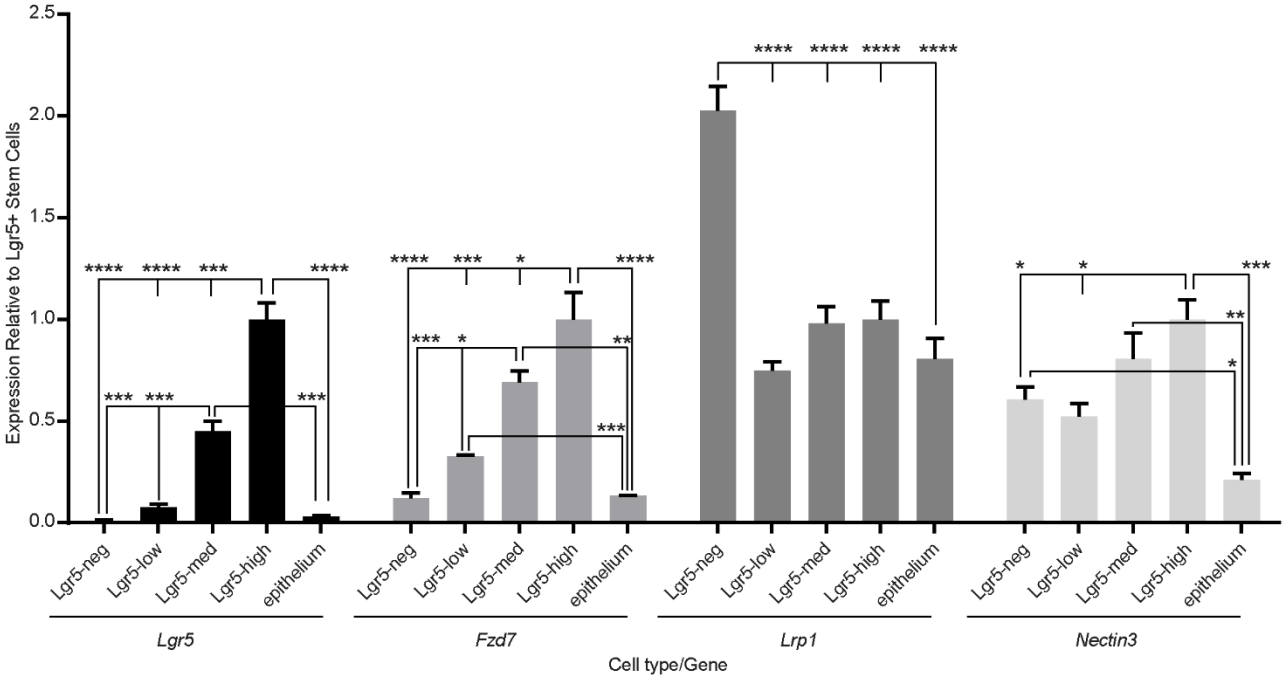

Figure 2-2. Colonic stem cells and their daughter cells express TcdB receptors

Colonic cells from adult LGR5-eGFP-IRES-CreERT2 mice were isolated, stained and sorted prior to RNA isolation and cDNA synthesis. qPCR was then used to quantify the expression levels of *Lgr5, Fzd7, Lrp1* and *Nectin3* in differentiated cells (LGR5-neg), progenitor cells (LGR5-low and LGR5 medium (med)), colonic stem cells (LGR5-high) and total epithelial cells. n=3. Data are represented as mean + S.E.M * $p \leq 0.05$, ** $p \leq 0.01$, *** $p \leq 0.001$, **** $p \leq 0.0001$. See also, **Figure 2-3**.

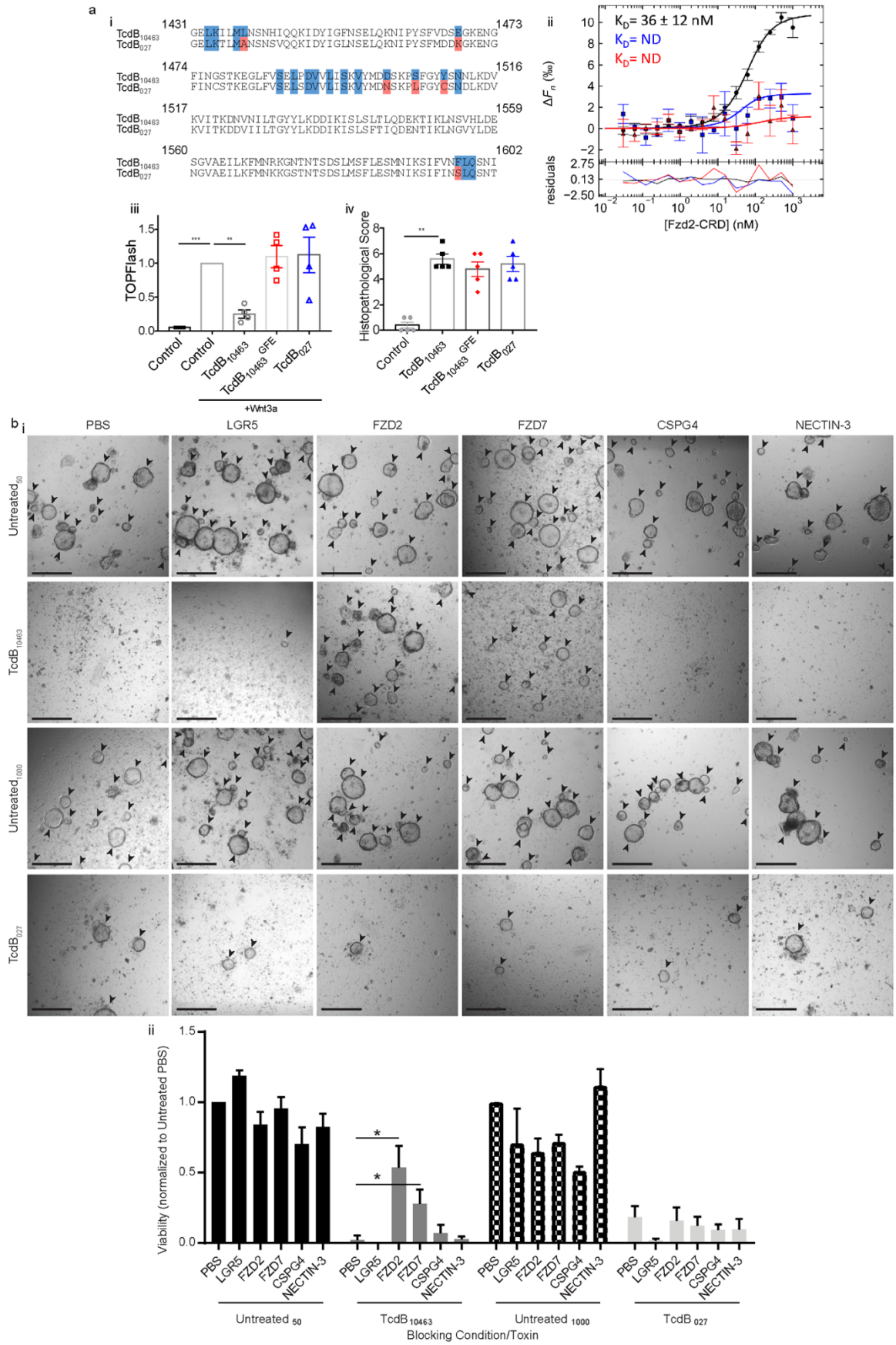
a
i
1431
1473
TcdB10463 GELKILMLNSNHIQQKIDYIGFNSELQKNIPYSFVDSEGKENG
TcdB027 GELKTLMANSNSVQQKIDYIGLNSELQKNIPYSFMDDKGKENG
1474
1516
TcdB10463 FINGSTKEGLFVSELPDVVLISKVYMDDSKFSFGYMSNNLKDV
TcdB027 FINCSTKEGLFVSELSDVVLISKVYMDNSKPLFGYCSNDLKDV
1517
1559
TcdB10463 KVITKDNVNILTGYYLKDDIKISLSLTLQDEKTIKLNSVHLDE
TcdB027 KVITKDDVIILTGYYLKDDIKISLSFTIQDENTIKLNGVYLDE
1560
1602
TcdB10463 SGVAEILKFMNRKGNTNTSDSLMSFLESMNIKSIFVNFLQSNI
TcdB027 NGVAEILKFMNKKGSTNTSDSLMSFLESMNIKSIFINSLQSNT
ii
KD= 36 ± 12 nM
KD= ND
KD= ND
ΔFn (‰)
residuals
[Fzd2-CRD] (nM)
iii
TOPFlash
Control
Control
TcdB10463
TcdB10463 GFE
TcdB027
+Wht3a
iv
Histopathological Score
Control
TcdB10463
TcdB10463 GFE
TcdB027
b
i
PBS
LGR5
FZD2
FZD7
CSPG4
NECTIN-3
Untreated50
TcdB10463
Untreated1000
TcdB027
ii
Viability (normalized to Untreated PBS)
PBS
LGR5
FZD2
FZD7
CSPG4
NECTIN-3
Untreated 50
TcdB 10463
Untreated 1000
TcdB 027
Blocking Condition/Toxin

Figure 2-3. RT027 *C. difficile TcdB* does not interact with FZD receptors, but still induces stem cell death and dysfunction

a) i) An alignment of the FZD binding domain of $TcdB_{10463}$ and $TcdB_{027}$ with $TcdB_{10463}$ contact residues (blue) and non-conserved $TcdB_{027}$ residues (red). **ii)** MST binding curves of $TcdB_{10463}$ (black), $TcdB_{027}$ (blue), and $TcdB_{10463}^{GFE}$ (red) to FZD2-CRD. The residuals with regards to the fit of the binding curve are depicted in the bottom panel (n=3). ND = not determined **iii)** TOPFlash assay performed in HEK293 STF cells incubated with 1:5 molar ratio of WNT3a and TcdB (n=4). **iv)** Mice were given 50 μg of TcdB intrarectally and were sacrificed after 4 hours post intoxication. Descending colon from each mouse was collected and stained with H&E (n=5). **b)** Equal numbers of colonic crypts were isolated from uninfected mice and then exposed to toxin, with or without recombinant receptor prior to organoid seeding. **i)** Representative images of organoids (arrowhead) cultured from crypts incubated for four hours with 5 nM of $TcdB_{10463}$ or 100 nM $TcdB_{027}$. Blocking was conducted with 50nM or 1000 nM, respectively, of either recombinant LGR5, FZD2, FZD7, CSPG4 or NECTIN-3 **ii)** with cell viability assessed *via* a PrestoBlue assay. n≥3. Data are represented as mean + S.E.M. * $p \leq 0.05$. ** $p \leq 0.01$, *** $p \leq 0.001$. Scale bars = 500 μm.

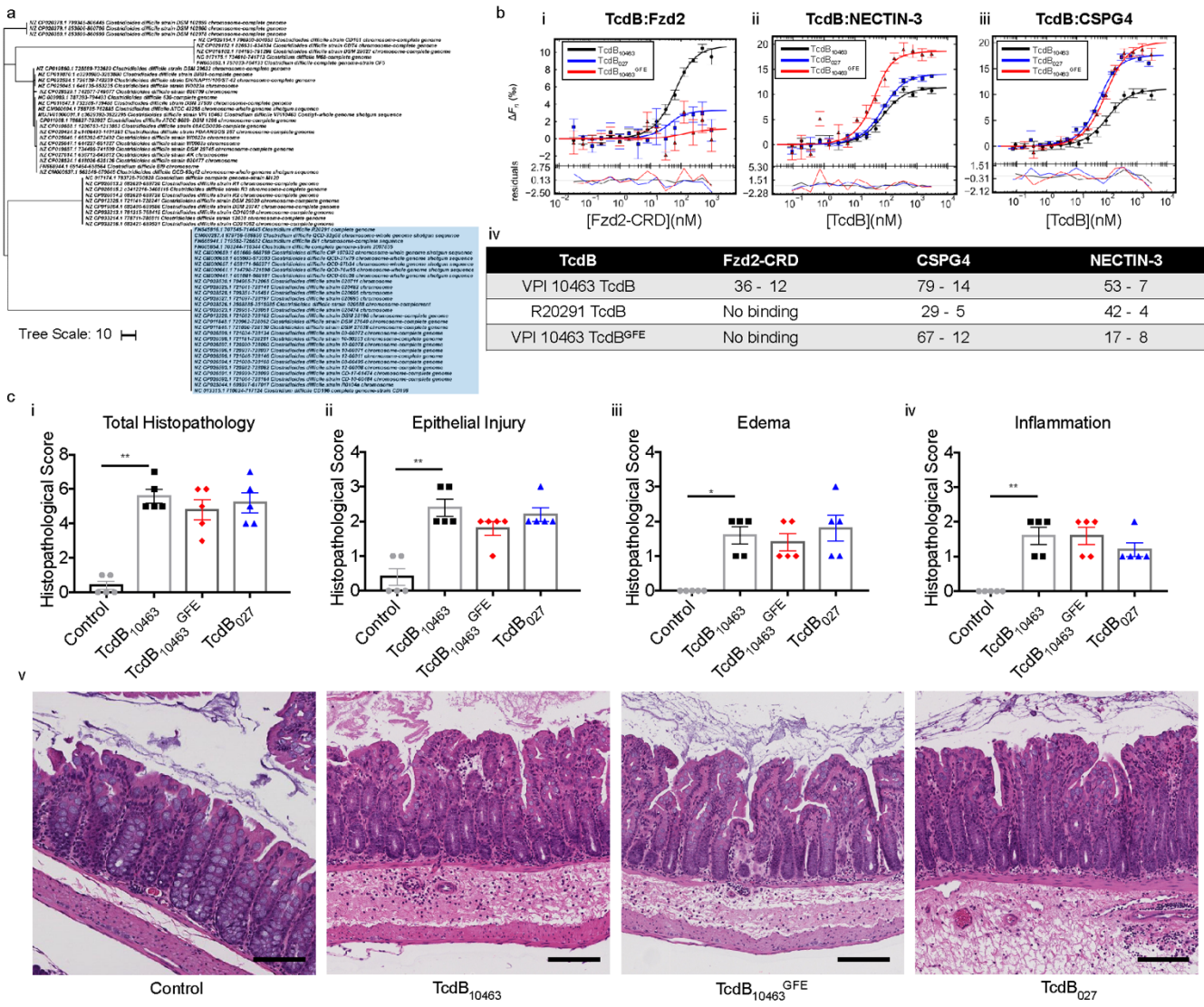

TcdB	Fzd2-CRD	CSPG4	NECTIN-3
VPI 10463 TcdB	36 - 12	79 - 14	53 - 7
R20291 TcdB	No binding	29 - 5	42 - 4
VPI 10463 TcdB^{GFE}	No binding	67 - 12	17 - 8

Figure 2-4. TcdB$_{027}$ does not bind FZD proteins, but still induces severe colonic damage.

a) A phylogenetic tree was generated from an alignment of TcdB amino acid sequences from annotated *C. difficile* genomes deposited in NCBI. The blue shade highlights RT027 strains of *C. difficile* and reveals that these strains have identical TcdB sequences. **b)** Dose-response curves of TcdBs titrated against a 16-step serial dilution of **i)** FZD2-CRD, **ii)** NECTIN-3 and **iii)** CSPG4 titrated against serial dilutions of TcdBs. Curves were fitted to a one-site binding model to determine K_D values (nM). The confidence intervals were calculated from three independent experiments in PALMIST using the variance-covariance method. **iv)** K_D values between TcdBs and their receptors determined by MST. ND = not determined. **c)** Individual scoring of mice colon exposed for 4 hours with PBS or 50 µg TcdB as described by **i)** total histopathology, **ii)** epithelial injury, **iii)** edema, and **iv)** inflammation. **v)** Representative H&E images of tissue from mice injected with either PBS or 50 µg of TcdB. Scale bar = 100 µM. n=5. Data are represented as mean + S.E.M. $p \leq 0.05$, ** $p \leq 0.01$, One-way Kruskal-Wallis with Dunn's post-hoc test for multiple comparisons.

each toxin to the purified ectodomains of CSPG4, FZD2-CRD, and NECTIN-3 (154–156, 159, 323). While the binding between TcdB10463 and FZD2-CRD could be reproducibly measured with a KD of 36 nM, the interactions of FZD2-CRD with TcdB027 or TcdB10463GFE (a TcdB10463 mutant lacking residues required for FZD2 binding) were weak and did not permit the calculation of KD (161). The affinities of TcdB027 for CSPG4 and NECTIN-3 were similar to those with TcdB10463 suggesting that the amino acid differences at the FZD binding site do not prevent the interaction of TcdB027 with other reported receptors (**Figure 2-3a i**, **Figure 2-4b**). As FZD1/2/7 are identical in the residues that contact TcdB10463 these data suggest that TcdB027 does not interact with FZD1/2/7 but retains the capacity to interact with CSGP4 and NECTIN-3 (**Figure 2-4b**) (161). Although TcdB10463 was able to inhibit WNT-signaling in a TOP-Flash assay and TcdB027 and the FZD-binding mutant, TcdB10463GFE, could not (**Figure 2-3a iii**), our in vivo data indicate that TcdB027 is still capable of altering WNT-signaling in vivo, likely as a consequence of inducing cell death at the crypt base, where the stem cell compartment resides. To further test this hypothesis, I used a rectal instillation mouse toxicity model with the help with J Shupe of the Lacy laboratory and found that there were no significant differences in histological scoring between toxins that could or could not interact with FZD as measured by injury, edema, and inflammation (**Figure 2-3a iv**, **Figure 2-4c**). These data indicate that TcdB can damage the colonic epithelium via receptors other than FZD and that there are likely multiple receptors that allow for TcdB entry into cells on the colonic epithelium, and more specifically colonic stem cells, altering their regenerative capacity.

To further define the concentration at which $TcdB_{10463}$ and $TcdB_{027}$ induces murine stem cell death, we were able to perform a dose response from 0.5 nM to 10 nM for $TcdB_{10463}$ and 1 nM to 100 nM for $TcdB_{027}$ with the help of the Lyras and Abud laboratories (**Figure 2-5a).** Crypts from uninfected mice were isolated and intoxicated with purified $TcdB_{10463}$ and $TcdB_{027}$ toxins for 4 hours, before washing and using in organoid seeding. After 7 days, organoid viability was measured, to establish at what concentration each toxin could induce near complete stem cell death. These data indicated that 5 nM of $TcdB_{10463}$ and 100 nM of $TcdB_{027}$ were sufficient to induce a similar level of stem cell death, without complete ablation of organoid seeding, with organoid viability counts around 10% of that detected for untreated control organoids (**Figure 2-5a**).

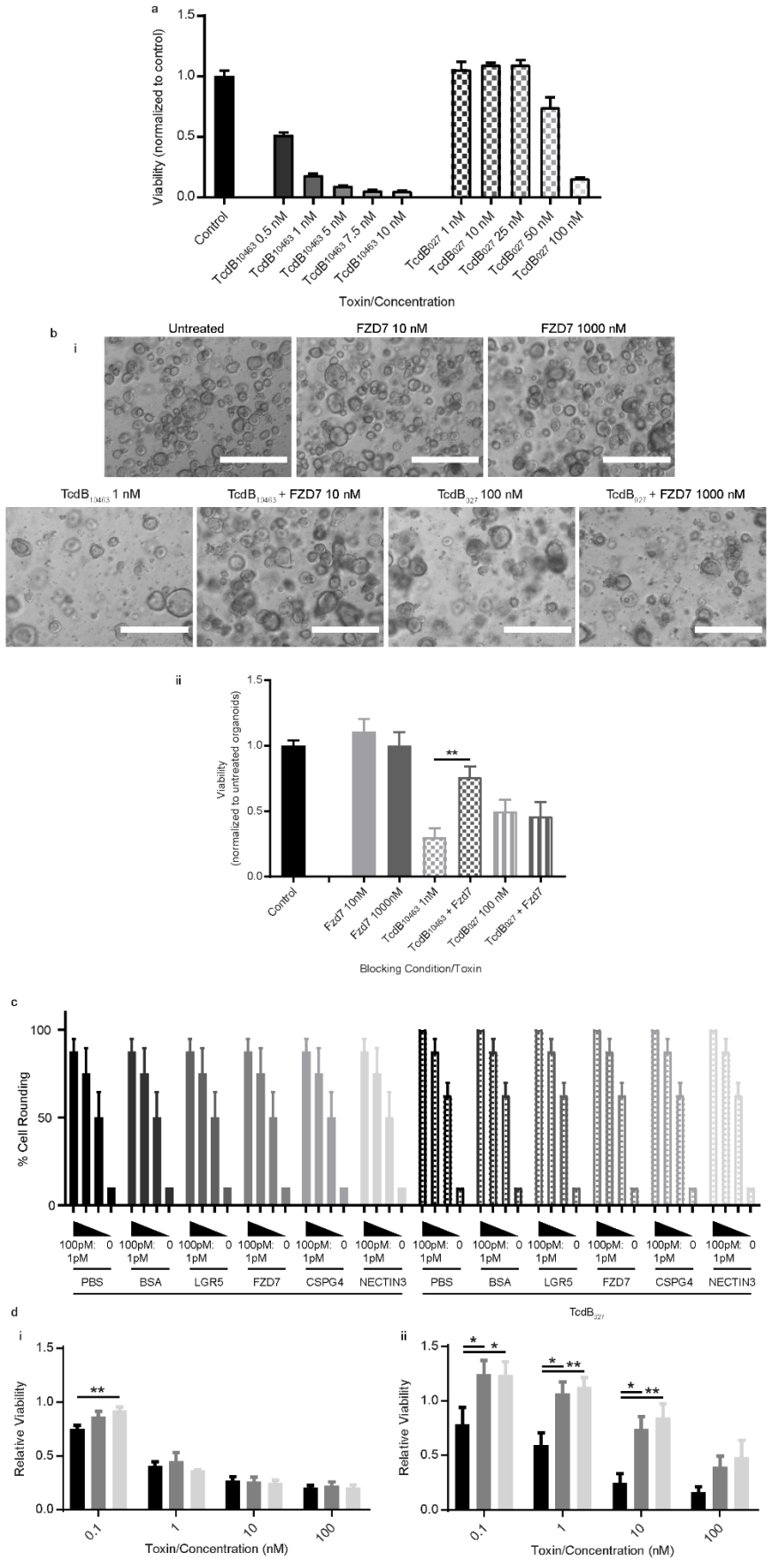
a
Viability (normalized to control)
Control
TcdB10463 0.5 nM
TcdB10463 1 nM
TcdB10463 5 nM
TcdB10463 7.5 nM
TcdB10463 10 nM
TcdB027 1 nM
TcdB027 10 nM
TcdB027 25 nM
TcdB027 50 nM
TcdB027 100 nM
Toxin/Concentration
b
i
Untreated
FZD7 10 nM
FZD7 1000 nM
TcdB10463 1 nM
TcdB10463 + FZD7 10 nM
TcdB027 100 nM
TcdB027 + FZD7 1000 nM
ii
Viability (normalized to untreated organoids)
Control
Fzd7 10nM
Fzd7 1000nM
TcdB10463 1nM
TcdB10463 + Fzd7
TcdB027 100 nM
TcdB027 + Fzd7
Blocking Condition/Toxin
c
% Cell Rounding
100pM: 0
1pM
PBS
BSA
LGR5
FZD7
CSPG4
NECTIN3
TcdB027
d
i
Relative Viability
Toxin/Concentration (nM)
ii
Relative Viability
Toxin/Concentration (nM)

Figure 2-5. $TcdB_{10463}$ and $TcdB_{027}$ can bind to cells in FZD dependent and independent mechanisms.

a) Equal numbers of colonic crypts were isolated from uninfected mice and then exposed to a range of $TcdB_{10463}$ and $TcdB_{027}$ doses (0.5 – 10 nM and 1 – 100 nM, respectively) to identify a suitable dose for intoxication blocking experiments. **b)** Equal numbers of dissociated human colonic organoid cells were exposed to toxin, with or without recombinant receptor prior to organoid seeding. **i)** Representative images of organoids cultured from cells for four hours with 1 nM of $TcdB_{10463}$ or 100 nM $TcdB_{027}$. Blocking was conducted with 10nM or 1000 nM, respectively, of recombinant FZD7. n=3, scale bar = 400 μM. **ii**) cell viability as assessed *via* a PrestoBlue assay. **c)** Vero cells seeded at 10^4 cell/per well were cultured following a four-hour exposure to $TcdB_{10463}$ and $TcdB_{027}$ that was treated with either PBS, BSA, or recombinant receptor using a range of TcdB concentrations (1 pM, 0.5 pM and 0.25 pM) in a ratio of 1:100 of toxin to added protein or left untreated (media alone). **d)** Hela and Caco-2 cells seeded at 7.5 x 10^3 and 5 x 10^3 cells per well, respectively, were cultured following exposure to $TcdB_{10463}$ (black), $TcdB_{10463}^{GFE}$ (dark grey), and $TcdB_{027}$ (light grey) at a range of concentrations (0.1 nM, 1 nM, 10 nM and 100 nM). Cell viability was measured using an ATP viability indicator (CellTiterGlo) at **i)** 2.5 hours of exposure on Hela cells or **ii)** 24 hours on Caco-2 cells. n = 3; Data are represented as mean + S.E.M. See also **Figure 2-3**.

To examine this differential receptor binding in the context of our in vivo infection data, colonic crypts from uninfected mice were isolated, and intoxicated with purified TcdB10463 and TcdB027 toxins (at 5 nM and 100 nM, respectively) to induce crypt death. These crypts were also pre-treated with purified recombinant soluble CSPG4, FZD2, FZD7, NECTIN-3 and LGR5 (at 50 nM and 1000 nM for each respective toxin), for 30 minutes, and used in organoid seeding, to assess if stem cell intoxication could be prevented by blocking toxin binding. Only unintoxicated intestinal stem cells that survive will generate mature organoids. Thus, these assays serve as a functional readout of the potential for TcdB to kill stem cells and the ability of each purified receptor to prevent this. Treatment with each receptor alone did not significantly alter organoid seeding, with similar numbers of mature organoids in each control condition (**Figure 2-3b**). TcdB10463 and TcdB027 treatment alone induced crypt death, with a lack of viable organoids following intoxication, and little to no cell viability detected (**Figure 2-3b**).

Pre-treatment with FZD2 and FZD7 blocked TcdB10463-mediated stem cell intoxication, indicated by increased mature organoid formation and cell viability at a significantly higher level than PBS treated TcdB10463-exposed crypts (p=0.0286; **Figure 2-3b**). However, soluble CSPG4, NECTIN-3 and LGR5 had no effect in modifying TcdB10463 toxicity, and may reflect low cell surface expression levels of these alternate receptors (**Figure 2-3b**). As predicted, pre-treatment with FZD2 and FZD7 did not block TcdB027-mediated stem cell intoxication, indicated by the similar levels of mature colonic organoids and cell viability between the FZD2/7 treated and PBS treated TcdB027-exposed groups (**Figure 2-3b**). Furthermore, soluble CSPG4, NECTIN-3 and LGR5 also had no effect in modifying TcdB027 toxicity, and as such, TcdB027 may bind to a previously unknown receptor on colonic stem cells. Similar blocking experiments were performed on human colonic organoids, indicating that FZD7 can prevent TcdB10463 but not TcdB027 intoxication of colonic stem cells, evidenced by a significant increase in organoid viability and organoid numbers in FZD7 treated TcdB10463 intoxicated stem cells (p=0.0021; **Figure 2-5b**). However, similar assays performed on Vero cells indicated that despite being protective in organoid culture, FZD7 could not prevent TcdB10463-mediated Vero cell rounding, with levels of cell rounding consistent across all test conditions (**Figure 2-5c**). I also measured the toxicity of TcdB10463, TcdB10463GFE and TcdB027-in HeLa and Caco-2 cells, two cell lines that differ in their receptor profiles. HeLa cells are known to express high levels of CSPG4 but low levels of FZD1/2/7, and can differ in whether or not NECTIN-3 is present (323). Caco-2 cells express NECTIN-3 and low levels of FZD1/2/7 but have little to no CSPG4 (323). Cells were treated with 0.1, 1, 10, and 100 nM of each

toxin, assessing viability after 2.5 hours (HeLa) or 24 hours (Caco-2). In HeLa cells, all of the toxins are equally active in the presence of the shared HeLa-dominant receptor CSPG4, implying that interaction with FZD1/2/7 is not required for this toxicity (**Figure 2-5d i**). In contrast, TcdB10463 had significantly higher cytotoxicity than TcdB10463GFE and TcdB027 in Caco-2 cells that correlated with the capacity to bind FZD1/2/7, evidenced by cells treated with TcdB10463GFE and TcdB027 exhibiting an increased viability over the concentration range of 0.1 nM to 10 nM TcdB ($p<0.05$; **Fig. 2-5d ii**). Taken together, our data indicate TcdB027 is able to induce stem cell death during infection but this does not result from binding to FZD. Additionally, these observations appear to be relevant in both human and mouse colonic stem cells.

Discussion

Although multiple receptors have been identified to interact with TcdB, little is known of their contributions to disease during infection. Through a successful collaboration with the Lyras and Abud laboratories from Monash University, we show that FZD interactions with TcdB are dispensable for mediating epithelial injuries and severe disease during CDI. These collaborations were necessary as the Lacy laboratory did have the capabilities of easily performing *C. difficile* infections at the time, and thus our collaboration with the Lyras laboratory allowed us to investigate CDI. Dena Lyras in turn introduced us to the Abud laboratory and convinced us to utilize and test the activities of TcdB on human and mouse derived organoids.

While the primary mechanism is unknown, I found that TcdB from our tested RT027 strain (R20291) does not interact with FZD proteins (**Figure 2-3a ii**). I predict that this loss of interaction is mediated by mutations within the FZD binding interface (**Figure 2-3a i**). Interestingly, I found that this loss of interaction does not impact the potency of TcdB on HeLa cells (**Figure 2-5d i**) and intestinal epithelial cells *in vivo* (**Figure 2-3a iv**). Furthermore, *C. difficile* that produces only TcdB from RT027 is still capable of inducing severe disease in the mouse model of CDI (**Figure 2-1a**). Mechanistically, this can be explained by the possibility that TcdB can utilize receptors other than FZDs for mediating epithelial injuries. While we were unable to block the activity of TcdB RT027 with Nectin-3 on organoids, I found, with the aid of my fellow lab member Dr. Jaime Jensen and Dr. Sheedlo, that TcdB RT027 is capable of interacting with Nectin-3 with nanomolar affinities (**Figure 2-4b ii**). Therefore, it is possible that TcdB RT027 can interact with Nectin-3 on the intestinal mucosa to mediate intestinal injuries. The lack of

neutralization of TcdB RT027 with Nectin-3 ectodomain can potentially be explained by (1) a fast dissociation of the Nectin-3:TcdB RT027 complex in solution and (2) the ability of this complex to interact with an alternative unknown receptor.

Another implication of these findings is the possibility the *C. difficile* toxins display receptor tropism between its clades. Receptor tropism has been observed in toxins such as *S. aureus* leukocidin, *Salmonella* typhoid toxin, and *Clostridium botulinum* neurotoxins to promote tissue and host specificity (324–326). It is possible that some strains of *C. difficile* utilize FZDs as receptors in specific hosts to mediate epithelial injuries. *C. difficile* can infect a variety of hosts, including humans, mice, hamsters, dogs, rabbits, chickens, pigs, and horses (327). Thus, *C. difficile* TcdB may have evolved interactions with FZDs to allow it to intoxicate colonic tissue in hosts where its primary receptor is absent. The attenuation of TcdB RT027 activity relative to TcdB VPI10463 on Caco-2 cells (**Figure 2-5d ii**) but not on HeLa cells (**Figure 2-5d i**) supports this hypothesis. Interestingly, sequence typing has revealed the existence of five TcdB clades (109, 176). Future studies are needed to determine if receptor tropism and potency differ across TcdB clades.

Materials and Methods

Bacterial strains, growth conditions, cell lines and reagents

C. difficile strains (**Table 2-1**) were cultured on HIS-T agar (heart infusion (HI) (Oxoid) supplemented with 1.5% glucose, 0.1% (w/v) L-cysteine, 1.5% (w/v) agar and 0.1% (w/v) sodium taurocholate (New Zealand Pharmaceuticals)), prior to inoculation into 500 mL Tryptone Yeast (TY) broth (3% tryptone (Oxoid), 2% yeast extract (Oxoid) and 0.1% sodium thioglycolate (Sigma-Aldrich)) and grown for seven days anaerobically at 37˚C. Spores were harvested by centrifugation at 10,000 g for 20 minutes at 4˚C, washed eight times with chilled dH2O and resuspended in Phosphate Buffered Saline (PBS) containing 0.05% Tween-80 (PBS-T) prior to heat-shocking at 65˚C for 20 minutes.

Recombinant protein cloning, expression and purification.

Site directed mutagenesis was used to generate VPI10463 TcdBGFE (pBL881) in pHis1622-VPI10463-TcdB-C-term-8X-His (pBL377) with primers F-GAAAGTATGAATATAAAAAGTATTTTCGGATTCGA-GAATATTAAGTTTATA and R-CTTATTATAAAATTAGCATCTAATATAAACTTAATATTCTCGAATCC-GAAAATACTTTTTAT. pHis1622-M7404-TcdB-C-term-6X-His plasmid (pBL598) was a gift from Dr.

J. Ballard (University of Oklahoma Health Sciences Center). Recombinant TcdB proteins were expressed in Bacillus megaterium and purified as previously described (328).

PNGase F expression vector pOPH6 (pBL831) was a gift from Shaun Lott (Addgene plasmid # 40315). pOPH6 was transformed into E. coli BL21 DE3 cells. Overnight cultures were prepared in 5 mL Luria Broth (LB) at 37˚C and inoculated into 250 mL LB the following day. This culture was shaken at 220 rpm at 37˚C and grown to an OD600 of 0.6. Expression of PNGase F was induced with 0.25 mM IPTG, followed by an overnight incubation at 18˚C. PNGase F was purified as outlined (329).

FZD2-CRD (residues 24-156), CSPG4 (residues 400-764), and NECTIN-3 (residues 58-302) DNA was cloned into pCDNA3.4 with an N-terminal human serum albumin secretion peptide (MKWVTFISLLFLFSSAYS) and a C-terminal TEV protease site and 6X-His tag (Thermo Fisher Scientific) to generate the plasmids pBL808, pBL790, and pBL787 respectively. The receptors were expressed in ExpiCHO cells (Thermo Fisher Scientific) in 25 mL according to the manufacturer's protocol. ExpiCHO supernatant was collected, and receptors were purified using cobalt-nitriloacetic acid resin (GE) and concentrated to 1 mL using 3 kDa or 10 kDa molecular weight cutoff filters (MilliporeSigma). FZD2-CRD and CSPG4 were treated with a 1:10 molar ratio of PNGaseF to receptor for 16 hours at 37˚C. The receptors were further purified using size exclusion chromatography with an S-75 column. The receptors were stored in 20 mM HEPES pH 8.0, 100 mM NaCl.

Microscale Thermophoresis

Microscale thermophoresis (MST) experiments were performed on a NanoTemper Monolith NT.115 (NanoTemper Technologies GmbH, Munich, Germany). VPI $TcdB_{10463}$, $TcdB_{027}$, VPI $TcdB_{10463}^{GFE}$, FZD2-CRD, CSPG4, and NECTIN-3 were equilibrated prior to labelling with size exclusion chromatography using either a Superdex 200 10/300 or Superdex 75 10/300 column (GE) with 20 mM HEPES pH 8.0, 100 mM NaCl. Toxins, CSPG4, and NECTIN-3 were labelled with the Monolith NT His-tag Labelling Kit RED-tris-NTA, following the manufacturer's instructions. TcdB or receptor concentration was held constant at 50 nM. Serial dilutions of FZD2-CRD or TcdB were prepared using a 1:1 dilution from 3-10 μM to 90-300 pM in 20 mM HEPES pH 8.0, 100 mM NaCl, 0.05% Tween-20, and protease inhibitor cocktail for His-tagged proteins (Sigma). Samples were loaded into Monolith NT.115 capillaries (NanoTemper), and measurements carried out at 21˚C with 40% MST power and 60% excitation power. MO.Control v1.6 was used for data collection, and MO.Affinity Analysis v2.3 and

PALMIST were used for data analysis (330). The K_D constants were calculated in PALMIST utilizing the saturation binding curve at equilibrium.

Animal model of *C. difficile* infection

Animal handling and experimentation was performed according to Victorian State Government regulations, approved by the Monash University Animal Ethics Committee (Monash University AEC no. SOBSB/M/2010/25 and MARP/2014/135). Time-course animal infections were conducted using the Monash mouse model of CDI as previously described with the following modifications (106, 331). Three days prior to infection, at the completion of the seven day antibiotic cocktail pre-treatment described previously, mice were switched to water containing cefaclor (300 μg/mL), ad libitum, and returned to untreated water on the day of infection (106, 331). Male, six to eight week old, C57BL/6J mice (Walter and Eliza Hall Institute of Medical Research) were challenged with 106 spores of a single strain of C. difficile by gastric inoculation and were monitored twice daily as described previously for disease signs (including weight loss, behavioral changes and diarrhea) (106). For the time course of infection experiments, mice were euthanized at either 12, 24 or 48-hours post-infection or upon reaching the following endpoints for the genetically diverse strains comparison: acute weight loss of greater than 10% relative to the day of infection (day zero) in the first 24-hours or chronic weight loss of greater than 15% relative to day zero thereafter, or on animals becoming moribund, showing low activity, labored breathing, severe diarrhea, and a scruffy coat. For the recovery model of infection, mice that reached a weight loss of greater than 10% relative to the day of infection but less than 15% relative to day zero at the peak of infection (48-hours) were allowed to recover for either 7 days or 14 days before being euthanized. Fecal pellets were collected from all animals and resuspended at 100 mg/mL in sterile PBS before culturing on supplemented Heart Infusion agar, as previously described (331). Weight loss relative to day zero (D0) was plotted for each group/time-point and analyzed with Graph Pad Prism 7 using a one-way ANOVA and Tukey's test. For the panel of clinical and animal C. difficile strains, feces collected at 24 hours post infection was further diluted to 50 mg/ml in PBS. The diluted feces were used to determine toxin levels within the infected mice. To do this, these preparations were filter sterilized using 0.45 μm and 0.22 μm filters (Sartorius) and two-fold serial dilutions of the fecal supernatants were prepared in Minimal Essential Medium (MEM) α (Gibco, ThermoFisher Scientific) or McCoy's 5A (modified) Medium (Gibco, ThermoFisher Scientific) supplemented with 1% (v/v) heat inactivated fetal calf serum (HI-FCS).

Vero and HT-29 cells were cultured and prepared as previously described (101). Cells were seeded in 96-well plates at 1 x 104 cells/well, and incubated for 24 hours at 37°C in 5% CO2 prior to exposing these cells to the filtered fecal content. All conditions were prepared in technical duplicated and at least four biological replicates. Morphological changes were observed after 18 hours using an Olympus 1X71 inverted microscope at 20x magnification. The toxin titre was evaluated as the final dilution at with 100% cell rounding, in comparison to the negative control wells, and was scored before analyzing with Graph Pad Prism 7 using a Mann-Whitney U test.

Four micron sections of formalin fixed (10% neutral buffered), Swiss-rolled colon and caecum were periodic acid–Schiff/Alcian blue stained by the Monash Histology Platform and assessed using a previously described scoring system (106). Stained sections were scanned for visualization using an Aperio Scanscope AT Turbo, at 20x magnification. For recovery mice, crypt length was measured for 30 crypts/mouse at equal points across the entire length of the colon, using the measure tool within Aperio ImageScope. All histopathological analysis was performed blind and analyzed with Graph Pad Prism 7 using a Mann-Whitney U test.

Animal model of *C. difficile* intoxication

All mouse experiments were approved by Vanderbilt Institutional Animal Care and Use Committee (IACUC). Female, five to eight-week old C57BL/6 mice (Jackson Laboratories) were housed five to a cage with free access to food and water. After a four-day acclimation period, mice were switched to water containing cefoperazone (500 μg/mL) for five days, with changes every 48-hours. After five days, cefoperazone treated water was switched back to untreated water and a 48-hour recovery period was allowed before being intoxicated with a 200 μL volume of 50 μg TcdB (VPI10463, VPI10463 GFE, or 027) or PBS as a control.

For the intoxication procedure, mice were anesthetized with isoflurane. A 21 gauge flexible gavage was inserted approximately 2 cm in via the rectum and each condition was slowly administered. Rectal pressure was applied for 30 seconds to prevent immediate leakage, and mice were placed in a clean cage to recover. After four hours, the mice were euthanized by CO2 gas, the abdomens were opened up, and colons extracted. Each colon was flushed with PBS, Swiss-rolled, and fixed in 10% formalin. After embedding in paraffin, the colonic tissue was sliced, mounted to a microscope slide, and stained with H&E by the

Translational Pathology Shared Resource (TPSR) center at Vanderbilt University Medical Center. The tissue was then scored for edema, inflammation, and epithelial injury as previously described by a pathologist blinded to the experimental conditions (332).

Immunohistochemistry and Immunofluorescence analysis

Paraffin-embedded colonic tissues were processed using standard procedures. Slides were de-waxed and antigen retrieval was performed using 10 mM citrate (Sigma-Aldrich) buffer, with 0.05% Tween-20 (Amresco), pH 6.0. Slides were blocked for 60 minutes with CAS-Block™ (Thermo-Fisher Scientific) at room temperature. For immunofluorescence staining, slides were incubated with either mouse anti-ezrin (Thermo-Fisher Scientific; 1:200 dilution in 1% Bovine serum albumin (BSA; Sigma Aldrich) in PBS) or mouse anti-β-catenin (BD; 1:200 dilution in 1% BSA) and rabbit anti-E-cadherin (Cell Signaling; 1:200 dilution in 1% BSA) overnight at 4˚C. Slides were rinsed three times in PBS before incubation with secondary antibodies for 60 minutes at room temperature. For ezrin and β-catenin, goat anti-mouse IgG, Alexa Fluor® 488 (Thermo-Fisher Scientific; 1:1000 dilution in 1% BSA) was used, for E-cadherin goat anti-rabbit IgG, Alexa Fluor® 568 (Thermo-Fisher Scientific; 1:1000 dilution in 1% BSA) was used. Slides were washed three times in PBS before staining the nuclei with DAPI (300 nM, Thermo Fisher). Slides were mounted with ProLong® Gold (Thermo Fisher), sealed and imaged using a Leica SP8 Confocal Invert microscope on a 20x/1.0 oil objective with LasX Software (Leica).

Colonic stem cell sorting and quantitative PCR for stem cell and TcdB receptors

Mouse colonic crypt isolation and organoid establishment were based on protocols previously described (333–335). Intact, dissected colons from adult LGR5-eGFP-IRES-CreERT2 mice (a pool of 10 colons was used per biological replicate) were flushed with 50 mL of cold PBS to remove luminal contents, cut longitudinally and scraped with a glass cover slip to remove epithelial fragments, mucus and feces (259). Colons were cut into 5 mm pieces and washed in cold PBS before digestion with 4 mM EDTA. To isolate crypts, the tissue fragments were vigorously suspended in cold PBS using a 10 mL pipette. This procedure was repeated a total of three times. Crypts were pelleted by centrifugation at 240 g for five minutes, at 4˚C. The collected crypts were then dissociated in TrypLE Express (Invitrogen) supplemented with 10 μM Y-27632 Rock inhibitor (Abcam) and DNAse 1 (Sigma-Aldrich) for four minutes at 37˚C. Cell clumps and mucus were removed using a 70 μm cell strainer (BD Biosciences). The remaining dissociated cells were washed twice with PBS and collected by centrifugation at 4˚C at 240 g for five minutes.

Antibody labelling step as well as the final resuspension of the sample were performed with PBS supplemented with 2 mM EDTA, 2% FBS and 10 μM Y-27632 Rock inhibitor. As previously described, cellularized crypts were incubated with anti-CD31-BV510 (1:200, clone: MEC 13.3, BD Horizon), anti-CD45-BV510 (1:200, clone: 30-F11, BD Horizon) and anti-CD24-PeCy7 (1:100, clone: M1/69, eBioscience) antibodies in a 500 μL volume for 15 minutes on ice (334). After washing twice with PBS, the cells were resuspended in a final volume of 1 mL, passed through a 70 μm strainer and transferred into appropriate FACS tubes containing propidium idodine (PI) at a concentration of 2 μg/mL. Cell sorting was carried out with a 100 μm nozzle on an Influx instrument (BD Biosciences). Aggregates, debris, dead cells (PI+), and CD45+/CD31+ hematopoietic/endothelial contaminates were depleted. For the LGR5-GFPhigh cell population, around 2% of the CD24+ LGR5-GFP brightest cells were selected. The subsequent 2% of the CD24+ LGR5-GFP+ cells were considered as LGR5-GFPmed and LGR5-GFPlow cell populations. A fully differentiated cell population, identified as CD24- LGR5-, was also isolated. Purity of collected fractions was confirmed by reanalysis of a small fraction of the sorted cells.

Following FACS, cells were centrifuged at 240 g for five minutes at 4˚C and resuspended in RLT buffer. RNA was then extracted using the Qiagen RNeasy Microkit following the manufacturer's instructions, and used to synthesize cDNA, using a QuantiTect Reverse Transcription kit (Qiagen), using 70 ng of RNA. The cDNA was quantified using the QIAExpert prior to dilution for use in quantitative PCR (qPCR). The qPCR was conducted as previously described, normalizing to β-2-microglobulin (*B2m*) and β-actin (*Actb*), using the corresponding forward and reverse primers: *Actb*, F-TGTTACCAACTGGGACGACA, R-GGGGTGTTGAAGGTCTCAAA; *B2m*, F-CTTTCTGGTGCTTGTCTCACTG, R-AGCATTTGGATTTCAATGTGAG; *Cspg4*, F-CCTGGTAGGCTGCATAGAAGAT, R-CCAGGGTGGAGAAAGTTTCATA; *Fzd7*, F-AGAGATTTGGGGCGAGAGAT, R-CAGTTAGCATCGTCCTGCAA; *Lgr5*, F-CCTTGGCCCTGAACAAAATA, R-ATTTCTTTCCCAGGGAGTGG; *Lrp1*, F-GACCAGGTGTTGGACACAGATG, R-AGTCGTTGTCTCCGTCACACTTC; *Nectin3*, F-TTGCCCTTTCCTTTGTCAAC, R-GCATGTCTGATGGTGGAATG (336).

RNA extraction, cDNA preparation and digital droplet PCR-analysis

Colonic tissues collected from infected mice were placed in RNAlater™ (Ambion) prior to RNA extraction. The tissues were then homogenized and total RNA was extracted using the RNeasy mini kit

(Qiagen). One microgram of RNA was used for cDNA synthesis using a QuantiTect Reverse Transcription kit (Qiagen). The cDNA was quantified using the QIAExpert prior to dilution for use in digital droplet PCR (ddPCR). The ddPCR was conducted as previously described, normalizing to β-2-microglobulin (*B2m*), using the corresponding forward and reverse primers, as follows:

Ascl2, F-CAGGAGCTGCTTGACTTTTCCA, R-GGGCTAGAAGCAGGTAGGTCCA; *Axin1*, F-GCAGCTCAGCAAAAAGGGAAAT, R-TACATGGGGAGCACTGTCTCGT; *B2m*, F-CTTTCTGGTGCTTGTCTCACTG, R-AGCATTTGGATTTCAATGTGAG; *Bmi1*, F-ATGCATCGAACAACCAGAATC, R-GTCTGGTTTTGTGAACCTGGA; *c-myc*, F-CTAGTGCTGCATGAGGAGACAC, R-GTAGTTGTGCTGGTGAGTGGAG; *Ephb2*, F-AGAATGGTGCCATCTTCCAG, R-GCACATCCACTTCTTCAGCA; *Fzd7*, F-AGAGATTTGGGGCGAGAGAT, R-CAGTTAGCATCGTCCTGCAA; *Lgr5*, F-CCTTGGCCCTGAACAAAATA, R-ATTTCTTTCCCAGGGAGTGG (336).

Following this, ddPCR was performed using 2x QX200 ddPCR EvaGreen Supermix (Bio-Rad), and 100 nM of each corresponding forward and reverse primer, as above. For each PCR reaction variable quantities of template cDNA were used (target gene dependent), with each reaction being performed in a final volume of 25 µL. From this, 20 µL was added to a DG8™ Cartridge for droplet generation using QX200 Droplet Generation Oil for EvaGreen (Bio-Rad). The generated droplets were transferred to a 96-well PCR-plate (Eppendorf) and subjected to thermo-cycling as previously described (336). Transcript levels were quantified and adjusted to copies per 10 µg of cDNA before normalizing to the housekeeping gene B2m. The adjusted transcript levels were plotted as a fold-change relative to uninfected using GraphPad Prism 7, with statistical significance assessed using a Mann Whitney U test.

Growth of murine colonic-organoids from *C. difficile* infected mice

Mouse colonic crypt isolation and organoid establishment were based on protocols previously described(333, 334). Intact, dissected colons from C57BL/6J mice (MARP) were flushed and scraped, as above. Colons were cut into 5 mm pieces and washed in cold PBS before digestion with 4 mM EDTA. Crypts were isolated from the tissues through vigorous re-suspension in cold PBS using a 10 mL pipette. This procedure was repeated a total of three times. Crypts were pelleted by centrifugation at 240 g for five minutes, at 4˚C. The crypt pellet was resuspended in PBS, passed through a 70 µm cell strainer (BD) and

centrifuged. The supernatant was discarded and the pellet containing the crypts was resuspended in matrigel (BD). Equal numbers of crypts in matrigel were seeded into each well of a 48-well plate (Nunc) and incubated for 10 minutes at 37°C until solidified. Crypt culture media (DMEM/F12 supplemented with B27 (Gibco), Glutamax (Gibco), N2 (Gibco), 10 mM HEPES (Gibco), Fungizone (Gibco), 50 ng/mL EGF (Peprotech), 100 ng/mL Noggin (Peprotech), penicillin/streptomycin (Gibco), 2.5 μM CHIR99021 (Bioscientific), 10 μM Y-27632 Rock inhibitor (Abcam), 10% R-spondin 1 conditioned media, and 50% WNT3a conditioned media) was added to each well. Organoid forming ability was assessed using the reazurin-based PrestoBlue reagent (Life Technologies), as previously described (336). Cell viability was measured according to the manufacturer's instructions and organoids were imaged using an EVOS FL Auto Cell Imaging System (Invitrogen). Viability was plotted using GraphPad Prism 7, with statistical significance assessed using a Mann Whitney U test.

TOPFlash assay

500,000 HEK 293 STF cells were seeded in a 12 well dish for 18 hours. The media was then replaced with 1 mL of pre-warmed media with or without combinations of 1:5 molar ratio of human WNT3a (100 ng/mL, 2.67 nM, StemRD) to toxin (13.35 nM) for 20 hours. Following the incubation, the media was removed and cells were lysed in 110 μL of Passive Lysis Buffer (Promega) for 15 minutes while shaking. The solubilized supernatant was collected and immediately used for the determination of the TOPFlash luciferase activities with the Steady-Glo Luciferase assay (Promega) and CellTiter Glo (Promega).

Treatment of colonic crypts with purified toxins and receptor-blocking proteins, and assessment of organoid formation

Colonic crypts were isolated from C57BL/6J mouse tissues as described previously. The crypt pellets were resuspended in PBS containing 1% fetal bovine serum (FBS) and supplemented with 5 nM purified VPI10463TcdB (Abcam) or 100 nM purified RT-027 TcdB. Blocking of toxin variants was conducted with respectively 50 nM or 1000 nM of either recombinant human FZD2 (see above), recombinant human FZD7 Fc chimera (R&D Systems), recombinant human CSPG4 (see above), recombinant human NECTIN-3 (see above), recombinant human LGR5 Fc chimera (R&D Systems). After four hours at 4°C, the crypt pellets were washed twice with PBS and resuspended in Matrigel (BD), and 12 μL were seeded into each well of a 48-well plate (Nunc) and incubated for 10 minutes at 37°C until solidified. The crypt culture media described above was added to each well. After 3 days, the medium was replaced with

fresh culture medium without Y-27632 Rock inhibitor. After four days in culture, cell viability was measured using the PrestoBlue reagent (Life Technologies) and imaged using an EVOS FL Auto Cell Imaging System (Invitrogen). Viability was plotted using GraphPad Prism 7, with statistical significance assessed using a Mann Whitney *U* test.

Treatment of colonic crypts with purified toxins and receptor-blocking proteins, and assessment of organoid formation

Colonic crypts were isolated from C57BL/6J mouse tissues as described previously. The crypt pellets were resuspended in PBS containing 1% FBS and supplemented with 5 nM purified VPI10463TcdB (Abcam) or 100 nM purified RT-027 TcdB. Blocking of toxin variants was conducted with respectively 50 nM or 1000 nM of either recombinant human FZD2 (see above), recombinant human FZD7 Fc chimera (R&D Systems), recombinant human CSPG4 (see above), recombinant human NECTIN-3 (see above), recombinant human LGR5 Fc chimera (R&D Systems). After four hours at 4˚C, the crypt pellets were washed twice with PBS and resuspended in Matrigel (BD), and 12 µL were seeded into each well of a 48-well plate (Nunc) and incubated for 10 minutes at 37˚C until solidified. The crypt culture media described above was added to each well. After 3 days, the medium was replaced with fresh culture medium without Y-27632 Rock inhibitor. After four days in culture, cell viability was measured using the PrestoBlue reagent (Life Technologies) and imaged using an EVOS FL Auto Cell Imaging System (Invitrogen). Viability was plotted using GraphPad Prism 7, with statistical significance assessed using a Mann Whitney *U* test.

Treatment of human colonic-organoids with *C. difficile* TcdB

Surgically resected normal colon samples were obtained following written informed consent from four patients at Cabrini hospital, Malvern, Australia. This study was approved by the Cabrini Human Research Ethics Committee (CHREC 04-19-01-15) and the Monash Human Research Ethics committee (MHREC ID 2518 CF15/332-2015000160). Patient recruitment was led by the colorectal surgeons in the Cabrini Monash University Department of Surgery. Tissue was washed and underlying muscle layers were removed with surgical scissors. Tissue was cut into 5 mm pieces and washed eight times in cold chelation buffer (distilled water with 5.6 mM/L Na2HPO4, 8.0 mM/L KH2PO4, 96.2 mM/L NaCl, 1.6 mM/L KCl, 43.4 mM/L sucrose, 54.9 mM/L D-sorbitol). Following incubation for 45 minutes at 4˚C in 4 mM EDTA in chelation buffer, intestinal crypts were released from colonic tissue fragments by

mechanically pipetting them with a 10 mL pipette in PBS as above. This procedure was repeated a total of three times. Crypts were pelleted by centrifugation at 240*g* for 5 minutes, at 4˚C. The crypt pellet was resuspended in PBS, passed through a 100 μm cell strainer and centrifuged. The supernatant was discarded and the pellet containing the crypts was resuspended in matrigel (BD). Matrigel was seeded into each well of a 48 well plate and incubated until solidified. Crypt culture media (advanced DMEM/F12 supplemented with B27 (Gibco), Glutamax (Gibco), N2 (Gibco), 10 mM HEPES (Gibco), 100 μg/mL Primocin (InvivoGen), 100 ng/mL Noggin (Peprotech), 50 ng/ml EGF (Peprotech), 10 nM Gastrin (Sigma Aldrich), 500 nM A83-01 (Torcis), 10 μM SB2002190 (Sigma Aldrich), 2.5 μM CHIR99021 (Bioscientific), 10% R-spondin 1 conditioned media, and 50% Wnt3a conditioned media) was added to each well. Ten micromoles of Y-27632 dihydrochloride kinase inhibitor (Torcis) was added after initial seeding for two days.

After the establishment of four human colonic-organoid lines, organoids were dissociated using TrypLE Express enzyme (Life technology). After dissociation, cells were pelleted and were resuspended in PBS containing 1% FBS and supplemented with 1 nM purified VPI10463 TcdB (Abcam) or 100 nM purified RT-027 TcdB. Blocking of toxin variants was conducted with 10 nM or 1000 nM of recombinant human FZD7 (R&D Systems), respectively. After four hours at 4˚C, the cells were washed twice with PBS and resuspended in Matrigel (BD), and re-seeded into 48 well plates. Organoids were cultured in crypt culture media for eight days before imaging using an EVOS FL Auto Cell Imaging System (Invitrogen). Additionally, cell viability was measured using the PrestoBlue reagent (Life Technologies). The experiments were performed in technical triplicate, per organoid line. Viability was plotted using GraphPad Prism 7, with statistical significance assessed using a One-way ANOVA and Tukey's multiple comparisons test.

Treatment of Vero cells with *C. difficile* TcdB

Vero cells were cultured and prepared as previously described (101). Cells were seeded in 96-well plates at 1 x 104 cells/well, and incubated for 24 hours at 37˚C in 5% CO2. Purified TcdB from strain VPI10463 (Abcam) or purified RT-027 TcdB was diluted in MEM-α containing 1% (v/v) FCS to concentrations of 1 pM, 0.5 pM, and 0.25 pM. Toxin preparations were incubated for 30 minutes on ice with either recombinant human FZD2 (see above), recombinant human FZD7 Fc chimera (R&D Systems), recombinant human CSPG4 (see above), recombinant human NECTIN-3 (see above), recombinant

human LGR5 Fc chimera (R&D Systems) or Bovine Serum Albumin (Sigma) each at concentrations of 100 pM, 50 pM, or 25 pM, to give a final ratio of 1:100 toxin:recombinant protein. The toxin or toxin/recombinant protein complexes were added to the Vero cells (100 μL/well) and incubated for four hours prior to removal, rinsing with PBS and replacement with fresh media. Cells treated with media alone were used as negative controls. All conditions were prepared in technical and biological triplicate. Morphological changes were observed after 18 hours using an Olympus 1X71 inverted microscope at 20x magnification. The cytopathic effect was determined as a percentage of rounded cells in comparison to the negative control wells.

Treatment of HeLa and Caco-2 cells with TcdB

HeLa cells were plated at 7,500 cells per well in a 100 μl volume into 96 well dishes and grown for 18 hours prior to intoxication. Caco-2 cells were plated at 5000 cells per well in a 50 μl volume and grown for 48 hours before intoxication. Cells were maintained in Dulbecco's Modified Eagle's medium (DMEM; Gibco) in 10% fetal bovine serum (FBS; Atlanta Biologicals), and were grown in a humidified incubator at 37 °C with 5% CO2 atmosphere. HeLa cells were treated with TcdB (TcdB10463, TcdB10463GFE and TcdB027) for 2.5 hours before measuring viability, while Caco-2 cells were treated for 24 hours before measuring viability by a CellTiterGlo (Promega) viability assay. CellTiterGlo assays were performed according to the manufacturer's protocol and were normalized to untreated conditions. Viability was plotted using GraphPad Prism 7, with statistical significance assessed using a Two-way ANOVA with comparisons made with respect to TcdB10463 using Dunnett's multiple comparisons test.

Sequence Analysis and Phylogeny

Fully annotated genomes of *C. difficile* strains deposited on the National Center for Biotechnology Information (NCBI) was used as the source of sequences in this study. As of the time of writing, 78 annotated sequences have been deposited into the NCBI. The *C. difficile* PubMLST database (https://pubmlst.org/cdifficile/) was used to define the *C. difficile* sequence types for these 78 annotated sequences (109, 337). Redundant strains or strains that could not be sequence typed were excluded from sequence analysis. The *tcdB* gene from the unannotated *C. difficile* VPI 10463 strain used in this study was also included in the alignment, amounting to a total of 65 strains for analysis. The loci corresponding to *tcdB* from these 65 strains were translated to determine their TcdB amino acid sequence (338). The TcdB sequences were aligned using the ClustalW algorithm within the R package msa version 1.14.0 (339). The

distance and relationships of these aligned sequences was then determined using the FastME V2 NJ Tree algorithm associated with the GrapeTree Python 2.7 package (340). A dendrogram and alignment was created using the Interactive Tree of Life (341).

Table 2-1. Strains and Characteristics

Strain	Characteristics	Reference
M7404	*tcdA*$^+$/*tcdB*$^+$/*cdtAB*$^+$, Clade 2, Ribotype 027, human clinical isolate, Canada, 2005.	(342)
DLL3045 (TcdA$^-$B$^+$)	M7404 derivative (M7404 *tcdA* TargeTron) *tcdA*$^-$/*tcdB*$^+$/*cdtAB*$^+$	
DLL3101 (TcdA$^+$B$^-$)	M7404 derivative (M7404Ω*tcdB* TargeTron) *tcdA*$^+$/*tcdB*$^-$/*cdtAB*$^+$	(106)
DLL3121 (TcdA$^-$B$^-$)	M7404 derivative (M7404Ω*tcdA* TargeTron, Ω *tcdB* TargeTron), *tcdA*$^-$/*tcdB*$^-$/*cdtAB*$^+$.	(106)
R20291	*tcdA*$^+$/*tcdB*$^+$/*cdtAB*$^+$, Clade 2, Ribotype 027, human clinical isolate, United Kingdom, 2006.	(343)
DLL3109	*tcdA*$^+$/*tcdB*$^+$/*cdtAB*$^+$, Clade 2, Ribotype 027, human clinical isolate, Australia, 2010.	(308, 344, 345)
VPI10463	*tcdA*$^+$/*tcdB*$^+$/*cdtAB*$^-$, Clade 1, Ribotype 003, Human isolate, reference strain, America, before 1982.	(74, 346)
630	*tcdA*$^+$/*tcdB*$^+$/*cdtAB*$^-$, Clade 1, Ribotype 012, human clinical isolate, Switzerland, 1982.	(347, 348)
JGS6133	*tcdA*$^+$/*tcdB*$^+$/*cdtAB*$^+$, Clade 5, Ribotype 078, porcine isolate, America, before 2013.	(349)
AI35	*tcdA*$^-$/*tcdB*$^+$(variant)/*cdtAB*$^+$, Clade 5, Ribotype 237, porcine isolate, Australia, 2013.	(349)
CD133	*tcdA*$^-$/*tcdB*$^-$/*cdtAB*$^-$, Clade 1, AUS-ribotype 091*, human clinical isolate, Australia, 2008.	This Study

Chapter 3

Nectin-3 and Shed Forms of CSPG4 Can Serve as Epithelial Cell Receptors for *Clostridioides difficile* TcdB

Adapted from: Childress K.O., Cencer C.S., Tyska M.J., Lacy D.B. Nectin-3 and Shed Forms of CSPG4 Can Serve as Epithelial Cell Receptors for Clostridioides difficile TcdB. Submitted

Abstract

Clostridioides difficile is a Gram-positive bacterium that can cause mild to severe diarrhea, inflammation, and colonic tissue damage in animal hosts. Symptoms of disease can be attributed to the activity of TcdB secreted by *C. difficile* during infection. TcdB can engage multiple host cell surface receptors *in vitro*, however, little is known about where these receptors localize on colonic tissue and how these interactions promote disease. In this chapter, I used immunofluorescence microscopy to first visualize TcdB interactions with two of the reported receptors, CSPG4 and Nectin-3, on cells *in vitro*. In cells expressing both receptors, I found that TcdB preferentially interacts with CSPG4 and stimulates CSPG4 entry. In host colonic tissue, I observed novel localization of Nectin-3 within the brush border of epithelial cells and CSPG4 localization at epithelial cell junctions. The unexpected junctional CSPG4 signal led me to the hypothesis that the signal could represent a soluble form of the CSPG4 extracellular domain (ECD) being shed from fibroblasts in the underlying stromal layer of the tissue. To test this hypothesis, I set up a co-culture of epithelial cells and fibroblasts separated by transwell inserts. I observed CSPG4-ECD shed into the media of cultured fibroblasts and an accumulation in epithelial cells following co-culture. I also found that soluble CSPG4-ECD present in the conditioned media from fibroblasts can potentiate TcdB mediated cytopathic responses in epithelial cells lacking CSPG4 expression. Based on these observations, I propose that Nectin-3 can facilitate binding of TcdB at the epithelial surface and that a soluble form of CSPG4 derived from stromal cells can contribute to TcdB intoxication of epithelial cells *in vivo*.

Importance

Toxin B (TcdB) is a major virulence factor of *C. difficile*, a Gram-positive pathogen that is a leading cause of hospital-acquired diarrhea. While previous studies have established that TcdB can engage multiple cell surface receptors *in vitro*, little is known of how these interactions promote disease and where these receptors localize on colonic tissue. Here, I used immunofluorescence microscopy to visualize Nectin-3 and CSPG4 on tissue, revealing unexpected localization of both receptors on colonic epithelial cells. I show that Nectin-3, which was previously characterized as an adherens junction protein, also localized to the brush border of colonocytes. Staining for CSPG4 revealed it is present along epithelial cell junctions, suggesting that it is shed by fibroblasts along the crypt-surface axis. Collectively, my study provides new insights into how TcdB can gain access to the receptors Nectin-3 and CSPG4 to intoxicate colonic epithelial cells.

Introduction

Clostridioides difficile is a Gram-positive, spore-forming anaerobe and is a leading cause of hospital-acquired diarrhea in the United States and Europe. While various antibiotic stewardship efforts have reduced cases of *C. difficile* infection (CDI) worldwide, there are still an estimated 462,000 infections annually in the United States alone, resulting in $1 billion dollars in excess healthcare costs (16, 350). Two major virulence factors of *C. difficile* are toxin A (TcdA) and toxin B (TcdB). These exotoxins damage the host epithelia and promote inflammation in the large intestine, causing symptoms ranging from diarrhea and inflammation in mild cases to pseudomembranous colitis, toxic megacolon, and death in severe cases. While TcdA contributes to symptoms of CDI, the activity of TcdB is necessary and sufficient for severe disease outcomes in various models of infection (101, 105, 110).

The intoxication of cells with TcdB begins with host receptor binding and endocytosis (286, 328). Acidification of the endosome facilitates the delivery of the toxin's N-terminal glucosyltransferase domain (GTD) into the cytosol which can target and inactivate Rho family GTPases such as RhoA, Rac1, and Cdc42. The inactivation of these GTPases results in cytopathic responses such as cell rounding, disruption of tight junctions, and apoptotic cell death (89, 302). In addition to an ability to bind glycans, multiple protein cell surface receptors for TcdB have been identified: chondroitin sulfate proteoglycan 4 (CSPG4), Frizzled (FZD) 1, FZD2, FZD7, Nectin-3, and tissue factor pathway inhibitor (TFPI) (152, 154–158). The receptor specificity can vary depending on toxinotype as there is significant TcdB sequence variation

among *C. difficile* strains. A recent analysis of 3,269 *C. difficile* genomes led to the classification of TcdB into 8 subtypes and concluded that TcdB was undergoing accelerated evolution to maximize diversity (162). Among the 8 subtypes, TcdB1, TcdB2, TcdB3 are the most potent when injected into mice, and the most prevalent among isolates with sequenced genomes (162). TcdB1 can be found in VPI10463, a commonly used lab strain, and has been shown to bind CSPG4, FZD1/2/7, and Nectin-3 with nanomolar affinities (177). The binding sites for CSPG4 and FZD1/2/7 are distinct and, in concept, can be engaged simultaneously, while the binding site for Nectin-3 remains unclear (160, 161). TcdB2 can be found in the epidemic ribotype 027 (RT027) strains and has been shown to bind CSPG4 and Nectin-3, but not FZD1/2/7 (163, 177, 178). TcdB3 can be found in ribotype 078 (RT078) strains and has been reported to bind TFPI (157, 158). While the knockout of each receptor can reduce TcdB mediated cytopathic or cytotoxic effects in cell lines, the role of each receptor in the physiological context of infection remains unclear.

The Nectins are a family of four transmembrane proteins (Nectin-1, -2, -3, -4) that are involved in the regulation of cell-cell adhesions. They are expressed in many cell types and contribute to the formation of apical-basal polarity in epithelial cells. The adhesion properties are mediated through three extracellular immunoglobulin-like domains, and the proteins are anchored by a cytosolic tail that can bind filamentous (F)-actin-binding protein afadin and the cell polarity protein partitioning defective-3 (PAR3) (293, 351). Nectin-3 (previously known as poliovirus receptor-like protein 3 or PVRL3) was identified as a receptor involved in TcdB mediated cytotoxic responses in epithelial cell lines (156, 351). Nectin-3 binds TcdB1 and TcdB2 with affinities of 53 nM and 17 nM, respectively, but the interaction does not facilitate the cytopathic response, leading some to propose that Nectin-3 promotes cellular cytotoxic responses through cell surface signaling events (159, 177). While possible, Nectin-3 is known to undergo cellular entry and recycling, and so the question of why Nectin-3 does not promote cytopathic responses *in vitro* is unclear (352). In addition, other members of the Nectin family serve as entry receptors for a variety of viruses, including the measles virus, herpes simplex virus, morbillivirus, and poliovirus (353–357).

Of the known host proteins that interact with TcdB, genetic deletion of CSPG4 confers the greatest protection from TcdB mediated cell rounding (154). CSPG4, also known as neural-glial antigen 2 (NG2), is a ~300 kDa transmembrane protein involved in cell survival, migration, and angiogenesis. It has been primarily characterized for its roles in the regulation of neuronal networks, endothelial and pericyte

function, and tumor progression in some forms of cancer (180, 230). The large extracellular domain (ECD) is post-translationally modified by chondroitin sulfate glycosaminoglycan chains and disulfide bonds and can serve as a scaffold for extracellular ligands or stimuli and amplifies their signals into the cell (230). For example, CSPG4 can bind platelet derived growth factors (PDGFs) and fibroblast growth factors (FGFs) and amplify their cognate receptor tyrosine kinase activities through direct interactions (193, 208, 209, 219). Other interactions of CSPG4 include the various components of the extracellular matrix and integrins, whose interactions with CSPG4 promote cell motility during angiogenesis and neuronal development (186, 187, 217).

Our initial goal in this study was to characterize TcdB interactions with Nectin-3 and CSPG4 on cells using confocal microscopy. As visualization of TcdB has been historically challenging, we screened various cell lines and identified 18Co, a human colonic fibroblast cell line, for robust TcdB binding and visualization. In these cells, TcdB preferentially co-localized with CSPG4 and could promote CSPG4 endocytosis. I next wanted to visualize the localization of Nectin-3 and CSPG4 *in vivo*, as the physiological roles of these proteins in the colon have not been fully established. In both human and mouse colonic tissue, I observed Nectin-3 at adherens junctions (as expected) but also on the apical surface as part of the brush border. I also observed co-localization of TcdB and Nectin-3 in intoxicated tissue, suggesting that Nectin-3 could have a role in capturing or concentrating TcdB at the apical surface of the epithelium. I observed CSPG4 localization in fibroblasts (as expected) but also in epithelial junctions, leading us to wonder whether this protein could represent CSPG4-ECD shed from the underlying stromal cells. I show that fibroblast derived CSPG4-ECD can accumulate in epithelial cells and potentiate TcdB cytopathic effects. Together, these observations advance the mechanistic understanding of how specific TcdB-receptor interactions may contribute to the pathogenesis of *C. difficile* infection.

Results

Visualization of TcdB with receptors on 18Co cells

In the Lacy Lab and for many other researchers in the *C. difficile* field (*personal communications*), the visualization of TcdB on cells has been challenging. For example, when Caco-2 cells are intoxicated with 10 nM Janelia Fluor 669-labeled TcdB1 (JF669-TcdB1) at 37°C for 30 minutes, no TcdB signal can be observed (**Figure 3-1A**). Knowing that cell lines can differ significantly in their cell surface protein profiles, I analyzed published transcriptomic datasets using the GEO RNA-seq Experiments Interactive Navigator to search for a cell line that expresses abundant levels of the reported TcdB receptors (358). I identified 18Co cells, derived from human colonic myofibroblasts, as cells that express all reported TcdB receptors (**Figure S3-1)** (359–361). When imaged, I found that 18Co cells intoxicated with 10 nM JF669-TcdB1 contained abundant levels of TcdB signal (**Figure 3-1A**). While previous approaches used to visualize TcdB have required conditions with cold temperatures and long incubation periods, 18Co cells simply needed to be treated with labeled TcdB and incubated at 37°C (328).

With the ability to now visualize TcdB on 18Co cells, I looked for TcdB co-localization with Nectin-3 and CSPG4 using immunofluorescence microscopy (**Figure 3-2**). To quantify colocalization, I measured the overlap of receptors and TcdB signal using Manders' Coefficients (*M1=Receptor:TcdB and M2=TcdB:Receptor*) and the correlation of receptor signal with TcdB using the Pearson correlation coefficient (PCC). Analysis of confocal images of intoxicated 18Co cells immunostained for Nectin-3 revealed small levels of colocalization (average $M1$ = 0.31, $M2$ = 0.35) and positive correlation with TcdB (average PCC = 0.31) (**Figures 3-2A, 2C-D**). Analysis of CSPG4 and TcdB revealed medium to large levels of colocalization (average $M1$ = 0.33, $M2$ = 0.68) and positive signal correlation (PCC = 0.44) (**Figures 3-2B, 2C-D**). Thus, while Nectin-3 can colocalize with TcdB1 on 18Co cells, my analysis suggests that CSPG4 is the preferred interaction.

TcdB receptors undergo passive and active endocytosis

A previous study using mouse embryonic fibroblasts reported that neither Nectin-3 or CSPG4 are endocytosed, even in the presence of TcdB, during a typical intoxication period (159). Those observations

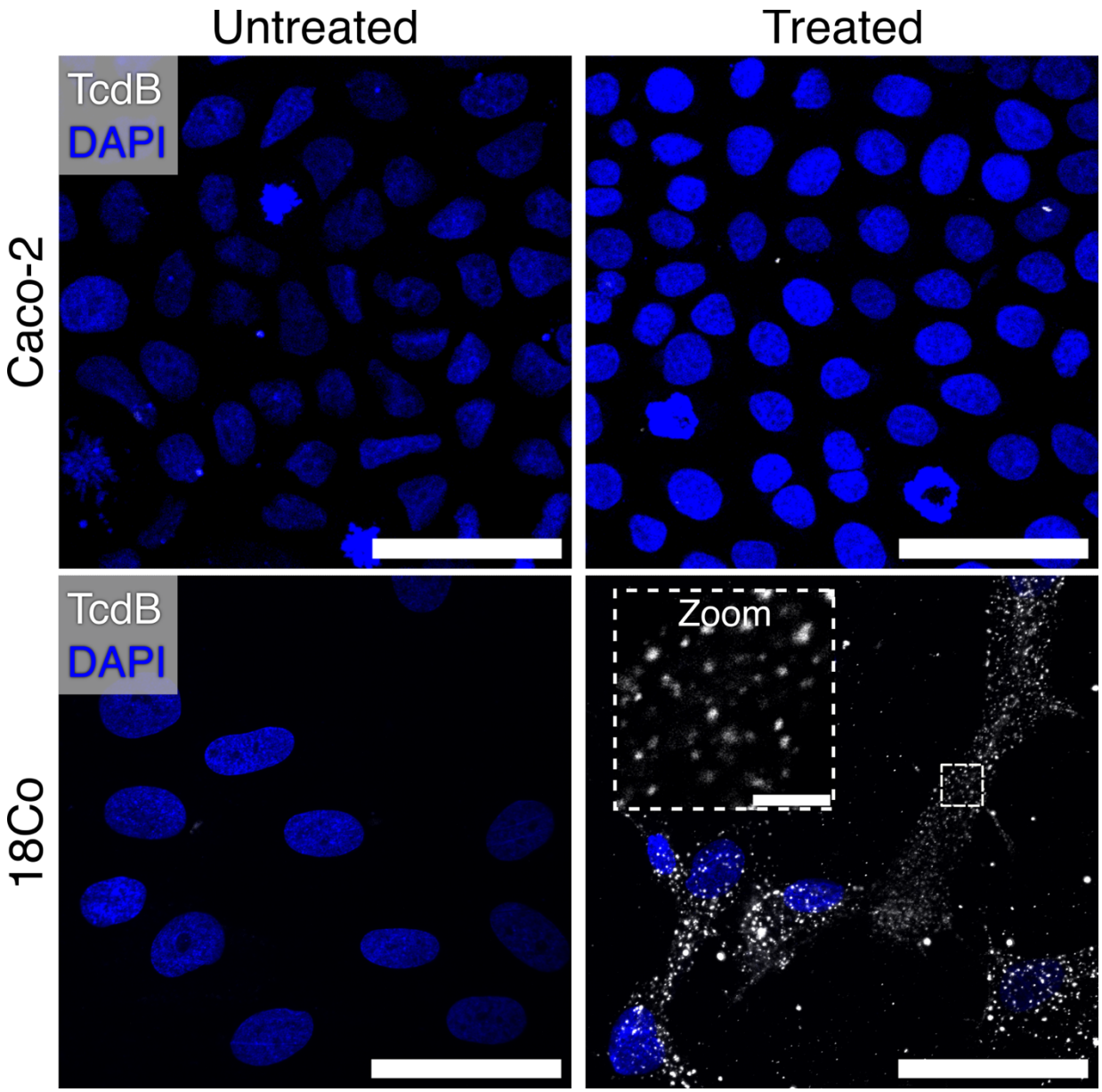

Figure 3-1. 18Co cells can be used to visualize TcdB

Confocal images comparing Caco-2 and 18Co cells intoxicated with 10 nM JF-669 TcdB1 (white) for 30 minutes and labeled with DAPI (blue). TcdB is not detected in Caco-2 cells while it is detected in 18Co cells. Images are shown as max intensity projections while the zoomed panel is shown as a single Z-plane. Scale bars, 50 μm and 5 μm (zoom).

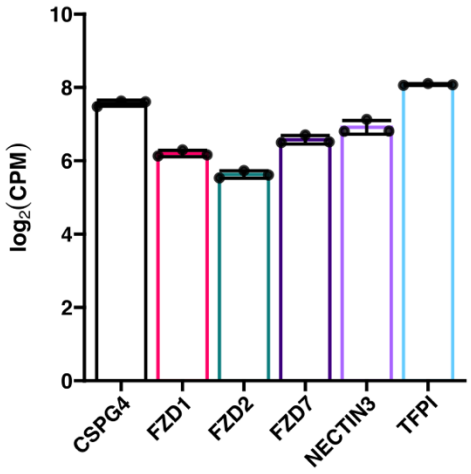

Figure S3-1. Transcriptional analysis of 18Co cells indicates the expression of all TcdB receptors

Normalized transcripts of TcdB receptors in 18Co cells were obtained from the GSE89124 dataset and analyzed with GREIN. The log2 transformed counts per million (CPM) are presented on the y-axis and the individual genes are on the x-axis. Individual data points are expression levels of each sample and error bars represent the standard deviation. **P<0.01.

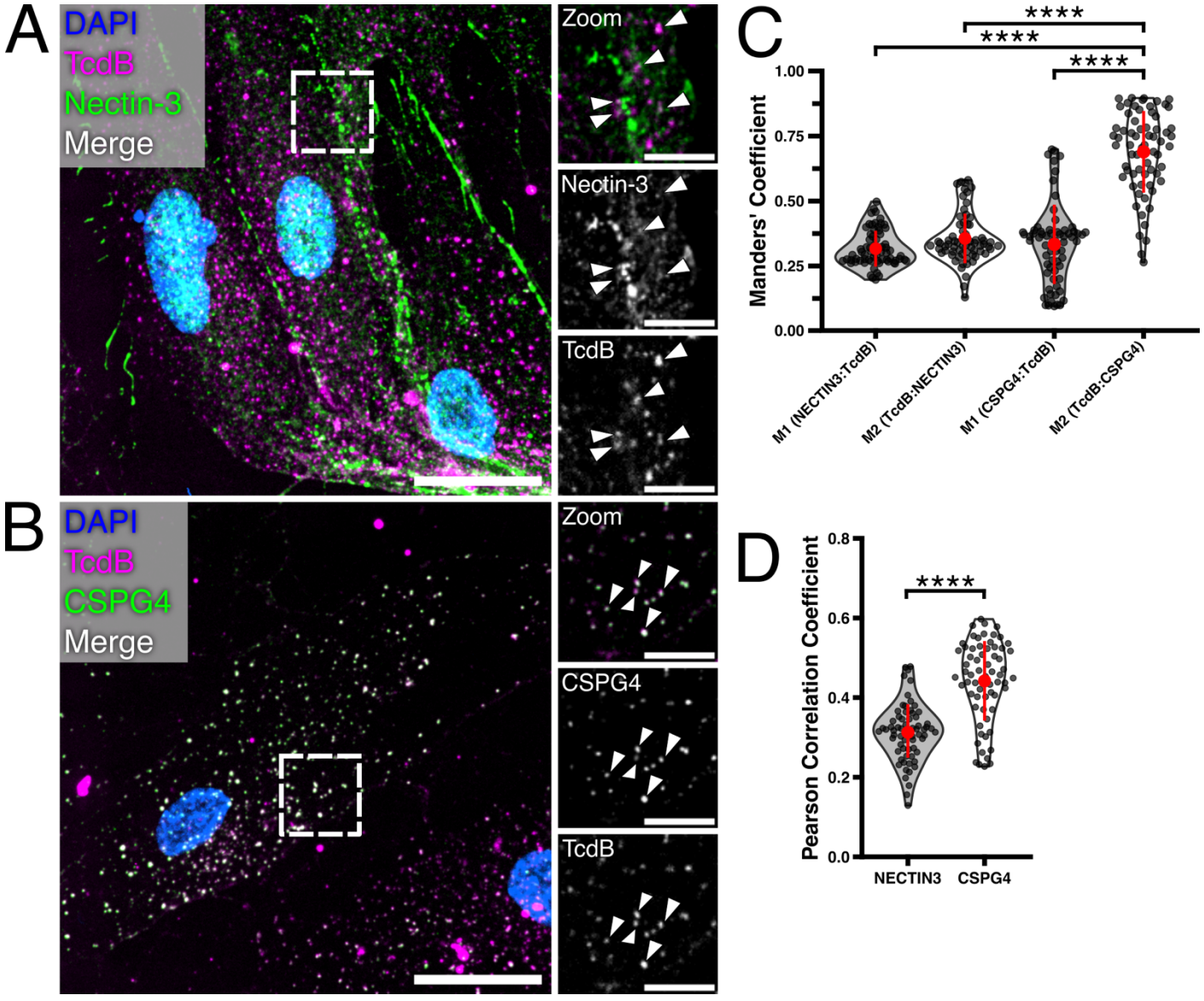
A
DAPI
TcdB
Nectin-3
Merge
Zoom
Nectin-3
TcdB
B
DAPI
TcdB
CSPG4
Merge
Zoom
CSPG4
TcdB
C
****
****
****
Manders' Coefficient
1.00
0.75
0.50
0.25
0.00
M1 (NECTIN3:TcdB)
M2 (TcdB:NECTIN3)
M1 (CSPG4:TcdB)
M2 (TcdB:CSPG4)
D
****
Pearson Correlation Coefficient
0.8
0.6
0.4
0.2
0.0
NECTIN3
CSPG4

Figure 3-2. TcdB primarily colocalizes with CSPG4 on 18Co cells

A) Confocal image of 18Co cells immunostained for Nectin-3 and treated with JF669-TcdB1 for 30 minutes. Dashed box represents location of zoomed panels. The main image is presented as a max intensity projection while the zoomed panels are shown as a single Z-plane. Scale bars, 30 μm and 10 μm (zoom). Arrows indicate locations of colocalized signal.

B) Confocal image of 18Co cells treated with JF669-TcdB1 for 30 minutes and immunostained for CSPG4. Dashed box represents location of zoomed panels. The main image is presented as a max intensity projection while the zoomed panels are shown as single Z planes. Scale bars, 30 μm and 10 μm (zoom). Arrows indicate locations of colocalized signal.

C) Manders' coefficient analyses of Receptor signal overlap with TcdB (M1) or TcdB signal overlap with Receptors (M2). Points represent individual Manders' coefficients. The error bar in red represents the mean and standard deviation. ****P<0.0001, Kruskal-Wallis ANOVA test and corrected for multiple comparisons using Dunn's post-hoc test. N=5

D) Pearson correlation coefficient analysis of TcdB colocalization with Nectin-3 or CSPG4. Points represent individual Pearson coefficients. The error bar in red represents the mean and standard deviation. ****P<0.0001, Mann-Whitney U Test. N=5

led to a proposal that CSPG4 and Nectin-3 sequester TcdB to the cell surface before transferring TcdB to its entry receptor. I performed a similar endocytosis assay on 18Co cells using reversible cell surface biotinylation to characterize the significance of the TcdB colocalization with its receptors. Briefly, 18Co cells were chilled at 4˚C for an hour to inhibit endocytosis and then treated with a cell membrane-impermeant reducible biotinylation reagent. Next, biotinylated cells were treated with TcdB2 to avoid endocytic responses mediated by FZDs at 37˚C for 20 minutes to allow for endocytosis (177). Cells were then treated with a cell membrane-impermeant reducing reagent to remove biotin from non-endocytosed proteins, lysed, and a pulldown using streptavidin beads was performed to capture endocytosed biotinylated proteins. PDGF-AA, a ligand reported to interact with CSPG4, was used as a control ligand while detection of LRP1, a constitutively endocytosed protein, was used to confirm the removal of surface biotin. Western blot analysis of endocytosed cargo revealed that both Nectin-3 and CSPG4 are recycled over a 20-minute period in the absence of any stimuli (**Figure 3-3**). I did not observe any TcdB-dependent enhancement in the levels of endocytosed Nectin-3 (**Figure 3-3A**). However, endocytosed CSPG4 was significantly increased in the presence of TcdB (**Figure 3-3B**). These data suggest that in 18Co cells, Nectin-3 and CSPG4 could provide either passive or active entry mechanisms for toxin.

Nectin-3 Localizes to the Colonic Epithelial Brush Border and Apical Cell Junctions

Nectin-3 belongs to a family of adhesion proteins that promote the formation of adherens junctions during the initial interactions between polarized cells (362). Since the 18Co cells do not form polarized junctions, I decided to turn to the epithelial cells of colonic tissue for imaging TcdB interactions with Nectin-3. Previous studies have established that Nectin-3 is expressed *in vivo* on mouse colonic epithelial cells with epifluorescence microscopy (363). I attempted to replicate these previous studies using human colonic tissue. As expected, we observed Nectin-3 signal at the epithelial cell junctions (**Figure 3-4A**). In addition, Nectin-3 signal was present along the apical surface of the cell, potentially within the brush border (**Figure 3-4A, zoomed panels**). The brush border is an array of microvilli supported internally by bundles of actin and organized externally by adhesion proteins (364). To acquire higher resolution images, I collaborated with a graduate student from Matthew J. Tyska's Lab, Caroline S. Cencer, here at Vanderbilt University to more clearly resolve the brush border localized Nectin-3 signal using structured illumination microscopy (**Figure 3-4B, zoom**). These images revealed that Nectin-3 is indeed present within the brush border on colonic epithelial cells. While the role of Nectin-3 within the microvilli is unresolved, Nectin-3 can also

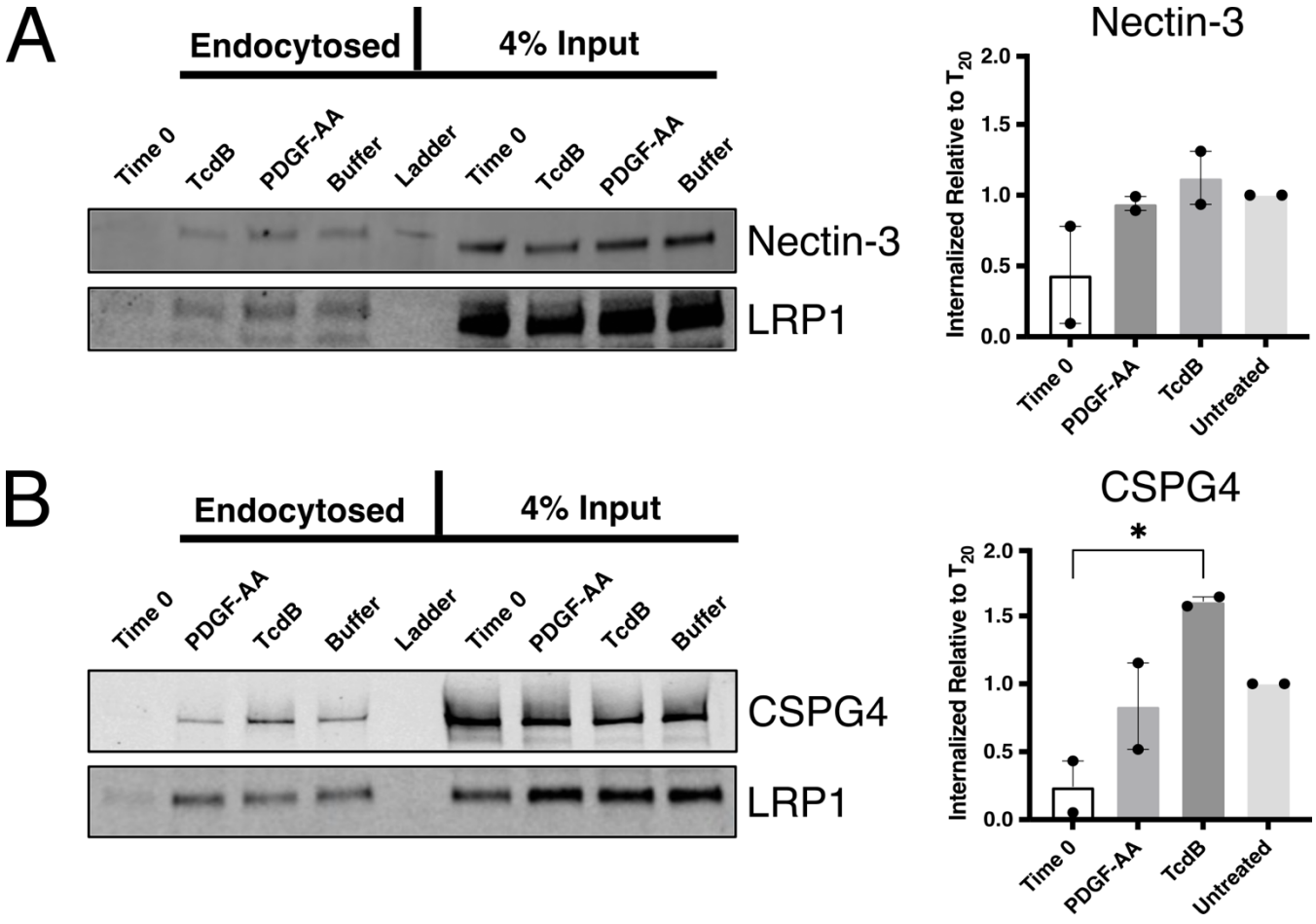

Figure 3-3. CSPG4 endocytosis is enhanced in the presence of TcdB

A) Western blot analysis from an endocytosis assay probed for Nectin-3. Levels of endocytosed Nectin-3 were determined using densitometry and normalized to levels of Nectin-3 at 20 minutes in cells treated with buffer alone. N=2

B) Western blot analysis from an endocytosis assay probed for CSPG4. Levels of endocytosed CSPG4 were determined using densitometry and normalized to levels of CSPG4 at 20 minutes in cells treated with buffer alone. Statistical analysis performed using a Kruskal-Wallis ANOVA test and corrected for multiple comparisons using Dunn's post-hoc test. *P<0.05, N=2

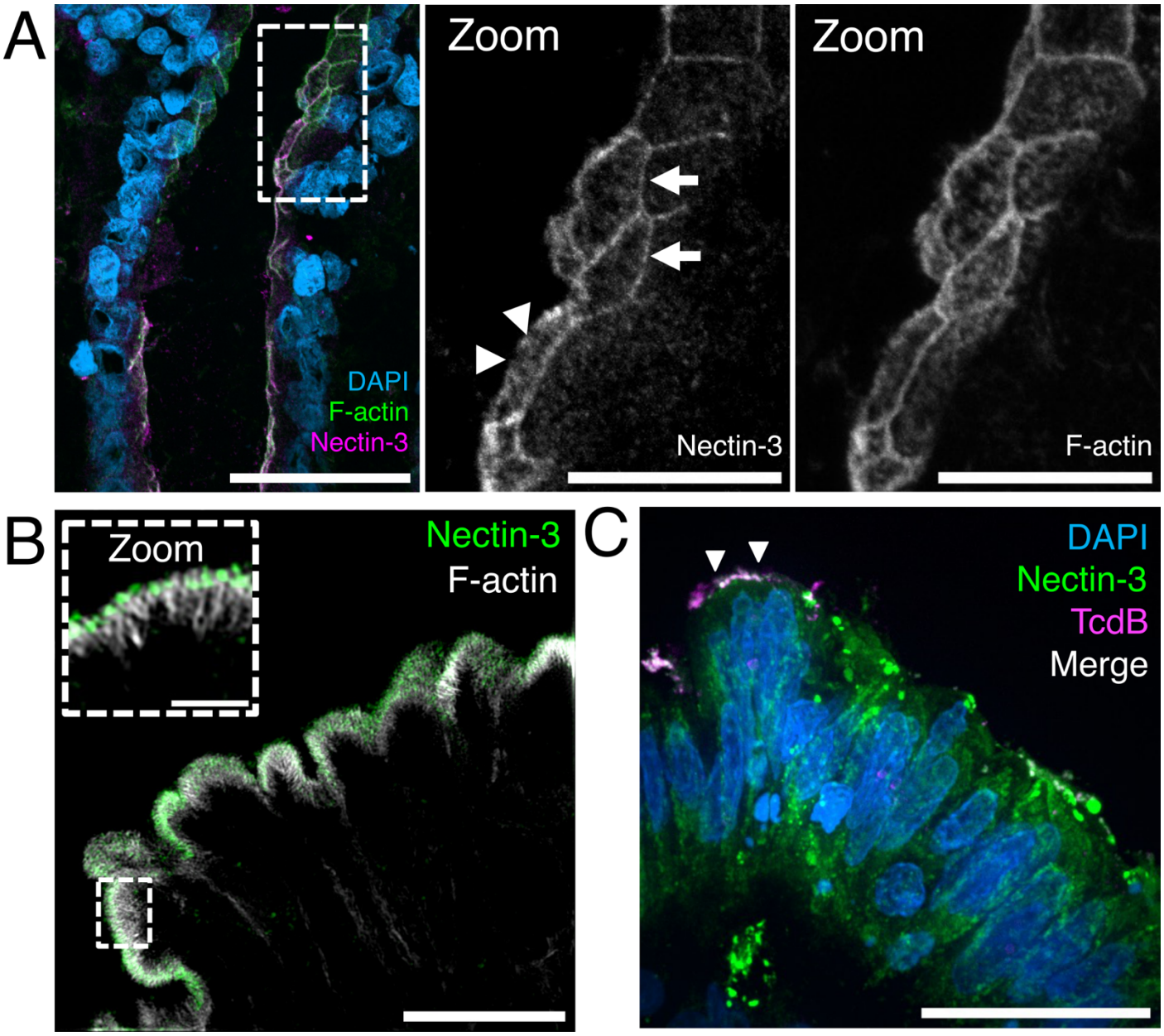
A
DAPI
F-actin
Nectin-3
Zoom
Nectin-3
Zoom
F-actin
B
Zoom
Nectin-3
F-actin
C
DAPI
Nectin-3
TcdB
Merge

Figure 3-4. NECTIN-3 localizes to the brush border on colonic epithelium

A) Confocal image of human colonic tissue stained for Nectin-3, F-actin, and DAPI. Dashed boxes represent origin of zoomed image. Arrowheads indicate signal localized to apical surface of cells while arrows indicate areas of junction. Scale bars, 50 μm and 20 μm (zoom).

B) Structured illumination microscopy image of human colonic epithelium stained for Nectin-3 and F-actin. Dashed boxes represent origin of zoomed imaged. The main image is presented as a max intensity projection while the zoomed panels are shown as a single Z-plane. Scale bars, 10 μm and 2 μm (zoom). Credit: C.S. Cencer from M.J. Tyska's Lab with permission.

C) Confocal image of a human colonic explant intoxicated with JF669-TcdB1 and stained for Nectin-3. Scale bar, 30 μm.

be observed within the brush border of polarized Caco-2 cells (**Figure S3-2**). These findings suggest that Nectin-3, and perhaps other Nectin family proteins, has a role in brush border structure and function.

With the unexpected finding that Nectin-3 localizes to the brush border of colonic epithelial cells, I wanted to determine if TcdB could interact with Nectin-3 on colonic tissue. I intoxicated human colonic explants with JF669-TcdB1 and immunostained the tissue for Nectin-3 (**Figure 3-4C**). While detection of JF669-TcdB1 was infrequently observed, colocalization between Nectin-3 and JF669-TcdB1 was observed along the apical surface of the colonic epithelium. These data suggest a role for Nectin-3 in binding to TcdB along the luminal surface of cells.

Colonic Epithelial Tissue is CSPG4(+)

While single cell sequencing studies have consistently shown *CSPG4* expression among various fibroblast populations along the crypt-surface axis of the intestines (**Figure 3-5A**), there is no evidence for *CSPG4* expression in colonic epithelial cells (199, 365). I analyzed a published single cell RNA-sequencing (scRNA-seq) dataset from the Human Gut Cell Atlas derived from 77,341 $EPCAM^+$ epithelial cells from the small intestine, large intestine, appendix, and rectum of healthy adults to determine if *CSPG4* expression could be found in any epithelial cell populations (260). Among these epithelial populations, I was unable to detect CSPG4 expression, confirming that *CSPG4* expression is isolated to stromal populations in the colon (**Figure 3-5B**).

While imaging CSPG4 on mouse colonic tissue, I observed the predicted CSPG4 signal in fibroblasts that line the crypt surface axis (**Figure 3-5C, zoom**). However, to our surprise, I also observed CSPG4 signal along the junctions of epithelial cells. To verify this staining pattern, I stained colonic tissue from $CSPG4^{-/-}$ mice for CSPG4 (**Figure S3-3**). These mice lacked CSPG4 signal on both fibroblasts and the junctions of colonic epithelial cells. I also stained human colonic tissue for CSPG4 and found that both fibroblasts and epithelial tissue stained positive for CSPG4 (**Figure 3-5D**). These data led us to wonder whether fibroblasts along the crypt-surface axis could shed CSPG4 extracellular domain (ECD) that would then associate with the epithelium.

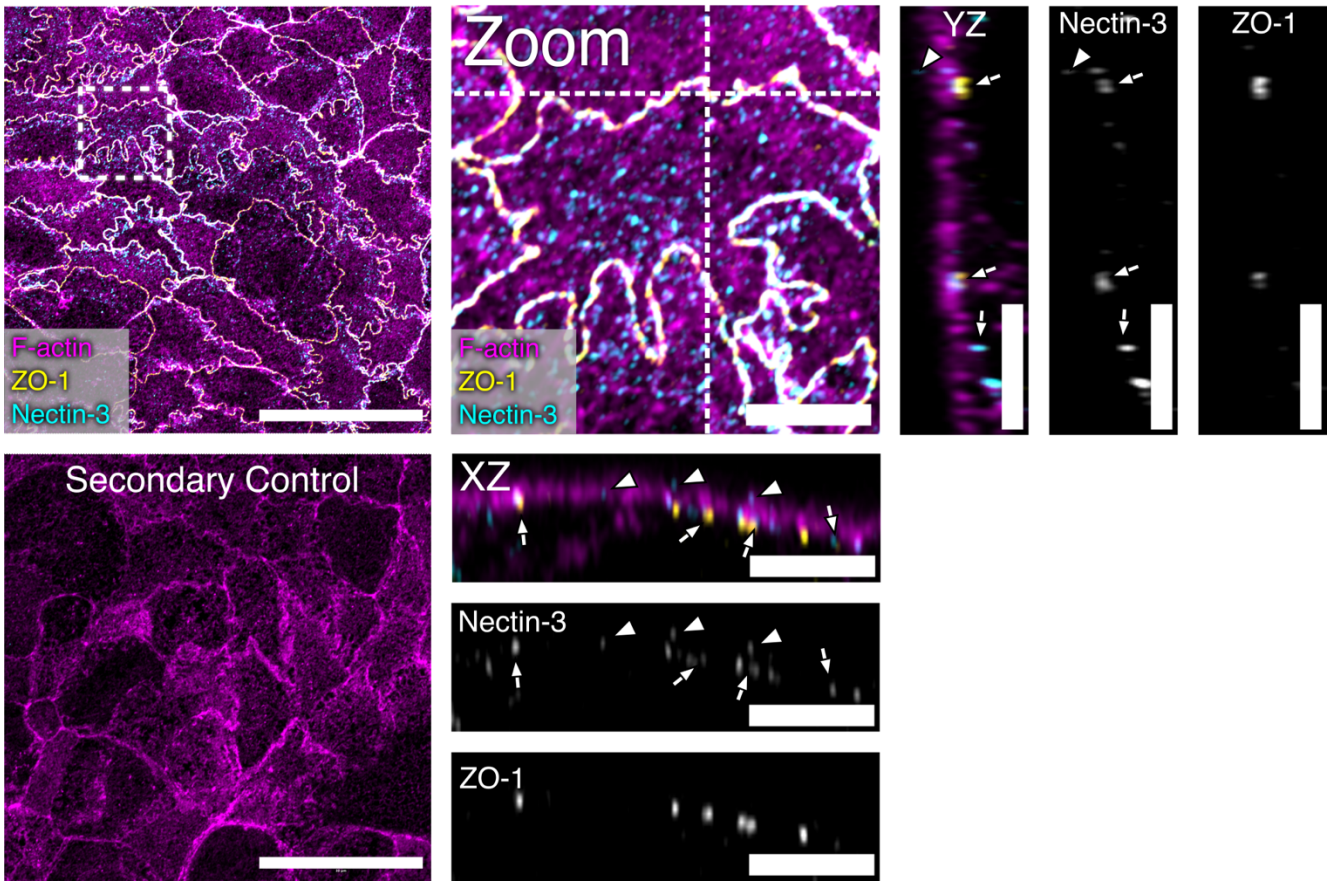

Figure S3-2. NECTIN-3 localizes to the brush border and cell junctions in Caco-2 cells.

Confocal image of Caco-2 cells stained for F-actin, Nectin-3, and ZO-1 or stained with only secondary antibodies and F-actin. Dashed box represents location of zoomed image. Dashed lines in zoom panel indicate location of orthogonal views. Arrowheads indicate Nectin-3 signal localized to the brush border and arrows indicate Nectin-3 signal in junctions. Scale bars, 30 μm and 5 μm (zoom).

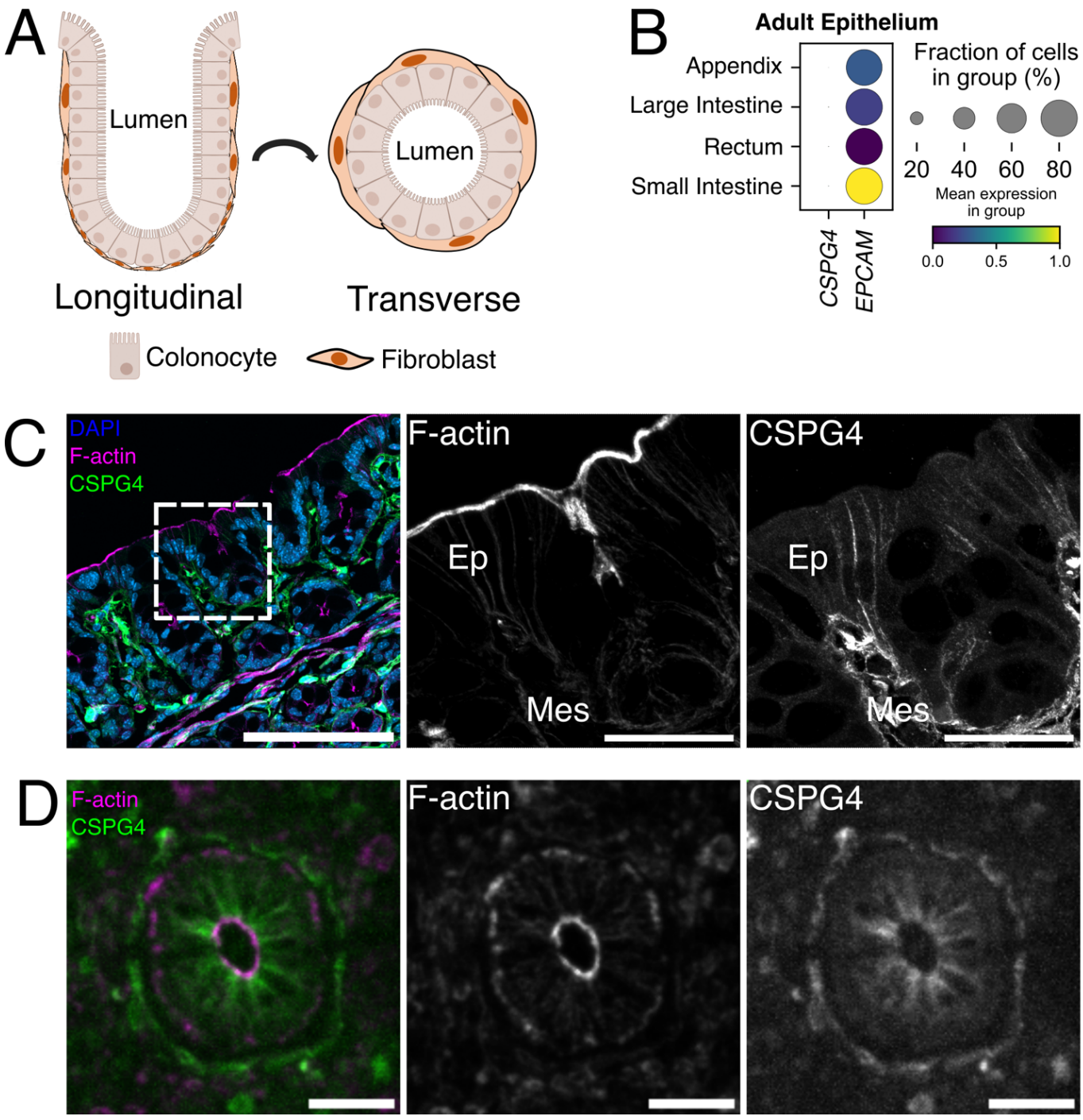
A
Lumen
Lumen
Longitudinal
Transverse
Colonocyte
Fibroblast
B
Adult Epithelium
Appendix
Large Intestine
Rectum
Small Intestine
CSPG4
EPCAM
Fraction of cells in group (%)
20
40
60
80
Mean expression in group
0.0
0.5
1.0
C
DAPI
F-actin
CSPG4
F-actin
Ep
Mes
CSPG4
Ep
Mes
D
F-actin
CSPG4
F-actin
CSPG4

Figure 3-5. Mouse and human colonic epithelial cells stain positive for CSPG4.

A) Model of the colonic crypt-surface axis

B) Analysis of single cell RNA expression data from human adult intestinal epithelial cells (*Gut Cell Atlas*) reveals that *cspg4* is not expressed in epithelial cells of human intestines.

C) Confocal images of wild-type B57/C6 mouse colon stained for CSPG4. Mouse epithelial cells and fibroblasts stained positive for CSPG4. Dashed boxes indicate location of zoomed images. Scale bars, 50 μm and 30 μm (Zoom)

D) Confocal images of a cross section of human ascending colon stained for CSPG4. Both fibroblasts and epithelial cells stained positive for CSPG4. Scale bars, 50 μm

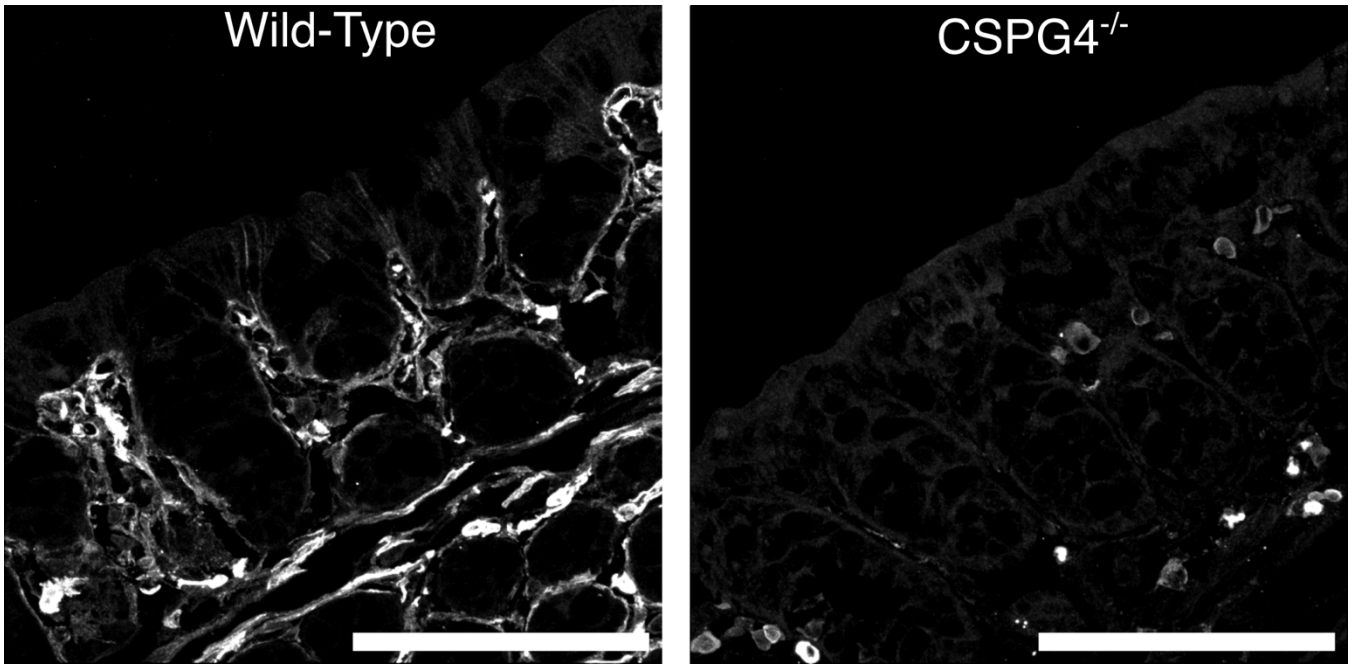

Figure S3-3. CSPG4 stains epithelial cells and fibroblasts in the colon.

Confocal images of wild-type B57/C6 mouse (from Figure 5C) or CSPG4 knockout mouse colon stained for CSPG4. Epithelial cells and fibroblasts stain positive for CSPG4 in wild-type colon tissue while staining is absent in CSPG4 knockout mice. Scale bars, 50 μm.

Caco-2 Cells Accumulate Fibroblast Derived CSPG4-ECD

The extracellular domain (ECD) of CSPG4 can be targeted by various proteinases, resulting in its release from the cell surface (232–234, 239). In various cancer cell lines, this can include what is essentially the full length CSPG4-ECD (238). I isolated and lysed crypts from mouse colons to determine if I could detect any cleaved forms of CSPG4 by Western blot (**Figure 3-6A**). Analysis of these lysates revealed that CSPG4 exists as two primary species, with one band >250 kDa matching the mature molecular weight of CSPG4 found in 18Co cells and another approximately 240 kDa band that is consistent with the size of the cleaved CSPG4-ECD.

A possible source of shed CSPG4 could be from stromal cells such as myofibroblasts found along the crypt-surface axis. As 18Co cells are a normal, non-transformed colonic myofibroblast cell line, I analyzed its conditioned media by Western blot to determine if these cells were capable of shedding CSPG4-ECD into its environment (**Figure 3-6B**). Conditioned media were collected and filtered after culturing the cells in complete DMEM for 5 days. The analysis revealed that soluble CSPG4-ECD is indeed present in conditioned media. I also verified that CSPG4-ECD is not a component of complete culture media (**Figure 3-6B**).

I next asked if this 18Co derived CSPG4-ECD could be transferred to Caco-2 cells, a human colonic epithelial cell line through co-culture. Caco-2 cells were grown in cell inserts above 18Co cells for 5 days before collecting and lysing the Caco-2 cells. A control condition of Caco-2 cells grown for 5 days without 18Co cells was included. Over a 5-day period, I observed increasing intensities of CSPG4 in the Caco-2 lysates (**Figure 3-6C**). Over the same period, I was unable to detect CSPG4 in the Caco-2 cells grown without 18Co cells. As fibroblasts of the crypts express CSPG4 and line the crypt-surface axis, these data suggest colonic epithelial cells possibly derive CSPG4-ECD from fibroblasts though an endocytic mechanism. I then stained Caco-2 cells for CSGP4 after growing them 5 days on cell inserts above 18Co cells. CSPG4 signal in Caco-2 cells grown above 18Co cells localized to the cytosolic compartment of the Caco-2 cells (**Figure 3-6D**). These data suggest that CSPG4-ECD derived from 18Co cells can enter Caco-2 cells.

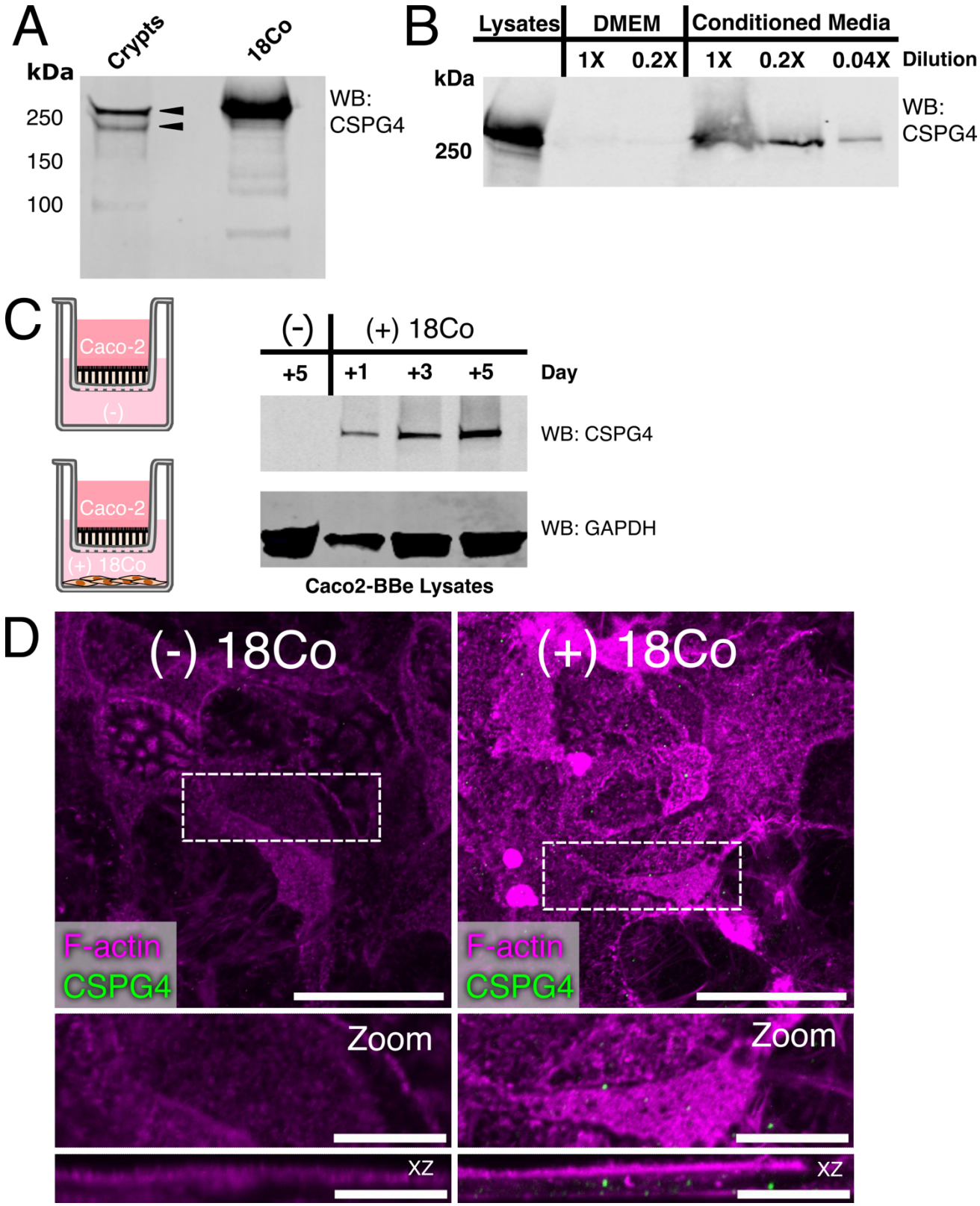
A
Crypts
18Co
kDa
250
150
100
WB:
CSPG4
B
Lysates
DMEM
Conditioned Media
1X
0.2X
1X
0.2X
0.04X
Dilution
kDa
250
WB:
CSPG4
C
Caco-2
(-)
Caco-2
(+) 18Co
(-)
(+) 18Co
+5
+1
+3
+5
Day
WB: CSPG4
WB: GAPDH
Caco2-BBe Lysates
D
(-) 18Co
(+) 18Co
F-actin
CSPG4
F-actin
CSPG4
Zoom
Zoom
XZ
XZ

Figure 3-6. Fibroblasts derived CSPG4 is endocytosed by Caco-2 cells

A) A CSPG4 fragment corresponding to the putative MW of a full length CSPG4-ECD is present in purified human colonic crypt lysates. Lysates from 18Co cells was used as a reference for the full length CSPG4.

B) 18Co cells were grown for 5 days and the conditioned media was analyzed for CSPG4 by Western blot. To resolve clearer bands of CSPG4 from the conditioned media, the media was diluted to 0.2X or 0.04X. Complete media, DMEM + 10% FBS, was also analyzed for CSPG4 by Western blot. CSPG4 was detected only in 18Co lysates and conditioned media.

C) Caco-2 cells were grown above 18Co cells in transwells and were collected and lysed on days 1, 3, and 5 and analyzed for CSPG4 by Western blot. Caco-2 lysates grown with 18Co cells contained CSPG4, while the negative condition grown without 18Co cells did not.

D) Confocal images of 5-day post confluency Caco-2 cells grown above 18Co cells in transwells and stained for CSPG4. Dashed boxes indicate the origin of zoomed panels and are shown as max projections in both xy and xz.

CSPG4(+) Conditioned Media Potentiates Cell Rounding

Given our observation that CSPG4-ECD can associate with Caco-2 cells, I next asked if the 18Co-derived CSPG4-ECD would promote TcdB-induced cytopathic effects in Caco-2 cells. For these studies, I used TcdB2 to eliminate any FZD 1/2/7 responses. I intoxicated Caco-2 cells with 1 pM TcdB2 and 18Co conditioned media and found that these intoxicated cells rounded faster in the presence of conditioned media (data not shown). To determine if this rounding was dependent on CSPG4-ECD, I collected conditioned media from 18Co cells treated with siRNA targeting *CSPG4* or with a non-targeting control. Treatment of 18Co cells with *siRNA* targeting *CSPG4* was effective at depleting CSPG4 in the media (**Figure 3-7A**). I then intoxicated Caco-2 cells with 1 pM TcdB2 in CSPG4(+) or CSPG4(-) 18Co conditioned media and observed that this potentiation of cell rounding was CSPG4-dependent (**Figure 3-7A, top**). I also asked if I could block CSPG4-ECD from interacting with cells by adding antibodies targeting CSPG4 to the conditioned media. Pre-incubation of conditioned media with an anti-CSPG4 antibody prior to intoxication of cells with 1 pM TcdB2 was sufficient at inhibiting potentiation of rounding (**Figure 3-7B**). Together, these data suggest that soluble CSPG4 can enhance the cytopathic effects of TcdB on epithelial cells, even in the absence of epithelial *CSPG4* transcript expression.

Discussion

TcdB is a key virulence factor in *C. difficile* infection (CDI). It is expressed by *C. difficile* in the lumen of the colon, and therefore the epithelial cells that form the barrier between the host and microbiota are expected to represent the first cells that the toxin will encounter. As intoxication requires receptor-mediated endocytosis, multiple studies have focused on the identification of epithelial cell surface proteins that can serve as TcdB receptors. The studies have largely been conducted *in vitro* using a combination of cell-based genetic screens and biochemical analyses and have led to the identification of multiple cell surface proteins that could be contributing to TcdB-induced symptoms (154–158). However, the understanding of if and how each receptor may contribute to intoxication *in vivo*, has been unclear for several reasons. First, the receptors that have been identified are not thought to be expressed on the apical surface of polarized cells. FZD 1/2/7, Nectin-3, and TFPI have all been reported to have lateral or basolateral expression, and CSPG4 is not thought to be expressed at all in epithelial cells. The proteins could still serve as receptors for TcdB that passes the barrier of the polarized epithelium, but the question of how the toxin makes initial contact with the epithelium has been unclear. Second, TcdB is a highly

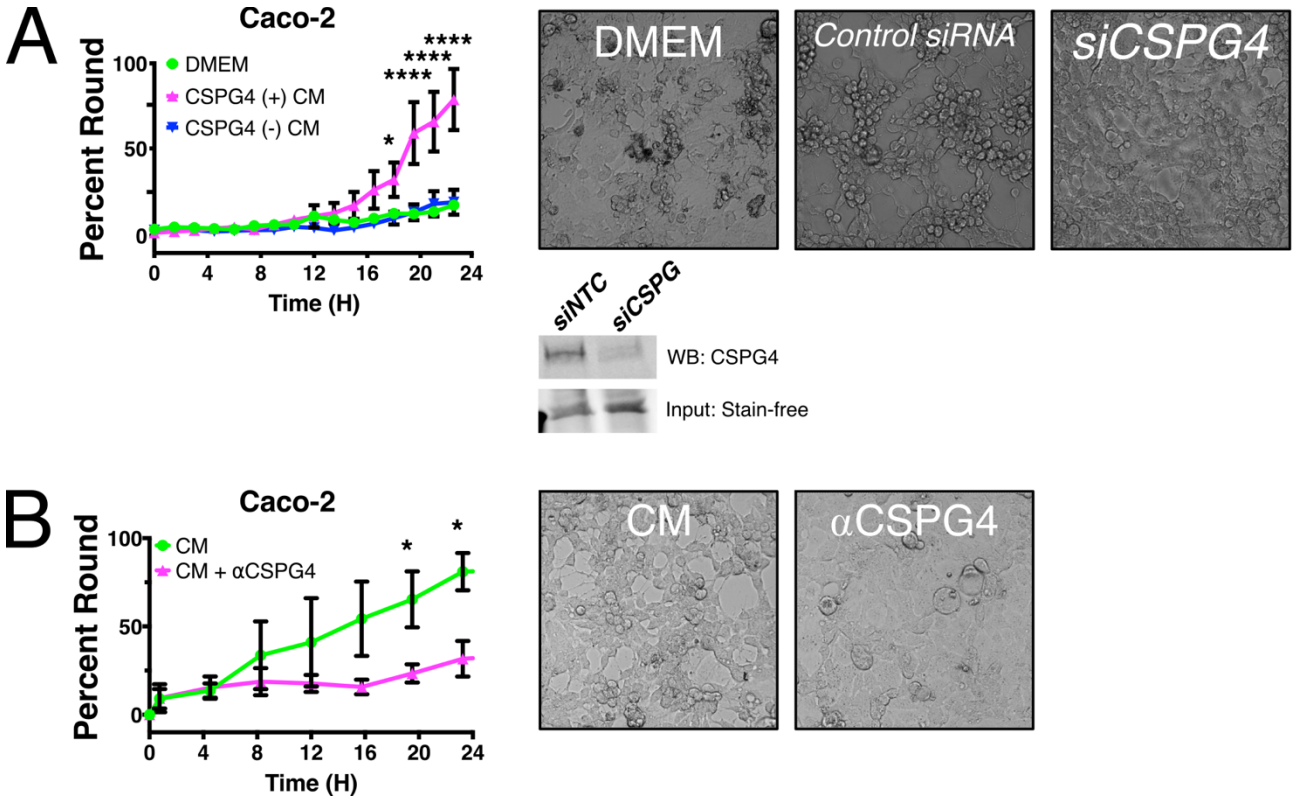

Figure 3-7. Fibroblast derived conditioned media containing CSPG4 promotes rounding in cells lacking CSPG4

A) Caco-2 cells were intoxicated with 1 pM TcdB2 in complete media (DMEM) or conditioned media from siRNA treated 18Co cells targeting *a non-targeting control* (Control siRNA) or *CSPG4*. Rounding was quantified from images acquired over the course of the experiment. Images to the right are representative images from these experiments. Statistical analysis performed using a two tailed ANOVA with a Sidak Post-hoc test for multiple comparisons. N=3 *P<0.05, ****P<0.001.

B) Conditioned media (CM) from 18Co cells was treated with antibodies targeting CSPG4 prior to the intoxication of Caco-2 cells with 1 pM TcdB2. Conditioned media lacking antibodies targeting CSPG4 rounded over a 24-hour period. Representative images from these assays are shown on the right. Statistical analysis performed using a two tailed ANOVA with a Sidak Post-hoc test for multiple comparisons. Images to the right of the graph are representative images from these experiments. N=3 *P<0.05

potent toxin capable of inducing cytopathic responses with EC_{50} values in the fM-pM range, depending on the cell type. The protein receptors identified to date, each bind TcdB with nM affinities. While these affinities are tight by some standards, they are weak when considering the potency of TcdB. The potency of TcdB suggests the need for co-receptor interactions, but it is unclear which receptor pairs are co-expressed and co-localized in the same cells to be available for binding to TcdB. Lastly, the question of endocytosis has largely been examined indirectly, using the cytopathic rounding response as a proxy for cellular endocytosis. The direct visualization of TcdB requires high concentrations that are rapidly cytotoxic and likely not representative of what one would find in an early stage of CDI.

In this study, we characterized the localization of Nectin-3 and CSPG4 within the colon using immunofluorescence confocal microscopy. Our initial predictions that Nectin-3 would localize to the junctions of epithelial cells and CSPG4 would localize to fibroblasts below the crypt-surface axis were confirmed. However, I also found that Nectin-3 and CSPG4 localized to additional and unexpected locations on epithelial cells. In addition to the epithelial cell junctions (**Figure 3-4A**), I found Nectin-3 localized at the epithelial brush border in microvilli (**Figure 3-4B**). With CSPG4, I saw robust localization with fibroblasts along the crypt-surface axis but also at the junctions of epithelial cells (**Figure 3-5C**). Since epithelial cells do not express *CSPG4* transcripts (**Figure 3-5B**), I reasoned that the CSPG4 signal represented soluble CSPG4-ECD shed by the underlying fibroblasts. Indeed, I showed that a shed form of CSPG4 is present in lysates from murine colonic crypts (**Figure 3-6A**), similar to an observation reported in another study showing that a shed form of CSPG4 is present in lysates from the small intestine of mice (203).

Since both receptors are capable of binding TcdB, I attempted to visualize fluorescently labeled TcdB with receptors on colonic tissue. While I could show evidence that TcdB colocalizes with Nectin-3 on colonic explants intoxicated with TcdB (**Figure 3-4C**), the TcdB signal was infrequent, consistent with the challenge of trying to visualize a potent toxin *in vivo*. Therefore, I used cell culture models to ask if TcdB is capable of colocalizing with these receptors. Historically, visualization of TcdB is challenging, with various cell lines showing little to no signal after intoxication (328). I show that 18Co cells provided strong signal for TcdB (**Figure 3-1**) and that both Nectin-3 and CSPG4 are capable of colocalizing with TcdB with modest to high levels of correlation (**Figure 3-2D**). Our measurement of colocalization using the Manders' correlation coefficient showed that on average 68% TcdB signal overlapped with CSPG4

(**Figure 3-2C**), revealing that CSPG4 is the preferred receptor on 18Co cells. The observation that TcdB had greater levels of colocalization with CSPG4 than Nectin-3 was surprising, as both receptors have similar reported affinities with TcdB. In considering the possible explanations for this difference, it could be that the receptors differ in their accessibility at the cell surface or that the affinity of TcdB for CSPG4 on the cell surface is tighter than what was observed with a recombinant fragment of the protein (155, 177). Alternatively, a higher affinity interaction between TcdB and CSPG4 could be mediated through co-receptor interactions with glycans on CSPG4 or with the various proteins CSPG4 interacts with along the cell surface (152, 180). Of note, while both CSPG4 and Nectin-3 appeared to enter 18Co cells, TcdB appeared to stimulate an increase in CSPG4 entry, suggesting either the engagement of co-receptors or a signaling component associated with the TcdB-CSPG4 interaction (**Figure 3-3**).

The observation that a shed form of CSPG4 exists within the colon led us to test if shed forms of CSPG4-ECD contribute to TcdB mediated cytopathic effects. I found that 18Co cells shed abundant levels of CSPG4 into the media over time (**Figure 3-6B**). I noted that Caco-2 cells, which lack CSPG4 expression, accumulate CSPG4 when supported by 18Co cells on transwells (**Figure 3-6C**). Moreover, I found that 18Co conditioned media containing shed CSPG4 potentiated Caco2 cell rounding in response to concentrations of TcdB2 that typically do not induce a cytopathic response (**Figure 3-7A**). The presence of CSPG4 in the conditioned media was required for this potentiation, as conditioned media derived from 18Co cells treated with siRNA targeting *CSPG4* (**Figure 3-7A**) or incubated with an antibody targeting CSPG4 (**Figure 3-7B**) were unable to promote cell rounding. Together, these data suggest that shed forms of CSPG4-ECD can bind the cellular junctions of epithelial cells and could contribute to TcdB intoxication *in vivo*.

The observations of this study raise a new series of questions, however. First, while the co-localization of TcdB and Nectin-3 on the brush border provides conceptual evidence that Nectin-3 could represent a readily accessible binding partner for TcdB being made in the colon, I still do not know if Nectin-3 can mediate TcdB entry and intoxication *in vivo*. Further studies to map the Nectin-3-TcdB binding interaction are needed to dissect the functional importance of this interaction.

Second, while I showed CSPG4 localized at epithelial junctions *in vivo* and that shed CSPG4-ECD can potentiate TcdB-induced cytopathic responses on epithelial cells *in vitro*, I still do not know if shed CSPG4-ECD potentiates TcdB intoxication of the epithelial layer *in vivo*. However, such a mechanism

would be consistent with studies showing that *cspg4*$^{-/-}$ mice infected with *C. difficile* or wild-type mice challenged with mutant TcdB lacking the ability to interact with CSPG4 experience significantly lower epithelial injury and overall disease (160).

Third, if the shed CSPG4 ectodomain is, in fact, acting as a TcdB receptor on epithelial cells, then what molecules are responsible for the binding and entry of TcdB-bound CSPG4-ECD? Given the vast number of known CSPG4 binding partners, which include growth factors as well as type V or VI collagens, perlecan, α-integrins, and Galectin-3 (186, 211, 217), I was not able to tackle this question in the scope of this study. However, it is also possible that the localization of CSPG4-ECD at the junctions provides TcdB with the necessary co-receptor pairing for Nectin-3, FZD1/2/7, and or TFPI- mediated events. Such pairings would not be plausible when considering cellular receptor expression profiles in isolation but could become relevant in the environment of colonic tissue. Further studies to examine these complex interactions *in vivo* are needed in the effort to identify the key intervention points for blocking TcdB-induced pathology in CDI.

Materials and Methods

Cell Lines and Reagents

18Co (CCD-18Co, ATCC), HEK293T cells were cultured in Dulbecco's Modified Eagle's Medium (DMEM), with high glucose, sodium pyruvate, L-glutamine (Gibco), and 10% fetal bovine serum (FBS, Corning). Caco-2 (C2BBe1, ATCC) cells were cultured with Eagle's Minimum Essential Medium (EMEM, ATCC) in 20% FBS. Cells were cultured in a humidified incubator at 37˚C at 5% CO_2.

Lentiviral Production

psPAX2 was a gift from Didier Trono (Addgene plasmid # 12260 ; http://n2t.net/addgene:12260 ; RRID:Addgene_12260). pMD2.G was a gift from Didier Trono (Addgene plasmid # 12259 ; http://n2t.net/addgene:12259 ; RRID:Addgene_12259). pLenti CMV GFP Puro (658-5) was a gift from Eric Campeau & Paul Kaufman (Addgene plasmid # 17448 ; http://n2t.net/addgene:17448 ; RRID:Addgene_17448). H2B-mCherry was a gift from Robert Benezra (Addgene plasmid # 20972 ; http://n2t.net/addgene:20972 ; RRID:Addgene_20972). To propagate lentiviruses, 2,000,000 HEK293T cells were seeded into T25 flasks in 5 ml of complete DMEM. The following day, 755 ng of psPAX2, 377 ng of pMD2.G, and 1.5 μg of H2B-mCherry or eGFP plasmids were mixed together and brought to

50.66 µl in serum free DMEM. A total of 21.67 µl of 1 mg/ml PEI, linear MW 25,000, was added to the plasmids and incubated for 10 minutes at room temperature to complex DNA. The complexed DNA:PEI mixture was then added to 2.7 ml of prewarmed complete DMEM. Media from the T25 flasks were replaced with this fresh media containing DNA:PEI to transfect HEK293T cells. Cells were grown for 72 hours, and the culture supernatant was collected. The supernatant was pelleted at 300·g for 10 minutes and filtered through a 0.45 µm filter. The filtered lentivirus preparations were aliquoted and stored at -70˚C until needed.

Transduction of Caco-2 Cells for H2B-mCherry and GFP expression

Caco-2 cells were seeded into 100 mm dishes, grown to 60% confluency, and the media were removed. Volumes of 2 ml, 1 ml, 0.5 ml, and 0.2 ml of GFP expressing lentiviruses aliquots were adjusted to 4 ml volumes in complete EMEM and added to cells. Cells were given fresh complete media after 24 hours. After 48 hours post-transduction, cells were treated with 10 µg/ml of puromycin and maintained in these conditions for 96 hours. Transduction conditions that resulted in a maximal viability of 10-30 % relative to an untreated control were kept while cells that resulted in higher viabilities or lower viabilities were discarded. The transduction of GFP expressing Caco-2 cells with H2B-mCherry was performed with the same method. However, transduced cells were selected with 2.5 µg/ml blasticidin and 10 µg/ml puromycin. Again, cells that resulted in a maximal viability of 10-30 % relative to an untreated control were kept. These cells were propagated and maintained in 10 µg/ml puromycin and 2.5 µg/ml puromycin and used for cell rounding assays.

Protein Expression and Purification

The vector for expressing TcdB2 (pBL598) was a gift from Dr. J Ballard (University of Oklahoma Health Sciences Center). Recombinant TcdB1 and TcdB2 were expressed and purified from *Bacillus megaterium* as previously described (328).

Labelling TcdB

TcdB1 was purified as described above but with modifications. TcdB was isolated over an S200 column in 20 mM HEPES pH 8.3 in 50 mM NaCl. Fractions containing TcdB were pooled and concentrated to 20-25 µM using a 100 kDa MWCO filter (MilliporeSigma). A 20-molar excess of NHS-JF-669 (Tocris) was added to TcdB and incubated at room temperature in the dark with occasional pipetting for 2 hours.

The labeling reaction was quenched with 50 mM Tris pH 8.0 and 50 mM NaCl for 10 minutes and applied through a PD-10 column (Cytiva) equilibrated with the same buffer to remove aggregates and unreacted dyes. Eluted samples were applied through an S200 column and collected in 20 mM HEPES pH 8 and 50 mM NaCl. Preparations of labeled TcdB resulted in no greater than1.5 labels moles of dye per mole of TcdB were used.

Tissue Preparation

Human colonic tissue was obtained from the Cooperative Human Tissue Network from consenting and deidentified donors under Institutional Review Board-approved protocol 031078. To prepare human frozen colonic tissue samples, ascending colon tissue was first dissected into sections and washed with PBS supplemented with 1.2 mM $CaCl_2$ and 1 mM $MgCl_2$. Sections were then incubated in Tissue-Tek optimal cutting temperature (OCT) compound and snap-frozen in a dry ice-cooled ethanol bath. Mouse colonic tissue from wild type and CSPG4 knockout mice were prepared by flushing luminal contents with PBS supplemented with 1.2 mM $CaCl_2$ and 1 mM $MgCl_2$. Colons were cut along their length and fixed in 2% paraformaldehyde in PBS for 2 hours at room temperature with gentle agitation. Tissues were then washed three times in PBS and incubated overnight at 4˚C in PBS supplemented with 30% sucrose and 1% sodium azide. The following day, samples were quickly dipped in the OCT compound, rolled along their length, submerged in OCT, and snap-frozen in a dry ice-cooled ethanol bath. All OCT embedded samples were cut into 10 μm sections and mounted onto positively charged slides for immunofluorescence staining and confocal microscopy.

Antibody Staining

18Co cells were intoxicated with 10 nM JF669-TcdB1 for 30 minutes at 37˚C. After intoxication, cells were washed once in PBS and fixed in 4% paraformaldehyde in PBS for 15 minutes. Fixed samples were washed 4 times in PBS with 5 minutes of incubation per wash and blocked in 5% normal donkey serum (NDS, Jackson ImmunoResearch Labs) in PBS with 0.3% Triton-X 100 for 1 hour at 37˚C for samples to be stained for Nectin-3 or in 5% normal goat serum (NGS, Jackson ImmunoResearch Labs) in PBS with 0.3% Triton-X 100 for 1 hour at 37˚C for samples to be stained for CSPG4. Coverslips were washed once in PBS prior to incubating overnight with primary antibodies. Staining was performed using antibodies targeting Nectin-3 (Thermo Fisher Scientific, 1:40) prepared in 1% NDS in PBS with 0.3% TritonX-100 or CSPG4 (abcam, 1:250) prepared in 1% NGS in PBS with 0.3% TritonX-100 overnight

at 4˚C. Coverslips were washed 3 times in PBS for at least 5 minutes per wash. Coverslips were then incubated in secondary antibody Alexa Fluor-488 donkey anti-goat (Thermo Fisher Scientific, 1:1000) in 1% NDS in PBS with 0.3% TritonX-100 or Alexa Fluor-488 goat anti-rabbit (Thermo Fisher Scientific, 1:1000) secondary antibody in 1% NGS in PBS with 0.3% TritonX-100 for 1 hour at room temperature. Next, coverslips were washed four times in PBS with at least 5 minutes per wash, stained with DAPI, mounted onto slides using ProLong Gold antifade (Thermo Fisher Scientific) and cured overnight in the dark. Images of 18Co cells are shown as max intensity projections unless otherwise noted in zoomed panels.

OCT from human and mouse colonic sections were removed by incubating sections in PBS for 5 minutes. For human tissue, slides were fixed in 4% paraformaldehyde for 10 minutes and washed 3 times in PBS with 5 minutes per wash. Human sections that were to be stained for Nectin-3 were blocked in 5% NDS in PBS with 0.3% Triton-X 100 for 1 hour. Human and mouse tissue sections that were to be stained for CSPG4 were blocked in 5% NGS in PBS with 0.3% TritonX-100 for 1 hour at room temperature. Sections were briefly washed in PBS and then incubated overnight in primary antibodies targeting Nectin-3 (Thermo Fisher Scientific, 1:40) in 1% NDS in PBS with 0.3% TritonX-100 or in primary antibodies targeting CSPG4 (abcam, 1:250) in 1% NGS in PBS with 0.3% TritonX-100 at 4˚C. The following day, slides were washed 3 times in PBS with 5 minutes per wash and incubated in secondary antibody Alexa Fluor-488 donkey anti-goat (Thermo Fisher Scientific, 1:200) and Alexa Fluor-546 phalloidin in 1% NDS in PBS with 0.3% TritonX-100 for slides stained for Nectin-3 or in secondary antibody Alexa Fluor-488 goat anti-rabbit (Thermo Fisher Scientific, 1:200) and Alexa Fluor-647 phalloidin (Thermo Fisher Scientific, 1:200) in 1% NGS in PBS with 0.3% TritonX-100 for slides stained for CSGP4 for 1 hour at room temperature. Finally, sections were briefly stained with DAPI and washed 4 times in PBS with 5 minutes per wash. Stained tissues were mounted in ProLong Gold antifade (Thermo Fisher Scientific), covered with 1.5 coverglass and cured overnight.

Caco-2 cells on coverslips were grown for 20 days before washing once in PBS and fixed in ice-cold 1:1 acetone:methanol at -20˚C for 15 minutes. Fixed cells were washed 4 times in PBS with 3.5 minutes of incubation per wash and blocked in 5% NDS in PBS with 0.3% Triton-X 100 for 1 hour at 37˚C. Coverslips were washed once in PBS prior to incubating overnight with primary antibodies. Staining was performed using antibodies targeting Nectin-3 (Thermo Fisher Scientific, 1:40) and ZO-1 (Thermo

Fisher Scientific, 1:50) prepared in 1% NDS in PBS with 0.3% TritonX-100 overnight at 4˚C. Coverslips were washed 3 times in PBS for at least 5 minutes per wash. Coverslips were then incubated in Alexa Fluor-488 donkey anti-rabbit (Thermo Fisher Scientific, 1:1000), Alexa Fluor-555 donkey anti-goat (Thermo Fisher Scientific, 1:1000), and Alexa Fluor-647 phalloidin (Thermo Fisher Scientific, 1:200) in 1% NDS in PBS with 0.3% TritonX-100. Next, coverslips were washed four times in PBS with at least 5 minutes per wash and mounted onto slides using ProLong Gold antifade (Thermo Fisher Scientific) and cured overnight. Images are shown as max intensity projections and contrast enhanced using ImageJ (NIH). Orthogonal views were generated in ImageJ.

Caco-2 cells on transwell membranes that were fixed and permeabilized were blocked for 1 hour in 5% NGS in PBS with 0.3% TritonX-100 for 1 hour at room temperature and briefly washed in PBS by removing the supernatant by inverting of the transwell insert. Blocked transwells were incubated in antibodies targeting CSPG4 (abcam, 1:250) overnight in 1% bovine serum albumin fraction V (BSA, VWR) in PBS with 0.3% TritonX-100 at 4˚C. The following day, the membranes were washed in PBS 3 times at 5 minutes per wash and incubated in secondary antibody Alexa Fluor-546 goat anti-rabbit (Thermo Fisher Scientific, 1:1000) and Alexa Fluor Plus-405 phalloidin (Thermo Fisher Scientific, 1:200) in 1% BSA in PBS with 0.3% TritonX-100 for 1 hour at room temperature. Transwells were then washed four times in PBS, and the membrane was excised from the transwell insert using a scalpel. Membranes were placed on a slide and a 1.5 coverslip containing Prolong Gold antifade (Thermo Fisher Scientific) was placed onto each membrane. Mounted membranes were cured overnight in the dark. Images are shown as max intensity projections as *en face* views of the entire cell and contrast enhanced using ImageJ (NIH). Cropped planes and X-Z images are shown as max projections along a single cell in the monolayer to present intracellular CSPG4 signal within the cell.

Confocal and Super-resolution Microscopy

Confocal imaging of Caco-2 cells and 18Co cells intoxicated with only JF669-TcdB1 was conducted using a Zeiss LSM 710 META inverted microscope equipped with a Plan-Apochromat (Apo) 63X/1.4 NA objective lens and 405 and 633 nM excitation LASERs. Confocal imaging of Nectin-3 or CSPG4 immunostained human tissue and 18Co cells immunostained for receptors and intoxicated with JF669-TcdB1 were imaged using a Nikon Spinning Disk microscope equipped with a Plan-Apo 60X/1.4 NA objective lens and 405, 488, 561, and 647 nm excitation LASERs. Confocal imaging of CSPG4

immunostained mouse tissue, Caco-2 cells immunostained for Nectin-3, or Caco-2 cells grown on transwells and immunostained for CSPG4 was performed using a Zeiss LSM980 microscope with Airyscan 2 equipped with a Plan-Apo 63X/1.4 NA objective lens, an Airyscan detector, and 405, 445, 488, 514, 561, and 639 nm excitation LASERs. Super-resolution imaging of human colonic tissue stained for Nectin-3 was performed using a Nikon Structured Illumination microscope equipped with an Andor DU-897 EMCCD camera, a 100X/1.49 NA TIRF oil immersion objective, and 405, 488, 561, and 647 nm LASERs. The Nikon Elements software was used to reconstruct images. LASER intensities and camera gain were matched between samples for each experimental condition.

Analysis of Colocalization of Receptors and TcdB in 18Co Cells

Confocal images were analyzed in ImageJ (NIH) using the EZcolocalization plugin (366). Images generated from the same imaging experiments were thresholded with the same values prior to quantifying colocalization using Ezcolocalization. No region of interest was used in this analysis. Manders' and Pearson correlation coefficients generated from Ezcolocalization was plotted in R (v4.2.0) using the R packages ggplot2 (v3.4.0), ggbeeswarm (v0.6.0) and ggprism (v1.0.4) (367–370).

Cell Surface Endocytosis Assays

Endocytic assays were performed as previously described but with some modifications (371). Briefly, 18Co cell were seeded into 100 mm dishes and grown to 80-90% confluency. Cells were washed three times in PBS supplemented with 100 mg/L $MgCl_2$ and 100 mg/L $CaCl_2$ (PBS-CM) and chilled for 1 hour at 4˚C in PBS-CM. After 1 hour, the PBS-CM was aspirated and cells were incubated with ice-cold HBSS containing 0.5 mg/ml EZ-Link Sulfo-NHS-SS-Biotin (Thermo Fisher Scientific) and incubated at 4˚C for 30 minutes with gentle rocking. Unreacted EZ-Link Sulfo-NHS-SS-Biotin was quenched by 6 ml of ice-cold 50 mM Tris pH 8.0 for 10 minutes. After 10 minutes, cells were washed again in 6 ml of ice-cold 50 mM Tris pH 8.0 for 5 minutes. Biotinylated cells were then treated for 30 minutes with 2.5 ml of pre-warmed HBSS containing 10 nM TcdB2 or 100 ng/ml PDGF-AA (STEMCELL Technologies) at 37˚C. A condition that wasn't biotinylated and a condition that was biotinylated but treated for 0 minutes were included as controls. Following treatment, cells were washed 3X in PBS-CM and cell-surface biotinylated proteins were reduced by adding 6 ml of an ice-cold solution containing 50 mM reduced glutathione, 75 mM NaCl, and 75 mM NaOH and incubating cells for 15 minutes at 4˚C. This step was repeated for an additional 15 minutes. Next, the reduced cell surfaces were quenched by incubating cells

in with 6 ml of a solution containing 50 mM iodoacetamide and 1% bovine serum albumin in PBS-CM for 15 minutes at 4˚C twice. Next, the cells were lysed in 500 µl of TritonX-100 lysis buffer containing Halt Protease inhibitor (Thermo Fisher Scientific). Dishes were scraped to ensure all cells were lysed and incubated for 30 minutes at 4˚C. Finally, lysates were collected and pelleted at 14,000·g for 30 minutes at 4˚C. Soluble lysates were collected and 20 µl of these lysates were removed to keep as an input sample. A BCA assay was performed to quantify total protein concentration in each sample. Next, 400 µg of cell lysates were added to 50 of magnetic streptavidin beads (NEB, cat#S1420S) pre-washed with TBS buffer and 0.1% Tween-20 (TBST). This mixture was rotated at room temperature for 20 minutes. Samples were then briefly pelleted, and beads were enriched using magnet racks. The supernatant was removed, and the beads were washed in 200 µl of TBST five times with five minutes per wash. Each wash rotating samples at room temperature and separating the supernatant from the beads using a magnetic rack. Finally, the magnetic streptavidin beads for each sample were resuspended in 50 µl of TBST and added into new tubes. 10 µl of 6X Laemmli buffer were added to each sample as well as 0.7 µl of 14.2 M 2-mercaptoethanol. Samples were boiled for 10 minutes at 95˚C, and the magnetic beads were separated from the sample using a magnetic rack. The supernatant was collected and analyzed by Western Blot for CSPG4 and TcdB.

siRNA knockdown of CSPG4

All siRNA stocks were resuspended to 10 µM and purchased from Horizon Discovery. To prepare the siRNA for transfection, 2 µl of the 10 µM stocks of non-targeting control siRNA (D-001210-2) or siRNA targeting CSPG4 (L-011632-01) were diluted into 18 µl of serum free DMEM. Meanwhile, 12 µl of RNAiMax (Thermo Fisher Scientific) was added to 388 µl of serum free DMEM. The transfection reagent mixture was then mixed with the siRNA and allowed incubated at room temperature for 15 minutes. This siRNA:RNAiMax solution was transferred into a 6 well dish and a suspension of 170000 18Co cells in 1.6 ml complete media was added. The molarity of siRNA in these conditions were 10 nM. After 24 hours, the media was replaced with fresh media and grown for an additional 48 hours. Knockdowns were confirmed by Western blot from cells lysed with TritonX-100 lysis buffer, consisting of 50 mM Tris pH 8.0, 150 mM NaCl, 1% Triton X-100, 0.1% SDS and HALT protease inhibitor (Thermo Fisher Scientific).

18Co Conditioned Media Collection

18Co cells were seeded into 6 well dishes at 170,000 cells per well in 2 ml of complete media. The conditioned media from all conditions were collected at 72 hours and the cellular debris was pelleted at 300·g for 10 minutes in a swinging-bucket centrifuge (372). The supernatant was filtered with a 0.45 μm filter and stored at -20˚C for short term storage or at -70˚C for long term storage.

Caco-2 CSPG4-ECD Uptake Assays

For experiments analyzed by Western blotting, 70,000 Caco-2 cells were seeded on 12 mm polycarbonate cell inserts with 8.0 μm pores (Millipore) and 100,0000 18Co cells were seeded into the bottom wells of the dish. The cell inserts were collected on days 1, 3, and 5 and lysed in 35 μl of TritonX-100 lysis buffer. Caco-2 cells grown for 5 days on the cell inserts were used as a negative control. The entire volume of cell lysates collected from these experiments were analyzed by Western blot. For imaging experiments, 70,000 Caco-2 cells were seeded into transwells made with 12 mm polyester membranes with 0.4 μm pores (Corning) and grown above 100,000 18Co cells for 5 days. Caco-2 cells on Transwells were washed twice in PBS and fixed for 20 minutes in 4% paraformaldehyde in PBS. Washes and removal of any reagents were performed by inverting the insert as mechanical forces could result in loss of the cell monolayer. After fixation, the cells were washed in PBS with 5 minutes per wash, permeabilized for 15 minutes using 0.3% TritonX-100 in PBS and stained as described in the Antibody Staining section.

Mouse Crypt Isolation

Crypt isolation was performed as previously described but with modifications (373). Mouse colonic tissue was prepared by first washing luminal contents with cold PBS to remove fecal pellets. The colon was then opened longitudinally and washed at least three times with cold PBS. Next, the samples were washed twice in cold 25 mM EDTA for approximately 3 minutes per wash. Colonic tissue was incubated in cold 25 mM EDTA on ice for 30 minutes with occasional inversions. After 30 minutes, the samples in 25 mM EDTA were shaken, and the supernatant was collected and kept on ice. This process was repeated two additional times. Collected supernatant was strained through a 70 μm mesh filter and pelleted at 600·g for 5 minutes. These crypt pellets were resuspended in PBS and visualized on a brightfield microscope at 10X magnification. Crypts were once again pelleted, and the supernatant was removed. Isolated crypts were then lysed in TritonX-100 lysis buffer and analyzed by Western Blot for CSPG4.

Intoxication of Caco-2 for Cell Rounding

Caco-2 expressing GFP and H2B-mCherry were seeded into a 96 well plate at 25,000 cells per well in complete EMEM. After growing cells for 48 hours, media from wells were removed and replaced with 90 µl with complete DMEM, or, for experiments using 18Co conditioned media, with 90 µl of si*NTC* media or 90 µl si*CSPG4* media. Finally, 10 µl of a stock solution of 10 pM TcdB2 was added to cells. After intoxication, brightfield, and fluorescence images were collected every 45 minutes on a Cytation 5 imager (BioTek) with an atmosphere of 5% CO_2 and 37˚C temperatures. Detailed methods and

CSPG4 Antibody Blocking Experiments

Caco-2 cells expressing GFP and H2B-mCherry were plated into 96 well dishes at a density of 25,000 cells per well. After 48 hours, an antibody targeting CSPG4 (SantaCruz, 20 µg/ml) was added to the conditioned media and incubated at room temperature for 30 minutes. Untreated conditioned media or antibody treated conditioned media was added to cells, and cells were intoxicated with 1 pM TcdB as previously described and imaged as previously described.

Western Blotting

Cell lysate concentrations were determined with a BCA Protein Assay Kit (Thermo Fisher Scientific). Unless specified, 20 µg of protein from cell lysates were boiled in Laemmli buffer prior to loading on 4-20% Mini-PROTEAN TGX stain-free gels (BioRad) for SDS-PAGE. Stain-free gels were activated and imaged on a BioRad Gel Doc EZ or a BioRad ChemiDoc MP prior to transfer. Proteins were transferred onto PVDF at 100V for 70 minutes in Towbin buffer lacking methanol and membranes were blocked in 5% milk in PBS for 1 hour. Membranes were incubated overnight in primary antibodies against CSPG4 (abcam, 1:2000), GAPDH (CST, 1:5000), or TcdB (ListLabs, 1:2000) at 4˚C in 5% milk in PBST. Membranes were washed three times in PBST, with 5 minutes per wash, and incubated for 1 hour in secondary antibodies Dylight-680 goat anti-mouse (CST, 1:10000), DyLight-800 goat anti-rabbit (CST, 1:10000) or horseradish peroxidase (HRP) goat anti-Chicken (Jackson ImmunoResearch Labs, 1:10000) in 5% Milk in PBST for 1 hour at room temperature. Membranes were washed three times in PBST and once in PBS prior to protein detection on a Licor Odyssey imager or imaged on film after activating the HRP with Immobilon Western Chemiluminescent HRP substrate (MilliporeSigma). Film generated from experiments were scanned at 600 DPI in color and converted to grayscale using ImageJ (NIH).

Single Cell RNA Sequencing Analysis

Pre-processed datasets of human colonic epithelial tissue was procured from the Space-Time Gut Cell Atlas (https://www.gutcellatlas.org/) (260). ScanPy (v1.9.1), NumPy (v1.22.4), Anndata (v0.8.0), Pandas (v1.1.2), and bbknn (v1.5.1) were used to analyze this published dataset as previously described (374–378). Cells annotated as healthy adult tissue from the appendix, large intestine, rectum, and small intestines were subsetted from the original dataset. Cell-type annotations were included by the original authors of the dataset and methods were verified for consistency. Epithelial cells along the intestines were plotted for *CSPG4* or *EPCAM* expression using ScanPy dotplot function. Dot plot figures were generated with ScanPy using a standard_scale=var and vmax=0.8. Human mesenchymal cells dataset was obtained from GSE114374. Genes were initially filtered in ScanPy to be detected in at least 3 cells, and all cells were filtered to have at least 250 genes expressed. Cells were further filtered to have less that 5% mitochondrial reads prior to scaling and normalizing the data as previously described. Highly variable genes were identified using a min_mean=0.0125, a max_mean=4, and min_disp=0.5 and total counts and percent mitochondrial counts were regressed. The data were scaled with a max_value=10 and principal component was performed using arpack. Neighbors were identified using n_neighbors=10 and n_pcs=20. Next, dimensionality reduction was calculated using a UMAP. Finally, clusters were identified using the Louvain clustering with a resolution=0.1 and clusters were named from gene markers of known markers (365). Stromal cells along the intestines were plotted for *CSPG4* or *PDGFRA* expression using ScanPy dotplot function using standard_scale=var and dot_max=0.8.

18Co RNA Sequencing Analysis

The 18Co transcriptomic dataset was acquired from the National Center for Biotechnology Information Gene Expression Omnibus (GEO) series GSE89124 (379). This dataset was processed by the GEO RNA-seq Experiments Interactive Navigator (GREIN) web platform hosted on the National Institutes of Health Library of Integrated Network-Based Cellular Signatures (358). The counts table was exported as normalized expression as counts per million (CPM) or trimmed mean of m-values (TMM) in GREIN. The normalized expression of *CSPG4*, *NECTIN3*, *FZD1/2/7*, and *TFPI* from the untreated control samples was log2 transformed and plotted in R (v4.2.0) using the R packages ggplot2 (v3.4.0), ggbeeswarm (v0.6.0) and ggprism (v1.0.4) (367–370).

Cell Rounding Quantification

Images acquired from cell rounding experiments were analyzed using an automated cell rounding analysis pipeline developed in the open source software CellProfiler (v4.2.1) using machine learning cell segmentation models from Cellpose (v2.0.5) and cell rounding classifiers generated in CellProfiler Analyst (v3.0.4) (380–382). To generate classifier models that differentiate round cells from non-round cells in Caco-2 cells, grayscale GFP and Texas Red images were imported into CellProfiler. Briefly, the RunCellpose module was applied using Cellpose's cyto2 detection model using GFP images. The nuclear images corresponding to the H2B-mCherry from the Texas Red images were used here. Cells were calculated to have an expected diameter of 40 and cell probability was set to -3. A flow threshold of 1 was used as well as a minimal size of 30. Other settings were kept at default settings. The size and shapes of classified objects were then filtered to have a MinFeretDiamter of minimally 17 and a maximal of 60. Objects touching the edges of images were filtered out as well. Next, objects were measured for size, shape, intensity of GFP and H2B-mCherry and their intensity distribution, and finally colocalization of GFP and H2B-mCherry within cells. Objects corresponding to segmented cells were then classified in CellProfiler Analyst as described earlier. The corresponding machine learning Gradient Boost model was then added to the end of the original Caco-2 cell segmentation pipeline to classify round cells from non-round cells. When needed, areas of images that were too bright to segment accurately were masked using CellProfiler prior to using RunCellpose. Images contained at least 500 cells per image. Finally, the percentage of round cells were calculated as previously described (155). These CellProfiler pipelines and the CellProfiler Analyst model are available on https://github.com/kochild/Cell-Rounding-Pipelines-and-Models.

Table 3-1. Bacterial Strains and plasmids

Plasmid or Strain	Relevant genotype or features	Source, construction, or reference
Strains		
B. megaterium		
bm003	TcdB1 expression strain containing	(138)
bm074	TcdB2 expression strain containing pBL598	J. Ballard
Plasmids		
pBL598	TcdB2 expression vector	J. Ballard
pLenti CMV GFP Puro (658-5)	Lentiviral expression vector encoding GFP under a CMV promoter	(383)
H2B-mCherry	Lentiviral expression vector encoding H2B fused to mCherry	(384)
psPAX2	2nd Generation lentiviral packaging plasmid	Cat#12260,Addgene; RRID: Addgene_12260
pMD2.G	VSV-G envelope expressing plasmid	Cat#12259, Addgene; RRID: Addgene_12259

Table 3-2. Materials and Reagents

Reagent	Source	Identifier
Antibodies and Cell Stains		
Rabbit monoclonal anti-CSPG4	Abcam	Cat#ab255811; RRID: N/A
Mouse monoclonal anti-CSPG4	Santa Cruz Biotechnology	Cat#sc-53389; RRID: AB_784821
Rabbit monoclonal anti-GAPDH	Cell Signaling Technology	Cat#2118; RRID: AB_561053
Rabbit anti-ZO-1	Thermo Fisher Scientific	Cat#61-7300; RRID: AB_2533938

Chicken polyclonal anti-TcdB	List Labs	Cat#754A; RRID: AB_2909446
Goat anti Nectin-3	Thermo Fisher Scientific	Cat#PA5-47441; RRID: AB_2577074
Goat anti-chicken HRP	Jackson ImmunoResearch	Cat#103-035-155; RRID: AB_2337381
Goat anti-rabbit 488	Thermo Fisher Scientific	Cat#A-11008; RRID: AB_143165
Goat anti-rabbit 546	Thermo Fisher Scientific	Cat# A-11035; RRID: AB_2534093
Goat anti-mouse DyLight 680	Cell Signaling Technology	Cat#5470; RRID: AB_10696895
Goat anti-rabbit DyLight 800	Cell Signaling Technology	Cat# 5151; RRID: AB_10697505
Donkey anti-rabbit 488	Thermo Fisher Scientific	Cat#A-21206; RRID: AB_2535792
Donkey anti-goat 555	Thermo Fisher Scientific	Cat#A-21432; RRID: AB_2535853
Alexa Fluor Plus 405 Phalloidin	Thermo Fisher Scientific	Cat#A30104
Alexa Fluor 546 Phalloidin	Thermo Fisher Scientific	Cat#A22283
Alexa Fluor 647 Phalloidin	Thermo Fisher Scientific	Cat#A22287
Chemicals		
NHS-Janelia Fluor 669	Tocris	Cat#6420
EZ-Link Sulfo-NHS-SS-Biotin	Thermo Fisher Scientific	Cat#21331
Cell Culture Reagents		
PDGF-AA	STEMCELL Technologies	Cat#78095

Final Discussion, Conclusions and Future Directions

Introduction

C. difficile infection continues to be a leading cause of antibiotic-associated diarrhea worldwide (114). As the clinical symptoms of the disease are mediated by its toxins, many researchers have worked to identify cell surface proteins involved in the intoxication process. While their efforts identified multiple proteins and glycans involved in the cytotoxic and cytopathic responses of the toxins, none of these cellular factors were demonstrated to facilitate the entry of the toxin into cells (152, 154–158, 221, 385–389). In fact, some of these interactions have been proposed to only promote toxin binding to the cell surface and are not involved in toxin endocytosis (159). If the interactions between the toxins and cellular factors do result in endocytosis, the use of the term *receptor* becomes ambiguous and suggests there is a need to distinguish between cell surface binding receptors and toxin entry receptors. However, some researchers have argued that even though the interactions between toxins and some receptors do not facilitate an immediate endocytic response, any toxin associated with a surface protein will likely be endocytosed over time through endocytic recycling pathways (36, 390). Therefore, even toxin interactions with so-call cell surface binding receptors are still predicted to enter the cell.

While the overall role of toxin binding to the cell surface is unknown, what was known when I began my thesis was that endocytosis of the toxin was necessary for mediating the toxin's cytotoxic and cytopathic activities (138, 145, 286, 328, 391). At that time, there were only two protein receptors for TcdB, Nectin-3 and CSPG4 (155, 156). My initial goal was to investigate how TcdB interactions with these receptors would promote the pathogenesis of the toxin in cells and hosts. Importantly, within the colon, these receptors were predicted to be localized to two distinct locations: (1) Nectin-3 was predicted to be expressed within epithelial adherens junctions and (2) CSPG4 was predicted to be expressed by fibroblasts along the crypt-villus axis (203, 299). I hypothesized that Nectin-3 would facilitate TcdB-mediated epithelial injuries alone and that CSPG4 would facilitate TcdB-mediated injuries to stromal cells. However, soon after I began testing this hypothesis, FZD1/2/7 was identified as an additional class of TcdB receptors (154). The FZD1/2/7 receptors were predicted to be expressed by colonic epithelial cells,

but unlike Nectin-3, their interactions with TcdB were shown to contribute to the cytopathic response (154, 156).

While the discovery of FZD1/2/7 as TcdB receptors did not negate my initial hypothesis, it was clear that I had to consider the contributions of FZDs in the overall intoxication mechanism of epithelial cells. As knockout of Nectin-3 was shown to result in decreased TcdB-mediated cytotoxicity on colonic epithelial cell lines, I had hypothesized that Nectin-3 served as a cytotoxic receptor and FZD1/2/7 proteins served as cytopathic receptors. As I began investigating these interactions, I performed a sequence alignment of the various annotated TcdB variants uploaded on NCBI GEO in hopes that I would identify conserved residues that were important for receptor interactions. These TcdB variants at the time were predicted to impact their virulence (165, 166, 343, 392). This investigation happened to coincide with the publication of a co-crystal structure of a portion of TcdB bound to the CRD of FZD2 (161). As the structure revealed many key residues that mediate TcdB interactions with FZD1/2/7, I inspected those sequences in my alignment. To my surprise, the alignment revealed mutations in six residues that mediate FZD interactions with TcdB1 were not conserved in TcdB2. While I did not expect that most of these mutations would be deleterious to the interaction with FZDs, I hypothesized that the F1597S mutation in TcdB2 would disrupt the hydrophobic interactions between TcdB2 and FZD1/2/7. As shown in Chapter 2, we were unable to detect any measurable binding between TcdB2 and the CRD of FZD2. Additionally, we found that TcdB2 is unable to inhibit the canonical Wnt signaling, a pathway that we confirmed to be inhibited by TcdB1. However, we saw that TcdB2 was as potent as TcdB1 and TcdB1^{GFE} (a FZD binding mutant) when rectally instilled into mice, with all toxins inducing similar pathologies. Finally, we found through a collaboration with Dena Lyras and Helen Abud that TcdB2 can still intoxicate stem cells independently of FZD interactions to perturb stem cell function.

With these findings, I became interested in the potential utility of immunofluorescence microscopy for characterizing TcdB and its receptor interactions. Although this may seem like a simple task, the visualization of TcdB was extremely challenging due to the toxin being undetectable in most contexts (328). However, if I could successfully apply the technique, I would be able to investigate TcdB interactions with receptors directly on cells. As shown in Chapter 3, I was able to identify 18Co cells as a cell line where TcdB could be visualized. In these cells, I found that TcdB1 colocalized with both CSPG4 and Nectin-3 and obtained evidence that both receptors are endocytosed in the presence of TcdB1.

Having developed a method for visualizing TcdB on cells, I next asked if I could use colonic tissue to investigate TcdB interactions with receptors. While imaging human colonic tissue sections immunostained for Nectin-3 and CSPG4 with confocal microscopy, I made two unexpected observations on the actual localization of the receptors. The first observation was that Nectin-3 localized to the colonic brush border in addition to cell junctions, and the second observation was that CSPG4 localized to epithelial cell junctions in addition to fibroblasts below the crypt-surface axis. While I found it very difficult to detect TcdB1 on intoxicated colonic tissue, I observed TcdB1 colocalization with Nectin-3 within the apical region of colonocytes. This result suggests that Nectin-3 may facilitate TcdB interactions on the colonic epithelial cells by binding TcdB within the brush border. As for the CSPG4 signal along the epithelial junctions, I found evidence that this signal is likely from CSPG4 shed by fibroblasts that line the crypt-surface axis. Specifically, I found that CSPG4 shed by fibroblasts can associate with epithelial cells grown in transwells. Surprisingly, this shed form of CSPG4 can potentiate the activity of TcdB2. Based on these observations, I propose that a soluble form of CSPG4 derived from stromal cells can serve as an epithelial receptor for TcdB. The observation of Nectin-3 in the brush border and shed CSPG4 on epithelial cells opens many exciting avenues for both epithelial biology and our understanding of TcdB mechanisms.

Future directions

Characterizing the relationship between TcdB interactions with receptor and cytotoxicity

Although my research revealed multiple unexpected results, I consider the lack of FZD interactions with TcdB2 to be the most surprising. While differences in receptor tropism has been observed in other toxins (e.g., Botulinum neurotoxins), TcdB2 was proposed to be more potent than historical variants and capable of inducing the severe symptoms associated with the epidemic of the 2000s in the United States (114, 169–171). How then could a toxin that lacked a receptor interaction be more potent? One potential explanation could be that TcdB2 interacts with an alternative receptor instead of FZDs. This may explain why I observed that TcdB2 is as potent as TcdB1 on mouse colonic tissue (**Figure 2-3, Figure S2-4**). Hoping to address this, I decided to first test the claim that TcdB2 is more potent than TcdB1. A simple metric for TcdB potency is the measurement of ATP present in cells following intoxication with necrotic concentrations of TcdB. As a control for TcdB2, I used TcdB1^{GFE} to prevent FZD interactions in the historical strain. If TcdB2 had only lost the ability to interact with FZD, I predicted that its cytotoxic

response should be identical to that of TcdB1^{GFE}. However, if TcdB2 had gained the ability to interact with an unknown receptor to compensate for the loss of FZD interactions, the cytotoxicity mediated by TcdB2 should be equivalent to or greater than that of TcdB1. On Caco-2 cells treated with these toxins, I found TcdB2-mediated cytotoxicity was nearly identical to that of TcdB1^{GFE} and that both TcdB2 and TcdB1^{GFE} were less cytotoxic than TcdB1 (**Figure 4-1A**). This suggests that TcdB2 has only lost the ability to interact with FZD receptors and that it is not more potent than TcdB1 as previously reported (343). However, when I repeated this experiment on HeLa cells, the activities of the toxins were identical (**Figure 4-1B**). These differences would suggest that the activities of TcdB1 and TcdB2 can be identical under specific contexts. In this case, the major difference is the expression of CSPG4 in HeLa cells and the absence of its expression in Caco-2 cells. Furthermore, while FZDs appear to not facilitate TcdB cytotoxicity in HeLa cells, the opposite is true in Caco-2 cells. These data suggest that the cytotoxic responses mediated by TcdB are cell line dependent. Indeed, similar observations have been reported for TcdB-mediated cytopathic responses (178). As Nectin-3 interactions with TcdB were originally reported to facilitate TcdB cytotoxicity in Caco-2 cells, it would be interesting to test the cytotoxicity of TcdB2 on a Nectin-3 knockout cell line. I would predict that TcdB2 would be completely non-toxic on these cells.

Recent phylogenetic studies have suggested that TcdB1 and TcdB2 have evolved from unique evolutionary paths (107). Sequencing analysis suggests that TcdB variants evolved from a TcdB1-like ancestor (type i) or a TcdB7-like ancestor (type ii) (107). The TcdB variants that evolved from the type i ancestor (TcdB1/5/6) reportedly all bind FZDs, while the TcdB variants that evolved from the type ii ancestor (TcdB4/7) do not (158). Instead, the TcdB variants that evolved from the type ii ancestor utilize TFPI as its putative receptor (157, 158). The remaining TcdB variants evolved through recombination events from both historical type i and type ii ancestors (107). While the TcdB1 variant is a direct descendent of the type i ancestor, the TcdB2 variant is predicted to have formed by fusion of the N-terminus from the type i ancestor (the GTD and APD) with the C-terminus from the type ii ancestor (the DD and CROPs) (107). However, even though the C-terminus of TcdB2 evolved from the predicted type ii TcdB ancestor, it does not interact with TFPI (158). This suggests that throughout the evolution of the TcdB2, the toxin acquired the C-terminus of the type ii ancestor prior to these variants evolving interactions with TFPI. Interestingly, CSPG4 interactions with TcdB is conserved across most TcdB variants with both type i and type ii ancestors (158).

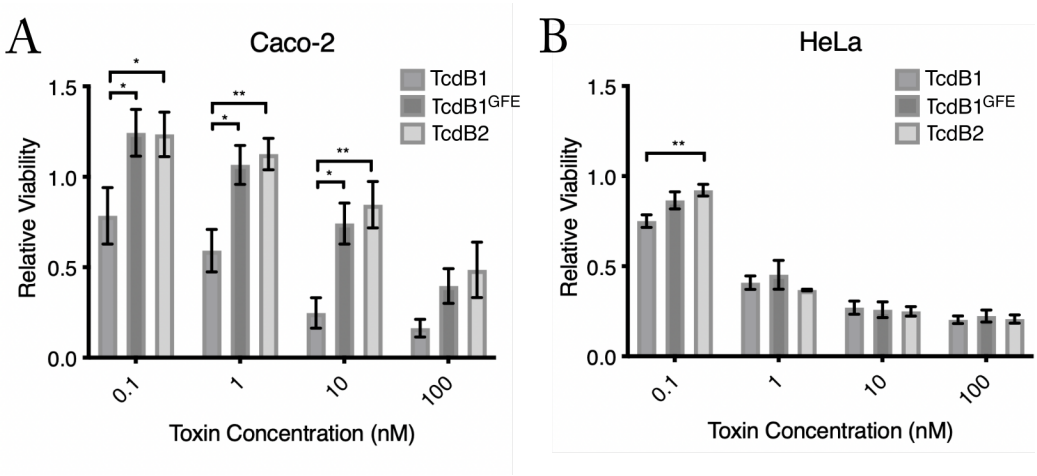

Figure 4-1. The cytotoxic properties of TcdB2 are cell line specific and CSPG4 dependent

A) Caco-2 cells were intoxicated with TcdB1, TcdB1^{GFE}, and TcdB2 for 4.5 hours before measuring ATP levels with CellTiter-Glo (Promega). N=3. *P<0.05, **P<0.01. Two-way ANOVA, corrected for multiple comparisons with Dunnett's test

B) HeLa cells were intoxicated with TcdB1, TcdB1^{GFE}, and TcdB2 for 4.5 hours before measuring ATP levels with CellTiter-Glo (Promega). N=3. **P<0.01. Two-way ANOVA, corrected for multiple comparisons with Dunnett's test

Is there a connection between CSPG4 and Nectin-3 expression?

While investigating TcdB receptor interactions, I generated knockouts of both Nectin-3 and CSPG4 in HeLa cells using CRISPR-cas9. When I intoxicated these cells with TcdB2, I found that while both CSPG4 knockout clones were protected from TcdB2, only one of my two Nectin-3 knockout clones was significantly protected (Figure 4-2). A Western blot analysis using cell lysates of these Nectin-3 knockout cells revealed varying levels of CSPG4 (Figure 4-2). Importantly, the Nectin-3 knockout clone with significant protection, clone 2, contained almost no detectable CSPG4 signal. Additionally, the Nectin-3 knockout clone with no significant protection, clone 1, also appeared to contain less CSPG4. The two CSPG4 knockout clones did not have any obvious changes in Nectin-3. While the differences in CSPG4 expression can possibly be explained by natural variations in cells, Nectin-3 is reported to regulate the localization of some transmembrane proteins on cells (290). One specific protein whose location is regulated by Nectin-3 is PDGFRα. PDGFRα is also a protein that CSPG4 can associate with on cells through direct interactions (193, 209). It would be interesting to determine if knockout of Nectin-3 also perturbs the localization of PDGFRα and CSPG4 on HeLa cells. This could be visualized through immunofluorescence microscopy. Additionally, even though knockout of CSPG4 did not appear to affect the concentration of Nectin-3 in cell lysates, it would be useful to determine if knockout of CSPG4 had any effects on the localization of Nectin-3 and PDGFRα.

Nectin-3 and its role in the brush border

The involvement of Nectin-3 in the development of various organs and cell architectures has been demonstrated using *Nectin3*$^{-/-}$ knockout and knockdown mice. These mice exhibit defects in cochlear hair cell organization, develop microphthalmia, have impaired neuronal synapse formation, and develop male-specific infertility (295, 296, 393–395). The localization of Nectin-3 in intestinal epithelium is influenced by afadin, a cytosolic protein that links Nectin proteins to the actin cytoskeleton (363). However, loss of Nectin-3 reportedly does not affect the architecture of the intestinal epithelium or its barrier function, a phenotype that may be attributed to compensatory interactions between other Nectin proteins (363). In addition to afadin, Nectin-1 and Nectin-3 can interact with the PAR complex, a ternary complex consisting of Par-3, Par-6, and αPKC that is required for cell polarity (293, 396). Nectin-1 and Nectin-2 have also been shown to interact with Patj *via* their PDZ domains using pulldowns (397). A recent study has shown that components of the Par complex and Patj are localized along the base and length of

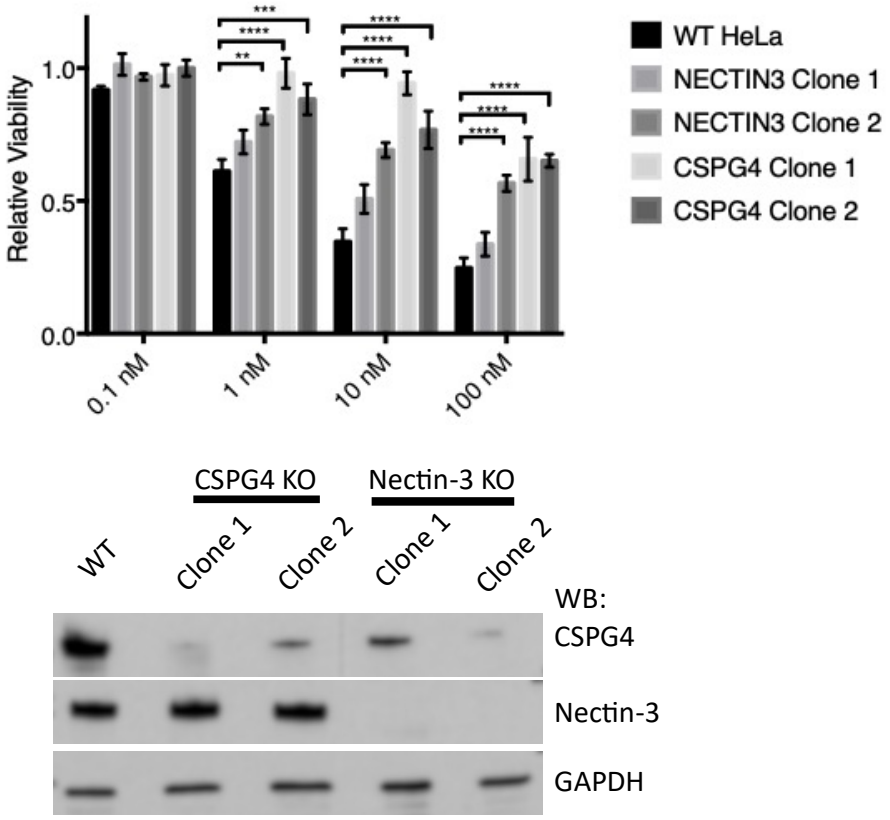

Figure 4-2 Knockout of Nectin-3 and CSPG4 in HeLa cells confers protection from TcdB2.

Clone 2 of NECTIN3 KO and clones 1 and 2 of CSPG4 knockout are significantly protected in the presence of RT027 TcdB. N=3 **P<0.01, *** P<0.001, ****P<0.0001. Two-way ANOVA, Dunnett's Multiple Comparison Test. The bottom panel is a representative Western blot (WB) confirming the knockout of either CSPG4 or Nectin-3.

microvilli in polarized Caco-2 cells. While Nectin-3 has not been demonstrated to interact with Patj, its PDZ domain is identical to Nectin-1 (398). Future studies will address if the interactions between Nectins and these cytosolic proteins are involved in the localization of Nectins to the microvilli. While we are unaware of other studies reporting the localization of Nectin proteins to microvilli along intestinal epithelial cells, Nectin-2 is reportedly present on the microvilli-like extensions found in oocytes (399). I have briefly investigated some of the proteins Nectin-3 possibly interacts with within the brush border. The most obvious proteins would be other Nectins. On a cell line commonly used to investigate the development of the brush border, I found that Nectin-1 and Nectin-3 colocalize with each other within the microvilli (**Figure 4-3**). This finding suggests that Nectin proteins could be involved in microvilli assembly, a field of research that is under active investigation. It was recently determined that microvilli assembly is regulated by the interactions of cadherin-like molecules (400, 401). Like the role of cadherins in cellular junctions, these cadherin-like molecules present throughout microvilli are proposed to interact with each other to facilitate the linkages between nascent microvilli (364). As Nectins can also form interactions with other Nectins, an attractive hypothesis is that these molecules facilitate a similar function.

What are the potential consequences of TcdB interactions with Nectin-3 if they occur in the microvilli? Although we lack a complete understanding of what residues in Nectin-3 facilitate its interactions with TcdB, we have data that suggests this occurs within the D1 subdomain. Additionally, the D1 subdomain is the region of Nectin-3 that facilitates its interactions with other Nectins (289). Therefore, one interesting hypothesis is that TcdB interactions with Nectin-3 could prevent it from interacting with other Nectins. If this occurs, TcdB interactions with Nectin-3 within the brush border could impact the assembly or stability of the brush border. These events could cause disease symptoms such as diarrhea due to the importance of brush border assembly in fluid absorption (401, 402).

CSPG4 and its interactions with the colonic epithelium

One important yet unresolved question is the source of shed CSPG4 *in vivo*. Multiple cell types within the colonic submucosa can express CSPG4 (**Figure 4-4**). From an analysis of a published sc-RNA seq dataset from mouse intestinal stromal cells, we can see that essentially all fibroblast populations along the crypt-surface axis can express CSPG4. Cell types such as pericytes and vascular smooth muscle cells (SMC) express the greatest amounts of CSPG4 transcripts. These data provide a starting point for future investigation. They also provide insight into the possible cell types TcdB can target within the submucosa.

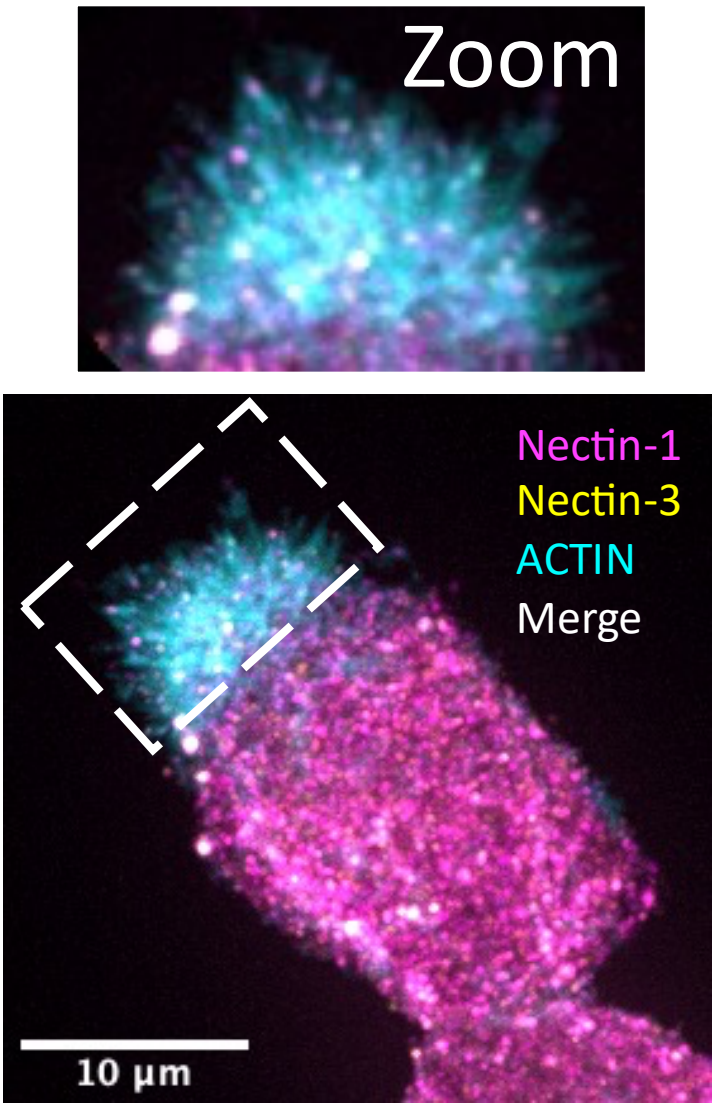

Figure 4-3 Nectin-1 and Nectin-3 colocalize with each other in the microvilli.

W4 cells were immunostained for Nectin-1, Nectin-3 and stained with phalloidin. Images were acquired on a Nikon Spinning Disk microscope at 60X. The white dashed box around the brush border outlines the location of the zoomed image.

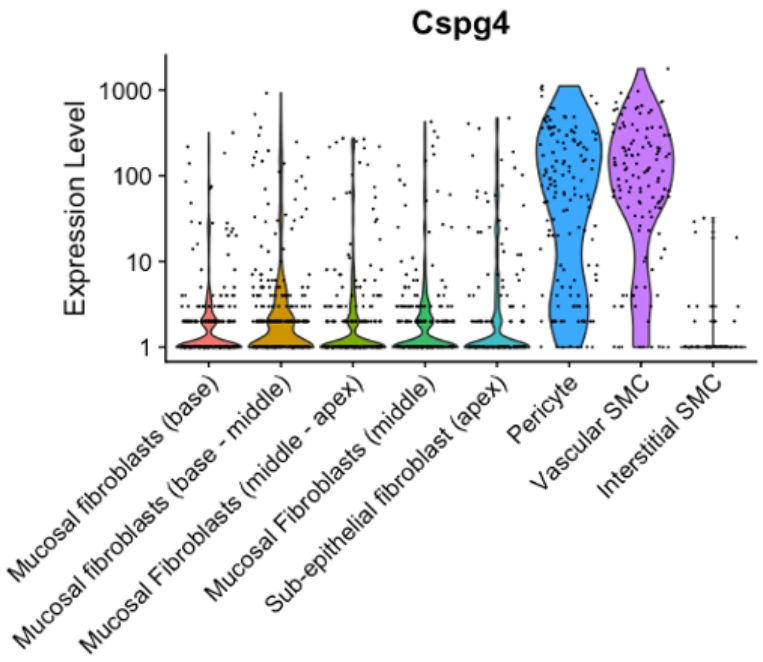

Figure 4-4. scRNA-seq reveals the expression of CSPG4 expressing cells in the colon.

scRNA-seq (GSE149859) analysis was performed using the same labels and clustering methods as previously described (403). CSPG4 expression per cell was plotted in Seurat (404). The clusters each represent individual fibroblast populations that are present along the crypt-surface axis. The terms base, middle, and apex, refer to the location of these fibroblast populations along the crypt surface axis.

The pericytes and vascular SMC are interesting due to their role in vasculature leakage during CDI (405).

While other proteoglycans are secreted directly into the extracellular environment, CSPG4 is expressed as a transmembrane protein and requires the activity of metalloproteinases to be shed into the extracellular environment (232–234, 406). Cleavage can occur within the D3 membrane proximal subdomain of CSPG4 (residues 1591-2221), producing a near equivalent of the full-length CSPG4 ectodomain (235, 238). Our data suggest that TcdB interactions with a shed form of CSPG4 promote cytopathic responses *in vitro*. However, we have not determined how endocytosis of this putative TcdB-CSPG4 ECD complex occurs. This complex may utilize the various signaling pathways the CSPG4 ECD domain can activate. Functionally, shed forms of CSPG4 have been shown to stimulate cell migration *via* the activation of β1-class integrin signaling (186). Additionally, interactions between the CSPG4 ECD with growth factors and receptor tyrosine kinases are predicted to still occur *in vivo* (230). Our future studies will address the contributions of various surface protein interactions of CSPG4 ECD for the endocytosis of TcdB.

Finally, it is interesting to speculate the role of shed CSPG4 ECD during CDI. As mentioned in Chapter 1, a recent study demonstrated that CSPG4$^{-/-}$ mice infected with *C. difficile* exhibited less epithelial injury and pathologies (160). The study also revealed that mouse ceca injected with TcdB1 that contained mutations that prevent CSPG4 interactions had reduced epithelial injuries and pathologies (160). I predict that shed forms of CSPG4 that associates with the colonic epithelium are responsible for mediating these reported CSPG4-dependent epithelial injuries in mice. In support of this prediction, it was determined that the inhibitory activity of bezlotoxumab, an anti-TcdB antibody approved by the United States Food and Drug Administration for the treatment of recurrent CDI, against TcdB is mediated by blocking TcdB interactions with CSPG4 (160, 407). Mice ceca injected with TcdB1 and bezlotoxumab are reported to have less epithelial injury and overall pathologies, a result that can be explained by my finding that soluble CSPG4 serves as an epithelial receptor for TcdB (160). With CSPG4 serving as a receptor for most TcdB variants, the development of drugs that block their interaction should protect hosts from the activity of TcdB (158).

References

1. Hall IC, O'Toole E. 1935. Intestinal flora in new-born infants: With a description of a new pathogenic anaerobe, *Bacillus difficilis*. Am J Dis Child 49:390–402.

2. Lawson PA, Citron DM, Tyrrell KL, Finegold SM. 2016. Reclassification of *Clostridium difficile* as *Clostridioides difficile* (Hall and O'Toole 1935) Prévot 1938. Anaerobe 40:95–99.

3. Smith LDs, King EO. 1962. Occurrence of *Clostridium difficile* in infections of man. J Bacteriol 84:65–67.

4. Bartlett JG, Moon N, Chang TW, Taylor N, Onderdonk AB. 1978. Role of *Clostridium difficile* in antibiotic-associated pseudomembranous colitis. Gastroenterology 75:778–782.

5. George WL, Goldstein EC, Sutter VL, Ludwig SL, Finegold SM. 1978. Aetiology of antimicrobial-agent-associated colitis. The Lancet 311:802–803.

6. Lyerly DM, Krivan HC, Wilkins TD. 1988. *Clostridium difficile*: its disease and toxins. Clin Microbiol Rev 1:1–18.

7. Taylor NS, Thorne GM, Bartlett JG. 1981. Comparison of two toxins produced by *Clostridium difficile*. Infect Immun 34:1036–1043.

8. Banno Y, Kobayashi T, Kono H, Watanabe K, Ueno K, Nozawa Y. 1984. Biochemical characterization and biologic actions of two toxins (D-1 and D-2) from *Clostridium difficile*. Rev Infect Dis 6 Suppl 1:S11-20.

9. Larson HE, Parry JV, Price AB, Davies DR, Dolby J, Tyrrell DA. 1977. Undescribed toxin in pseudomembranous colitis. Br Med J 1:1246–1248.

10. Cohen LE, McNeill CJ, Wells RF. 1973. Clindamycin-Associated Colitis. JAMA 223:1379–1380.

11. Kabins SA, Spira TJ. 1975. Outbreak of clindamycin-associated colitis. Ann Intern Med 83:830–831.

12. Theriot CM, Koenigsknecht MJ, Carlson PE, Hatton GE, Nelson AM, Li B, Huffnagle GB, Z. Li J, Young VB. 2014. Antibiotic-induced shifts in the mouse gut microbiome and metabolome increase susceptibility to *Clostridium difficile* infection. 1. Nat Commun 5:3114.

13. Dobson G, Hickey C, Trinder J. 2003. *Clostridium difficile* colitis causing toxic megacolon, severe sepsis and multiple organ dysfunction syndrome. Intensive Care Med 29:1030.

14. Chatila W, Manthous CA. 1995. *Clostridium difficile* causing sepsis and an acute abdomen in critically ill patients. Crit Care Med 23:1146–1150.

15. Lowenkron S, Waxner J, Khullar P, Ilowite J, Niederman M, Fein A. 1996. *Clostridium difficile* infection as a cause of severe sepsis. Intensive Care Med 22:990–994.

16. CDC. 2019. Antibiotic Resistance Threats in the United States, 2019. CDC.

17. Paredes-Sabja D, Shen A, Sorg JA. 2014. *Clostridium difficile* spore biology: sporulation, germination, and spore structural proteins. Trends Microbiol 22:406–416.

18. Stewart GS, Johnstone K, Hagelberg E, Ellar DJ. 1981. Commitment of bacterial spores to germinate. A measure of the trigger reaction. Biochem J 198:101–106.

19. Sterlini JM, Mandelstam J. 1969. Commitment to sporulation in Bacillus subtilis and its relationship to development of actinomycin resistance. Biochem J 113:29–37.

20. Lee CD, Rizvi A, Edwards AN, DiCandia MA, Vargas Cuebas GG, Monteiro MP, McBride SM. 2022. Genetic mechanisms governing sporulation initiation in *Clostridioides difficile*. Curr Opin Microbiol 66:32–38.

21. Buggy BP, Wilson KH, Fekety R. 1983. Comparison of methods for recovery of *Clostridium difficile* from an environmental surface. J Clin Microbiol 18:348–352.

22. Lawley TD, Clare S, Walker AW, Goulding D, Stabler RA, Croucher N, Mastroeni P, Scott P, Raisen C, Mottram L, Fairweather NF, Wren BW, Parkhill J, Dougan G. 2009. Antibiotic Treatment of *Clostridium difficile* Carrier Mice Triggers a Supershedder State, Spore-Mediated Transmission, and Severe Disease in Immunocompromised Hosts. Infect Immun 77:3661–3669.

23. Jump RLP, Pultz MJ, Donskey CJ. 2007. Vegetative *Clostridium difficile* Survives in Room Air on Moist Surfaces and in Gastric Contents with Reduced Acidity: a Potential Mechanism To Explain the Association between Proton Pump Inhibitors and *C difficile*-Associated Diarrhea? Antimicrob Agents Chemother 51:2883–2887.

24. Kim KH, Fekety R, Batts DH, Brown D, Cudmore M, Silva J Jr, Waters D. 1981. Isolation of *Clostridium difficile* from the Environment and Contacts of Patients with Antibiotic-Associated Colitis. J Infect Dis 143:42–50.

25. Ali S, Moore G, Wilson APR. 2011. Spread and persistence of *Clostridium difficile* spores during and after cleaning with sporicidal disinfectants. J Hosp Infect 79:97–98.

26. Neumann-Schaal M, Metzendorf NG, Troitzsch D, Nuss AM, Hofmann JD, Beckstette M, Dersch P, Otto A, Sievers S. 2018. Tracking gene expression and oxidative damage of O2-stressed *Clostridioides difficile* by a multi-omics approach. Anaerobe 53:94–107.

27. Kint N, Morvan C, Martin-Verstraete I. 2022. Oxygen response and tolerance mechanisms in *Clostridioides difficile*. Curr Opin Microbiol 65:175–182.

28. McFarland LV. 2008. Antibiotic-associated diarrhea: epidemiology, trends and treatment. Future Microbiol 3:563–578.

29. Dial S, Delaney JAC, Barkun AN, Suissa S. 2005. Use of Gastric Acid–Suppressive Agents and the Risk of Community-Acquired *Clostridium difficile*–Associated Disease. JAMA 294:2989–2995.

30. Oh J, Makar M, Fusco C, McCaffrey R, Rao K, Ryan EE, Washer L, West LR, Young VB, Guttag J, Hooper DC, Shenoy ES, Wiens J. 2018. A Generalizable, Data-Driven Approach to Predict Daily Risk of *Clostridium difficile* Infection at Two Large Academic Health Centers. Infect Control Hosp Epidemiol 39:425–433.

31. Keller JM, Surawicz CM. 2014. *Clostridium difficile* infection in the elderly. Clin Geriatr Med 30:79–93.

32. Revolinski SL, Munoz-Price LS. 2019. *Clostridium difficile* in Immunocompromised Hosts: A Review of Epidemiology, Risk Factors, Treatment, and Prevention. Clin Infect Dis 68:2144–2153.

33. Vollaard E J, Clasener H A. 1994. Colonization resistance. Antimicrob Agents Chemother 38:409–414.

34. Wilson KH. 1983. Efficiency of various bile salt preparations for stimulation of *Clostridium difficile* spore germination. J Clin Microbiol 18:1017–1019.

35. Sorg JA, Sonenshein AL. 2008. Bile Salts and Glycine as Cogerminants for *Clostridium difficile* Spores. J Bacteriol 190:2505–2512.

36. Kordus SL, Thomas AK, Lacy DB. 2022. *Clostridioides difficile* toxins: mechanisms of action and antitoxin therapeutics. Nat Rev Microbiol 20:285–298.

37. Bouillaut L, Dubois T, Sonenshein AL, Dupuy B. 2015. Integration of metabolism and virulence in *Clostridium difficile*. Res Microbiol 166:375–383.

38. Zackular JP, Moore JL, Jordan AT, Juttukonda LJ, Noto MJ, Nicholson MR, Crews JD, Semler MW, Zhang Y, Ware LB, Washington MK, Chazin WJ, Caprioli RM, Skaar EP. 2016. Dietary zinc alters the microbiota and decreases resistance to *Clostridium difficile* infection. 11. Nat Med 22:1330–1334.

39. Napolitano LM, Edmiston CE. 2017. *Clostridium difficile* disease: Diagnosis, pathogenesis, and treatment update. Surgery 162:325–348.

40. Dehority W. 2010. Use of Vancomycin in Pediatrics. Pediatr Infect Dis J 29:462.

41. Kelly CR, Khoruts A, Staley C, Sadowsky MJ, Abd M, Alani M, Bakow B, Curran P, McKenney J, Tisch A, Reinert SE, Machan JT, Brandt LJ. 2016. Effect of Fecal Microbiota Transplantation on Recurrence in Multiply Recurrent *Clostridium difficile* Infection. Ann Intern Med 165:609–616.

42. Ofori E, Ramai D, Dhawan M, Mustafa F, Gasperino J, Reddy M. 2018. Community-acquired *Clostridium difficile*: epidemiology, ribotype, risk factors, hospital and intensive care unit outcomes, and current and emerging therapies. J Hosp Infect 99:436–442.

43. Ramirez-Ronda CH. 1974. Letter: Incidence of clindamycin-associated colitis. Ann Intern Med 81:860.

44. Swartzberg JE, Maresca RM, Remington JS. 1977. Clinical study of gastrointestinal complications associated with clindamycin therapy. J Infect Dis 135 Suppl:S99-103.

45. Tedesco FJ, Barton RW, Alpers DH. 1974. Clindamycin-associated colitis. A prospective study. Ann Intern Med 81:429–433.

46. Kramer IRH. 1948. Fatal Staphylococcal enteritis developing during streptomycin therapy by mouth. The Lancet 252:646–647.

47. Hummel RP, Altemeier WA, Hill EO. 1964. Iatrogenic Staphylococcal Enterocolitis. Ann Surg 160:551–557.

48. Altemeier WA, Hummel RP, Hill EO. 1963. Staphylococcal Enterocolitis Following Antibiotic Therapy. Ann Surg 157.

49. Khan MY, Hall WH. 1966. Staphylococcal Enterocolitis—Treatment with Oral Vancomycin. Ann Intern Med 65:1–8.

50. Bartlett JG. 1990. *Clostridium difficile*: Clinical Considerations. Rev Infect Dis 12:S243–S251.

51. Birkenmeyer RD, Kagan F. 1970. Lincomycin. XI. Synthesis and structure of clindamycin. A potent antibacterial agent. J Med Chem 13:616–619.

52. Marr JJ, Sans MD, Tedesco FJ. 1975. Bacterial Studies of Clindamycin-Associated Colitis: A preliminary report. Gastroenterology 69:352–358.

53. Gurwith MJ, Rabin HR, Love K, Cooperative Antibiotic Diarrhea Study Group. 1977. Diarrhea Associated with Clindamycin and Ampicillin Therapy: Preliminary Results of a Cooperative Study. J Infect Dis 135:S104–S110.

54. Small JD. 1968. Fatal enterocolitis in hamsters given lincomycin hydrochloride. Lab Anim Care 18:411–420.

55. Bartlett JG, Onderdonk AB, Cisneros RL. 1977. Clindamycin-associated colitis in hamsters: protection with vancomycin. Gastroenterology 73:772–776.

56. Bartlett JG, Onderdonk AB, Cisneros RL, Kasper DL. 1977. Clindamycin-Associated Colitis Due to a Toxin-Producing Species of Clostridium in Hamsters. J Infect Dis 136:701–705.

57. Lindsey D, Wise HM, Knecht AT, Noyes HE. 1959. Influence of Route of Administration on Effectiveness of Clostridial Antitoxin. AMA Arch Surg 78:328–330.

58. Arseculeratne SN, Panabokké RG, Wijesundera S. 1969. The Toxins Responsible for the Lesions of *Clostridium sordelli* Gas Gangrene. J Med Microbiol 2:37–53.

59. Weinstein L, Barza MA. 1973. Gas gangrene. N Engl J Med 289:1129–1131.

60. Junior CAO, Silva ROS, Lobato FCF, Navarro MA, Uzal FA. 2020. Gas gangrene in mammals: a review. J Vet Diagn Invest 32:175–183.

61. Larson HE, Price AB. 1977. Pseudomembranous colitis: Presence of clostridial toxin. The Lancet 310:1312–1314.

62. Rifkin GD, Fekety FR, Silva J, Sack RB. 1977. Antibiotic-induced colitis implication of a toxin neutralised by *Clostridium sordellii* antitoxin. The Lancet 310:1103–1106.

63. Bornside GH, Floyd CE, Cohn I. 1964. *Clostridium sordelli* toxin in strangulation obstruction: Further studies of serial changes of intestinal contents. J Surg Res 4:233–239.

64. Bartlett JG, Chang TW, Gurwith M, Gorbach SL, Onderdonk AB. 1978. Antibiotic-Associated Pseudomembranous Colitis Due to Toxin-Producing Clostridia. N Engl J Med 298:531–534.

65. Bartlett JG, Chang TW, Onderdonk AB. 1978. Will the real Clostridium species responsible for antibiotic-associated colitis please step forward? Lancet Lond Engl 1:338.

66. Burdon DW, George RH. 1978. Pseudomembranous colitis. The Lancet 311:444–445.

67. Keighley M, Alexander-Williams J, Arabi Y, Youngs D, Burdon D, Shinagawa N, Thompson H, Bentley S, George R. 1978. Diarrhoea and pseudomembranous colitis after gastrointestinal operations: a prospective study. The Lancet 312:1165–1167.

68. Larson HE, Price AB, Honour P, Borriello SP. 1978. *Clostridium difficile* and the aetiology of pseudomembranous colitis. The Lancet 311:1063–1066.

69. Chang TW, Bartlett JG, Gorbach SL, Onderdonk AB. 1978. Clindamycin-induced enterocolitis in hamsters as a model of pseudomembranous colitis in patients. Infect Immun 20:526–529.

70. Humphrey CD, Condon CW, Cantey JR, Pittman FE. 1979. Partial Purification of a Toxin Found in Hamsters with Antibiotic-Associated Colitis: Reversible Binding of the Toxin by Cholestyramine. Gastroenterology 76:468–476.

71. Taylor NS, Bartlett JG. 1979. Partial Purification and Characterization of a Cytotoxin from *Clostridium difficile*. Rev Infect Dis 1:379–385.

72. Rolfe R D, Finegold S M. 1979. Purification and characterization of *Clostridium difficile* toxin. Infect Immun 25:191–201.

73. Lyerly DM, Lockwood DE, Richardson SH, Wilkins TD. 1982. Biological activities of toxins A and B of *Clostridium difficile*. Infect Immun 35:1147–1150.

74. Sullivan NM, Pellett S, Wilkins TD. 1982. Purification and characterization of toxins A and B of *Clostridium difficile*. Infect Immun 35:1032–1040.

75. Libby JM, Wilkins TD. 1982. Production of Antitoxins to Two Toxins of *Clostridium difficile* and Immunological Comparison of the Toxins by Cross-Neutralization Studies. Infect Immun 35:374–376.

76. Banno Y, Kobayashi T, Watanabe K, Ueno K, Nozawa Y. 1981. Two toxins (D-1 and D-2) of *Clostridium difficile* causing antibiotic-associated colitis - purification and some characterization. Biochem Int 2:629–635.

77. Libby JM, Jortner BS, Wilkins TD. 1982. Effects of the two toxins of *Clostridium difficile* in antibiotic-associated cecitis in hamsters. Infect Immun 36:822–829.

78. Lyerly DM, Saum KE, MacDonald DK, Wilkins TD. 1985. Effects of *Clostridium difficile* toxins given intragastrically to animals. Infect Immun 47:349–352.

79. Arnon SS, Mills DC, Day PA, Henrickson RV, Sullivan NM, Wilkins TD. 1984. Rapid death of infant rhesus monkeys injected with *Clostridium difficile* toxins A and B: Physiologic and pathologic basis. J Pediatr 104:34–40.

80. Lyerly DM, Roberts MD, Phelps CJ, Wilkins TD. 1986. Purification and properties of toxins A and B of *Clostridium difficile*. FEMS Microbiol Lett 33:31–35.

81. Lönnroth I, Lange S. 1983. Toxin A of *Clostridium difficile*: production, purification and effect in mouse intestine. Acta Pathol Microbiol Immunol Scand [B] 91:395–400.

82. Gill DM, Richardson SH. 1980. Adenosine Diphosphate-Ribosylation of Adenylate Cyclase Catalyzed by Heat-Labile Enterotoxin of *Escherichia coli*: Comparison with Cholera Toxin. J Infect Dis 141:64–70.

83. Cassel D, Pfeuffer T. 1978. Mechanism of cholera toxin action: Covalent modification of the guanyl nucleotide-binding protein of the adenylate cyclase system. Proc Natl Acad Sci 75:2669–2673.

84. Field M, Rao MC, Chang EB. 1989. Intestinal Electrolyte Transport and Diarrheal Disease. N Engl J Med 321:879–883.

85. Triadafilopoulos G, Pothoulakis C, O'Brien MJ, LaMont JT. 1987. Differential effects of *Clostridium difficile* toxins A and B on rabbit ileum. Gastroenterology 93:273–279.

86. Pothoulakis C, Sullivan R, Melnick DA, Triadafilopoulos G, Gadenne AS, Meshulam T, LaMont JT. 1988. *Clostridium difficile* toxin A stimulates intracellular calcium release and chemotactic response in human granulocytes. J Clin Invest 81:1741–1745.

87. Sullivan R, Melnick DA, Malech HL, Meshulam T, Simons ER, Lazzari KG, Proto PJ, Gadenne AS, Leavitt JL, Griffin JD. 1987. The effects of phorbol myristate acetate and chemotactic peptide on transmembrane potentials and cytosolic free calcium in mature granulocytes evolve sequentially as the cells differentiate. J Biol Chem 262:1274–1281.

88. Miller PD, Pothoulakis C, Baeker TR, LaMont JT, Rothstein TL. 1990. Macrophage-dependent stimulation of T cell-depleted spleen cells by *Clostridium difficile* toxin A and calcium ionophore. Cell Immunol 126:155–163.

89. Hecht G, Pothoulakis C, LaMont JT, Madara JL. 1988. *Clostridium difficile* toxin A perturbs cytoskeletal structure and tight junction permeability of cultured human intestinal epithelial monolayers. J Clin Invest 82:1516–1524.

90. Hecht G, Koutsouris A, Pothoulakis C, LaMont JT, Madara JL. 1992. *Clostridium difficile* toxin B disrupts the barrier function of T84 monolayers. Gastroenterology 102:416–423.

91. Wedel N, Toselli P, Pothoulakis C, Faris B, Oliver P, Franzblau C, LaMont T. 1983. Ultrastructural effects of *Clostridium difficile* toxin B on smooth muscle cells and fibroblasts. Exp Cell Res 148:413–422.

92. Shen L, Su L, Turner JR. 2009. Mechanisms and Functional Implications of Intestinal Barrier Defects. Dig Dis Basel Switz 27:443–449.

93. Riegler M, Sedivy R, Pothoulakis C, Hamilton G, Zacherl J, Bischof G, Cosentini E, Feil W, Schiessel R, LaMont JT. 1995. *Clostridium difficile* toxin B is more potent than toxin A in damaging human colonic epithelium in vitro. J Clin Invest 95:2004–2011.

94. Alfa MJ, Kabani A, Lyerly D, Moncrief S, Neville LM, Al-Barrak A, Harding GKH, Dyck B, Olekson K, Embil JM. 2000. Characterization of a Toxin A-Negative, Toxin B-Positive Strain of *Clostridium difficile* Responsible for a Nosocomial Outbreak of *Clostridium difficile*-Associated Diarrhea. J Clin Microbiol 38:2706–2714.

95. Limaye AP, Turgeon DK, Cookson BT, Fritsche TR. 2000. Pseudomembranous Colitis Caused by a Toxin A– B+ Strain of *Clostridium difficile*. J Clin Microbiol 38:1696–1697.

96. Depitre C, Delmee M, Avesani V, Roels A, L'haridon R, Popoff M, Corthier G. 1993. Serogroup F Strains of *Clostridium difficile* Produce Toxin B but not Toxin A. J Med Microbiol 38:434–441.

97. Rupnik M, Avesani V, Janc M, von Eichel-Streiber C, Delmée M. 1998. A Novel Toxinotyping Scheme and Correlation of Toxinotypes with Serogroups of *Clostridium difficile* Isolates. J Clin Microbiol 36:2240–2247.

98. Savidge TC, Pan W, Newman P, O'Brien M, Anton PM, Pothoulakis C. 2003. *Clostridium difficile* toxin B is an inflammatory enterotoxin in human intestine. Gastroenterology 125:413–420.

99. O'Connor JR, Lyras D, Farrow KA, Adams V, Powell DR, Hinds J, Cheung JK, Rood JI. 2006. Construction and analysis of chromosomal *Clostridium difficile* mutants. Mol Microbiol 61:1335–1351.

100. Heap JT, Pennington OJ, Cartman ST, Carter GP, Minton NP. 2007. The ClosTron: A universal gene knock-out system for the genus Clostridium. J Microbiol Methods 70:452–464.

101. Lyras D, O'Connor JR, Howarth PM, Sambol SP, Carter GP, Phumoonna T, Poon R, Adams V, Vedantam G, Johnson S, Gerding DN, Rood JI. 2009. Toxin B is essential for virulence of *Clostridium difficile*. Nature 458:1176–1179.

102. Kuehne SA, Cartman ST, Heap JT, Kelly ML, Cockayne A, Minton NP. 2010. The role of toxin A and toxin B in *Clostridium difficile* infection. 7316. Nature 467:711–713.

103. Ballard JD. 2010. A toxin contest. 7316. Nature 467:665–666.

104. Gill N, Finlay BB. 2011. The gut microbiota: challenging immunology. 10. Nat Rev Immunol 11:636–637.

105. Kuehne SA, Collery MM, Kelly ML, Cartman ST, Cockayne A, Minton NP. 2014. Importance of Toxin A, Toxin B, and CDT in Virulence of an Epidemic *Clostridium difficile* Strain. J Infect Dis 209:83–86.

106. Carter GP, Chakravorty A, Pham Nguyen TA, Mileto S, Schreiber F, Li L, Howarth P, Clare S, Cunningham B, Sambol SP, Cheknis A, Figueroa I, Johnson S, Gerding D, Rood JI, Dougan G, Lawley TD, Lyras D. 2015. Defining the Roles of TcdA and TcdB in Localized Gastrointestinal Disease, Systemic Organ Damage, and the Host Response during *Clostridium difficile* Infections. mBio 6.

107. Mansfield MJ, Tremblay BJM, Zeng J, Wei X, Hodgins H, Worley J, Bry L, Dong M, Doxey AC. 2020. Phylogenomics of 8,839 *Clostridioides difficile* genomes reveals recombination-driven evolution and diversification of toxin A and B. PLoS Pathog 16:e1009181.

108. Lemee L, Bourgeois I, Ruffin E, Collignon A, Lemeland J-F, Pons J-L. 2005. Multilocus sequence analysis and comparative evolution of virulence-associated genes and housekeeping genes of *Clostridium difficile*. Microbiology 151:3171–3180.

109. Griffiths D, Fawley W, Kachrimanidou M, Bowden R, Crook DW, Fung R, Golubchik T, Harding RM, Jeffery KJM, Jolley KA, Kirton R, Peto TE, Rees G, Stoesser N, Vaughan A, Walker AS, Young BC, Wilcox M, Dingle KE. 2010. Multilocus sequence typing of *Clostridium difficile*. J Clin Microbiol 48:770–778.

110. Peritore-Galve FC, Shupe JA, Cave RJ, Childress KO, Washington MK, Kuehne SA, Lacy DB. 2022. Glucosyltransferase-dependent and independent effects of *Clostridioides difficile* toxins during infection. PLOS Pathog 18:e1010323.

111. Popoff MR, Rubin EJ, Gill DM, Boquet P. 1988. Actin-specific ADP-ribosyltransferase produced by a *Clostridium difficile* strain. Infect Immun 56:2299–2306.

112. Perelle S, Gibert M, Bourlioux P, Corthier G, Popoff MR. 1997. Production of a complete binary toxin (actin-specific ADP-ribosyltransferase) by *Clostridium difficile* CD196. Infect Immun 65:1402–1407.

113. Bacci S, Mølbak K, Kjeldsen MK, Olsen KEP. 2011. Binary Toxin and Death after *Clostridium difficile* Infection. Emerg Infect Dis J 17.

114. Martin JSH, Monaghan TM, Wilcox MH. 2016. *Clostridium difficile* infection: epidemiology, diagnosis and understanding transmission. 4. Nat Rev Gastroenterol Hepatol 13:206–216.

115. Gülke I, Pfeifer G, Liese J, Fritz M, Hofmann F, Aktories K, Barth H. 2001. Characterization of the Enzymatic Component of the ADP-Ribosyltransferase Toxin CDTa from *Clostridium difficile*. Infect Immun 69:6004–6011.

116. Cowardin CA, Buonomo EL, Saleh MM, Wilson MG, Burgess SL, Kuehne SA, Schwan C, Eichhoff AM, Koch-Nolte F, Lyras D, Aktories K, Minton NP, Petri WA. 2016. The binary toxin CDT enhances *Clostridium difficile* virulence by suppressing protective colonic eosinophilia. 8. Nat Microbiol 1:1–10.

117. Buonomo EL, Cowardin CA, Wilson MG, Saleh MM, Pramoonjago P, Petri WA. 2016. Microbiota-Regulated IL-25 Increases Eosinophil Number to Provide Protection during *Clostridium difficile* Infection. Cell Rep 16:432–443.

118. Frisbee AL, Saleh MM, Young MK, Leslie JL, Simpson ME, Abhyankar MM, Cowardin CA, Ma JZ, Pramoonjago P, Turner SD, Liou AP, Buonomo EL, Petri WA. 2019. IL-33 drives group 2 innate lymphoid cell-mediated protection during *Clostridium difficile* infection. 1. Nat Commun 10:2712.

119. Schwan C, Stecher B, Tzivelekidis T, van Ham M, Rohde M, Hardt W-D, Wehland J, Aktories K. 2009. *Clostridium difficile* Toxin CDT Induces Formation of Microtubule-Based Protrusions and Increases Adherence of Bacteria. PLOS Pathog 5:e1000626.

120. Schwan C, Kruppke AS, Nölke T, Schumacher L, Koch-Nolte F, Kudryashev M, Stahlberg H, Aktories K. 2014. *Clostridium difficile* toxin CDT hijacks microtubule organization and reroutes vesicle traffic to increase pathogen adherence. Proc Natl Acad Sci 111:2313–2318.

121. Nölke T, Schwan C, Lehmann F, Østevold K, Pertz O, Aktories K. 2016. Septins guide microtubule protrusions induced by actin-depolymerizing toxins like *Clostridium difficile* transferase (CDT). Proc Natl Acad Sci 113:7870–7875.

122. Genth H, Dreger SC, Huelsenbeck J, Just I. 2008. *Clostridium difficile* toxins: More than mere inhibitors of Rho proteins. Int J Biochem Cell Biol 40:592–597.

123. Just I, Wilm M, Selzer J, Rex G, von Eichel-Streiber C, Mann M, Aktories K. 1995. The enterotoxin from *Clostridium difficile* (ToxA) monoglucosylates the Rho proteins. J Biol Chem 270:13932–13936.

124. Just I, Fritz G, Aktories K, Giry M, Popoff MR, Boquet P, Hegenbarth S, von Eichel-Streiber C. 1994. *Clostridium difficile* toxin B acts on the GTP-binding protein Rho. J Biol Chem 269:10706–10712.

125. Just I, Selzer J, Wilm M, Eichel-Streiber C von, Mann M, Aktories K. 1995. Glucosylation of Rho proteins by *Clostridium difficile* toxin B. 6531. Nature 375:500–503.

126. Genth H, Pauillac S, Schelle I, Bouvet P, Bouchier C, Varela-Chavez C, Just I, Popoff MR. 2014. Haemorrhagic toxin and lethal toxin from *Clostridium sordelli* strain vpi9048: Molecular characterization and comparative analysis of substrate specificity of the large clostridial glucosylating toxins. Cell Microbiol 16:1706–1721.

127. Popoff MR, Chaves-Olarte E, Lemichez E, von Eichel-Streiber C, Thelestam M, Chardin P, Cussac D, Antonny B, Chavrier P, Flatau G, Giry M, de Gunzburg J, Boquet P. 1996. Ras, Rap, and Rac small GTP-binding proteins are targets for *Clostridium sordelli* lethal toxin glucosylation. J Biol Chem 271:10217–10224.

128. Nagahama M, Ohkubo A, Oda M, Kobayashi K, Amimoto K, Miyamoto K, Sakurai J. 2011. *Clostridium perfringens* TpeL Glycosylates the Rac and Ras Subfamily Proteins. Infect Immun 79:905–910.

129. Selzer J, Hofmann F, Rex G, Wilm M, Mann M, Just I, Aktories K. 1996. *Clostridium novyi* α-Toxin-catalyzed Incorporation of GlcNAc into Rho Subfamily Proteins. J Biol Chem 271:25173–25177.

130. Orrell Kathleen E., Melnyk Roman A. 2021. Large Clostridial Toxins: Mechanisms and Roles in Disease. Microbiol Mol Biol Rev 85:e00064-21.

131. Sehr P, Joseph G, Genth H, Just I, Pick E, Aktories K. 1998. Glucosylation and ADP Ribosylation of Rho Proteins: Effects on Nucleotide Binding, GTPase Activity, and Effector Coupling. Biochemistry 37:5296–5304.

132. Genth H, Aktories K, Just I. 1999. Monoglucosylation of RhoA at threonine 37 blocks cytosol-membrane cycling. J Biol Chem 274:29050–29056.

133. Vetter IR, Hofmann F, Wohlgemuth S, Herrmann C, Just I. 2000. Structural consequences of mono-glucosylation of Ha-Ras by *Clostridium sordelli* lethal toxin. J Mol Biol 301:1091–1095.

134. Geyer M, Wilde C, Selzer J, Aktories K, Kalbitzer HR. 2003. Glucosylation of Ras by *Clostridium sordelli* Lethal Toxin: Consequences for Effector Loop Conformations Observed by NMR Spectroscopy. Biochemistry 42:11951–11959.

135. Pruitt RN, Chambers MG, Ng KK-S, Ohi MD, Lacy DB. 2010. Structural organization of the functional domains of *Clostridium difficile* toxins A and B. Proc Natl Acad Sci 107:13467–13472.

136. Amimoto Katsuhiko, Noro Taichi, Oishi Eiji, Shimizu Mitsugu. 2007. A novel toxin homologous to large clostridial cytotoxins found in culture supernatant of *Clostridium perfringens* type C. Microbiology 153:1198–1206.

137. Genisyuerek S, Papatheodorou P, Guttenberg G, Schubert R, Benz R, Aktories K. 2011. Structural determinants for membrane insertion, pore formation and translocation of *Clostridium difficile* toxin B. Mol Microbiol 79:1643–1654.

138. Pruitt RN, Chumbler NM, Rutherford SA, Farrow MA, Friedman DB, Spiller B, Lacy DB. 2012. Structural Determinants of *Clostridium difficile* Toxin A Glucosyltransferase Activity. J Biol Chem 287:8013–8020.

139. Egerer M, Giesemann T, Herrmann C, Aktories K. 2009. Autocatalytic Processing of *Clostridium difficile* Toxin B: Binding of inositol hexakisphosphate. J Biol Chem 284:3389–3395.

140. Shen A, Lupardus PJ, Gersch MM, Puri AW, Albrow VE, Garcia KC, Bogyo M. 2011. Defining an allosteric circuit in the cysteine protease domain of *Clostridium difficile* toxins. 3. Nat Struct Mol Biol 18:364–371.

141. Pruitt RN, Chagot B, Cover M, Chazin WJ, Spiller B, Lacy DB. 2009. Structure-function analysis of inositol hexakisphosphate-induced autoprocessing in *Clostridium difficile* toxin A. J Biol Chem 284:21934–21940.

142. Reineke J, Tenzer S, Rupnik M, Koschinski A, Hasselmayer O, Schrattenholz A, Schild H, von Eichel-Streiber C. 2007. Autocatalytic cleavage of *Clostridium difficile* toxin B. Nature 446:415–419.

143. Chumbler NM, Rutherford SA, Zhang Z, Farrow MA, Lisher JP, Farquhar E, Giedroc DP, Spiller BW, Melnyk RA, Lacy DB. 2016. Crystal structure of *Clostridium difficile* toxin A. Nat Microbiol 1:15002.

144. Verma S, Dixit R, Pandey KC. 2016. Cysteine Proteases: Modes of Activation and Future Prospects as Pharmacological Targets. Front Pharmacol 7.

145. Zhang Z, Park M, Tam J, Auger A, Beilhartz GL, Lacy DB, Melnyk RA. 2014. Translocation domain mutations affecting cellular toxicity identify the *Clostridium difficile* toxin B pore. Proc Natl Acad Sci U S A 111:3721–3726.

146. Just I, Gerhard R. 2005. Large clostridial cytotoxins, p. 23–47. *In* Reviews of Physiology, Biochemistry and Pharmacology. Springer, Berlin, Heidelberg.

147. Barroso LA, Moncrief JS, Lyerly DM, Wilkins TD. 1994. Mutagenesis of the *Clostridium difficile* toxin B gene and effect on cytotoxic activity. Microb Pathog 16:297–303.

148. Chen P, Lam K, Liu Z, Mindlin FA, Chen B, Gutierrez CB, Huang L, Zhang Y, Hamza T, Feng H, Matsui T, Bowen ME, Perry K, Jin R. 2019. Structure of the full-length *Clostridium difficile* toxin B. 8. Nat Struct Mol Biol 26:712–719.

149. Chen B, Basak S, Chen P, Zhang C, Perry K, Tian S, Yu C, Dong M, Huang L, Bowen ME, Jin R. 2022. Structure and conformational dynamics of *Clostridioides difficile* toxin A. Life Sci Alliance 5.

150. Aminzadeh A, Larsen CE, Boesen T, Jørgensen R. 2022. High-resolution structure of native toxin A from *Clostridioides difficile*. EMBO Rep 23:e53597.

151. Jiang M, Shin J, Simeon R, Chang J-Y, Meng R, Wang Y, Shinde O, Li P, Chen Z, Zhang J. 2022. Structural dynamics of receptor recognition and pH-induced dissociation of full-length *Clostridioides difficile* Toxin B. PLOS Biol 20:e3001589.

152. Hartley-Tassell LE, Awad MM, Seib KL, Scarselli M, Savino S, Tiralongo J, Lyras D, Day CJ, Jennings MP. 2019. Lectin Activity of the TcdA and TcdB Toxins of *Clostridium difficile*. Infect Immun 87:e00676-18.

153. Hofmann F, Rex G, Aktories K, Just I. 1996. The Ras-Related Protein Ral Is Monoglucosylated by *Clostridium sordelli* Lethal Toxin. Biochem Biophys Res Commun 227:77–81.

154. Tao L, Zhang J, Meraner P, Tovaglieri A, Wu X, Gerhard R, Zhang X, Stallcup WB, Miao J, He X, Hurdle JG, Breault DT, Brass AL, Dong M. 2016. Frizzled proteins are colonic epithelial receptors for C. difficile toxin B. Nature 538:350–355.

155. Yuan P, Zhang H, Cai C, Zhu S, Zhou Y, Yang X, He R, Li C, Guo S, Li S, Huang T, Perez-Cordon G, Feng H, Wei W. 2015. Chondroitin sulfate proteoglycan 4 functions as the cellular receptor for *Clostridium difficile* toxin B. Cell Res 25:157–168.

156. LaFrance ME, Farrow MA, Chandrasekaran R, Sheng J, Rubin DH, Lacy DB. 2015. Identification of an epithelial cell receptor responsible for *Clostridium difficile* TcdB-induced cytotoxicity. Proc Natl Acad Sci 112:7073–7078.

157. Luo J, Yang Q, Zhang X, Zhang Y, Wan L, Zhan X, Zhou Y, He L, Li D, Jin D, Zhen Y, Huang J, Li Y, Tao L. 2022. TFPI is a colonic crypt receptor for TcdB from hypervirulent clade 2 C. difficile. Cell 185:980-994.e15.

158. Tian S, Xiong X, Zeng J, Wang S, Tremblay BJ-M, Chen P, Chen B, Liu M, Chen P, Sheng K, Zeve D, Qi W, Breault DT, Rodríguez C, Gerhard R, Jin R, Doxey AC, Dong M. 2022. Identification of TFPI as a receptor reveals recombination-driven receptor switching in *Clostridioides difficile* toxin B variants. Nat Commun 13:6786.

159. Schöttelndreier D, Seeger K, Grassl GA, Winny MR, Lindner R, Genth H. 2018. Expression and (Lacking) internalization of the cell surface receptors of *Clostridioides difficile* toxin B. Front Microbiol 9:1483.

160. Chen P, Zeng J, Liu Z, Thaker H, Wang S, Tian S, Zhang J, Tao L, Gutierrez CB, Xing L, Gerhard R, Huang L, Dong M, Jin R. 2021. Structural basis for CSPG4 as a receptor for TcdB and a therapeutic target in *Clostridioides difficile* infection. Nat Commun 12:3748.

161. Chen P, Tao L, Wang T, Zhang J, He A, Lam K, Liu Z, He X, Perry K, Dong M, Jin R. 2018. Structural basis for recognition of frizzled proteins by *Clostridium difficile* Toxin B. Science 360:664 LP – 669.

162. Shen E, Zhu K, Li D, Pan Z, Luo Y, Bian Q, He L, Song X, Zhen Y, Jin D, Tao L. 2020. Subtyping analysis reveals new variants and accelerated evolution of *Clostridioides difficile* toxin B. 1. Commun Biol 3:1–8.

163. Pan Z, Zhang Y, Luo J, Li D, Zhou Y, He L, Yang Q, Dong M, Tao L. 2021. Functional analyses of epidemic *Clostridioides difficile* toxin B variants reveal their divergence in utilizing receptors and inducing pathology. PLOS Pathog 17:e1009197.

164. Von Eichel-Streiber C, Zu Heringdorf DM, Habermann E, Sartingen S. 1995. Closing in on the toxic domain through analysis of a variant *Clostridium difficile* cytotoxin B. Mol Microbiol 17:313–321.

165. Lanis JM, Barua S, Ballard JD. 2010. Variations in TcdB activity and the hypervirulence of emerging strains of *Clostridium difficile*. PLoS Pathog 6:e1001061.

166. Quesada-Gómez C, López-Ureña D, Chumbler N, Kroh HK, Castro-Peña C, Rodríguez C, Orozco-Aguilar J, González-Camacho S, Rucavado A, Guzmán-Verri C, Lawley TD, Lacy DB, Chaves-Olarte E. 2016. Analysis of TcdB Proteins within the Hypervirulent Clade 2 Reveals an Impact of RhoA Glucosylation on *Clostridium difficile* Proinflammatory Activities. Infect Immun 84:856–865.

167. Lanis JM, Heinlen LD, James JA, Ballard JD. 2013. *Clostridium difficile* 027/BI/NAP1 Encodes a Hypertoxic and Antigenically Variable Form of TcdB. PLOS Pathog 9:e1003523.

168. Clabots CR, Johnson S, Bettin KM, Mathie PA, Mulligan ME, Schaberg DR, Peterson LR, Gerding DN. 1993. Development of a rapid and efficient restriction endonuclease analysis typing system for *Clostridium difficile* and correlation with other typing systems. J Clin Microbiol 31:1870–1875.

169. Loo VG, Poirier L, Miller MA, Oughton M, Libman MD, Michaud S, Bourgault A-M, Nguyen T, Frenette C, Kelly M. 2005. A predominantly clonal multi-institutional outbreak of *Clostridium difficile*–associated diarrhea with high morbidity and mortality. N Engl J Med 353:2442–2449.

170. Warny M, Pepin J, Fang A, Killgore G, Thompson A, Brazier J, Frost E, McDonald LC. 2005. Toxin production by an emerging strain of *Clostridium difficile* associated with outbreaks of severe disease in North America and Europe. The Lancet 366:1079–1084.

171. McDonald LC, Killgore GE, Thompson A, Owens Jr RC, Kazakova SV, Sambol SP, Johnson S, Gerding DN. 2005. An epidemic, toxin gene–variant strain of *Clostridium difficile*. N Engl J Med 353:2433–2441.

172. See I, Mu Y, Cohen J, Beldavs ZG, Winston LG, Dumyati G, Holzbauer S, Dunn J, Farley MM, Lyons C, Johnston H, Phipps E, Perlmutter R, Anderson L, Gerding DN, Lessa FC. 2014. NAP1 Strain Type Predicts Outcomes from *Clostridium difficile* Infection. Clin Infect Dis Off Publ Infect Dis Soc Am 58:1394–1400.

173. Layton B, ML GD, Liedtke L, Strausbaugh L. 2005. Perceived increases in the incidence and severity of *Clostridium difficile* disease: an emerging threat that continues to unfold.

174. Walk ST, Micic D, Jain R, Lo ES, Trivedi I, Liu EW, Almassalha LM, Ewing SA, Ring C, Galecki AT, Rogers MAM, Washer L, Newton DW, Malani PN, Young VB, Aronoff DM. 2012. *Clostridium difficile* Ribotype Does Not Predict Severe Infection. Clin Infect Dis 55:1661–1668.

175. Stabler RA, Dawson LF, Phua LTH, Wren BW. 2008. Comparative analysis of BI/NAP1/027 hypervirulent strains reveals novel toxin B-encoding gene (tcdB) sequences. J Med Microbiol 57:771–775.

176. Dingle KE, Griffiths D, Didelot X, Evans J, Vaughan A, Kachrimanidou M, Stoesser N, Jolley KA, Golubchik T, Harding RM, Peto TE, Fawley W, Walker AS, Wilcox M, Crook DW. 2011. Clinical *Clostridium difficile*: Clonality and Pathogenicity Locus Diversity. PLOS ONE 6:e19993.

177. Mileto SJ, Jardé T, Childress KO, Jensen JL, Rogers AP, Kerr G, Hutton ML, Sheedlo MJ, Bloch SC, Shupe JA, Horvay K, Flores T, Engel R, Wilkins S, McMurrick PJ, Lacy DB, Abud HE, Lyras D. 2020. *Clostridioides difficile* infection damages colonic stem cells via TcdB, impairing epithelial repair and recovery from disease. Proc Natl Acad Sci 117:8064 LP – 8073.

178. López-Ureña D, Orozco-Aguilar J, Chaves-Madrigal Y, Ramírez-Mata A, Villalobos-Jimenez A, Ost S, Quesada-Gómez C, Rodríguez C, Papatheodorou P, Chaves-Olarte E. 2019. Toxin B variants from *Clostridium difficile* strains VPI 10463 and NAP1/027 share similar substrate profile and cellular intoxication kinetics but use different host cell entry factors. Toxins 11:348.

179. Chung S-Y, Schöttelndreier D, Tatge H, Fühner V, Hust M, Beer L-A, Gerhard R. 2018. The conserved Cys-2232 in *Clostridioides difficile* toxin B modulates receptor binding. Front Microbiol 9:2314.

180. Tamburini E, Dallatomasina A, Quartararo J, Cortelazzi B, Mangieri D, Lazzaretti M, Perris R. 2019. Structural deciphering of the NG2/CSPG4 proteoglycan multifunctionality. FASEB J 33:3112–3128.

181. Wilson S-S, Baetge EE, Stallcup WB. 1981. Antisera specific for cell lines with mixed neuronal and glial properties. Dev Biol 83:146–153.

182. Wilson BS, Imai K, Natali PG, Ferrone S. 1981. Distribution and molecular characterization of a cell-surface and a cytoplasmic antigen detectable in human melanoma cells with monoclonal antibodies. Int J Cancer 28:293–300.

183. Wilson BS, Ruberto G, Ferrone S. 1983. Immunochemical characterization of a human high molecular weight — melanoma associated antigen identified with monoclonal antibodies. Cancer Immunol Immunother 14:196–201.

184. Bumol TF, Reisfeld RA. 1982. Unique glycoprotein-proteoglycan complex defined by monoclonal antibody on human melanoma cells. Proc Natl Acad Sci 79:1245–1249.

185. Pluschke G, Vanek M, Evans A, Dittmar T, Schmid P, Itin P, Filardo EJ, Reisfeld RA. 1996. Molecular cloning of a human melanoma-associated chondroitin sulfate proteoglycan. Proc Natl Acad Sci 93:9710–9715.

186. Fukushi J, Makagiansar IT, Stallcup WB. 2004. NG2 Proteoglycan Promotes Endothelial Cell Motility and Angiogenesis via Engagement of Galectin-3 and α3β1 Integrin. Mol Biol Cell 15:3580–3590.

187. You W-K, Yotsumoto F, Sakimura K, Adams RH, Stallcup WB. 2014. NG2 proteoglycan promotes tumor vascularization via integrin-dependent effects on pericyte function. Angiogenesis 17:61–76.

188. Cooney CA, Jousheghany F, Yao-Borengasser A, Phanavanh B, Gomes T, Kieber-Emmons AM, Siegel ER, Suva LJ, Ferrone S, Kieber-Emmons T, Monzavi-Karbassi B. 2011. Chondroitin sulfates play a major role in breast cancer metastasis: a role for CSPG4 and CHST11gene expression in forming surface P-selectin ligands in aggressive breast cancer cells. Breast Cancer Res 13:R58.

189. Girolamo F, Dallatomasina A, Rizzi M, Errede M, Wälchli T, Mucignat MT, Frei K, Roncali L, Perris R, Virgintino D. 2013. Diversified Expression of NG2/CSPG4 Isoforms in Glioblastoma and Human Foetal Brain Identifies Pericyte Subsets. PLOS ONE 8:e84883.

190. Schiffer D, Mellai M, Boldorini R, Bisogno I, Grifoni S, Corona C, Bertero L, Cassoni P, Casalone C, Annovazzi L. 2018. The Significance of Chondroitin Sulfate Proteoglycan 4 (CSPG4) in Human Gliomas. 9. Int J Mol Sci 19:2724.

191. Farnedi A, Rossi S, Bertani N, Gulli M, Silini EM, Mucignat MT, Poli T, Sesenna E, Lanfranco D, Montebugnoli L, Leonardi E, Marchetti C, Cocchi R, Ambrosini-Spaltro A, Foschini MP, Perris R. 2015. Proteoglycan-based diversification of disease outcome in head and neck cancer patients identifies NG2/CSPG4 and syndecan-2 as unique relapse and overall survival predicting factors. BMC Cancer 15:352.

192. Keleg S, Titov A, Heller A, Giese T, Tjaden C, Ahmad SS, Gaida MM, Bauer AS, Werner J, Giese NA. 2014. Chondroitin Sulfate Proteoglycan CSPG4 as a Novel Hypoxia-Sensitive Marker in Pancreatic Tumors. PLOS ONE 9:e100178.

193. Grako KA, Ochiya T, Barritt D, Nishiyama A, Stallcup WB. 1999. PDGF (alpha)-receptor is unresponsive to PDGF-AA in aortic smooth muscle cells from the NG2 knockout mouse. J Cell Sci 112:905–915.

194. Hossain-Ibrahim MK, Rezajooi K, Stallcup WB, Lieberman AR, Anderson PN. 2007. Analysis of axonal regeneration in the central and peripheral nervous systems of the NG2-deficient mouse. BMC Neurosci 8:80.

195. Huang C, Sakry D, Menzel L, Dangel L, Sebastiani A, Krämer T, Karram K, Engelhard K, Trotter J, Schäfer MKE. 2016. Lack of NG2 exacerbates neurological outcome and modulates glial responses after traumatic brain injury. Glia 64:507–523.

196. Jones LL, Yamaguchi Y, Stallcup WB, Tuszynski MH. 2002. NG2 is a major chondroitin sulfate proteoglycan produced after spinal cord injury and is expressed by macrophages and oligodendrocyte progenitors. J Neurosci 22:2792–2803.

197. Rezajooi K, Pavlides M, Winterbottom J, Stallcup W, Hamlyn P, Lieberman A, Anderson P. 2004. NG2 proteoglycan expression in the peripheral nervous system: upregulation following injury and comparison with CNS lesions. Mol Cell Neurosci 25:572–584.

198. Kaestner KH. 2019. The intestinal stem cell niche: a central role for Foxl1-expressing subepithelial telocytes. Cell Mol Gastroenterol Hepatol 8:111–117.

199. Kim J-E, Fei L, Yin W-C, Coquenlorge S, Rao-Bhatia A, Zhang X, Shi SSW, Lee JH, Hahn NA, Rizvi W, Kim K-H, Sung H-K, Hui C, Guo G, Kim T-H. 2020. Single cell and genetic analyses reveal conserved populations and signaling mechanisms of gastrointestinal stromal niches. Nat Commun 11:334.

200. Huang F-J, You W-K, Bonaldo P, Seyfried TN, Pasquale EB, Stallcup WB. 2010. Pericyte deficiencies lead to aberrant tumor vascularizaton in the brain of the NG2 null mouse. Dev Biol 344:1035–1046.

201. Kucharova K, Stallcup WB. 2010. The NG2 proteoglycan promotes oligodendrocyte progenitor proliferation and developmental myelination. Neuroscience 166:185–194.

202. Kucharova K, Stallcup WB. 2015. NG2-proteoglycan-dependent contributions of oligodendrocyte progenitors and myeloid cells to myelin damage and repair. J Neuroinflammation 12:161.

203. Terada N, Ohno N, Murata S, Katoh R, Stallcup WB, Ohno S. 2006. Immunohistochemical study of NG2 chondroitin sulfate proteoglycan expression in the small and large intestines. Histochem Cell Biol 126:483–490.

204. Stallcup WB. 2002. The NG2 proteoglycan: Past insights and future prospects. J Neurocytol 31:423–435.

205. Jumper J, Evans R, Pritzel A, Green T, Figurnov M, Ronneberger O, Tunyasuvunakool K, Bates R, Žídek A, Potapenko A, Bridgland A, Meyer C, Kohl SAA, Ballard AJ, Cowie A, Romera-Paredes B, Nikolov S, Jain R, Adler J, Back T, Petersen S, Reiman D, Clancy E, Zielinski M, Steinegger M, Pacholska M, Berghammer T, Bodenstein S, Silver D, Vinyals O, Senior AW, Kavukcuoglu K, Kohli P, Hassabis D. 2021. Highly accurate protein structure prediction with AlphaFold. 7873. Nature 596:583–589.

206. Varadi M, Anyango S, Deshpande M, Nair S, Natassia C, Yordanova G, Yuan D, Stroe O, Wood G, Laydon A, Žídek A, Green T, Tunyasuvunakool K, Petersen S, Jumper J, Clancy E, Green R, Vora A,

Lutfi M, Figurnov M, Cowie A, Hobbs N, Kohli P, Kleywegt G, Birney E, Hassabis D, Velankar S. 2022. AlphaFold Protein Structure Database: massively expanding the structural coverage of protein-sequence space with high-accuracy models. Nucleic Acids Res 50:D439–D444.

207. Staub E, Hinzmann B, Rosenthal A. 2002. A novel repeat in the melanoma-associated chondroitin sulfate proteoglycan defines a new protein family. FEBS Lett 527:114–118.

208. Cattaruzza S, Ozerdem U, Denzel M, Ranscht B, Bulian P, Cavallaro U, Zanocco D, Colombatti A, Stallcup WB, Perris R. 2013. Multivalent proteoglycan modulation of FGF mitogenic responses in perivascular cells. Angiogenesis 16:309–327.

209. Nishiyama A, Lin X-H, Giese N, Heldin C-H, Stallcup WB. 1996. Interaction between NG2 proteoglycan and PDGF α-receptor on O2A progenitor cells is required for optimal response to PDGF. J Neurosci Res 43:315–330.

210. Nishiyama A, Lin X-H, Giese N, Heldin C-H, Stallcup WB. 1996. Co-localization of NG2 proteoglycan and PDGF α-receptor on O2A progenitor cells in the developing rat brain. J Neurosci Res 43:299–314.

211. Tang F, Lord MS, Stallcup WB, Whitelock JM. 2018. Cell surface chondroitin sulphate proteoglycan 4 (CSPG4) binds to the basement membrane heparan sulphate proteoglycan, perlecan, and is involved in cell adhesion. J Biochem (Tokyo) 163:399–412.

212. Song S, Ewald AJ, Stallcup W, Werb Z, Bergers G. 2005. PDGFRβ+ perivascular progenitor cells in tumours regulate pericyte differentiation and vascular survival. Nat Cell Biol 7:870–879.

213. Bumol T, Walker L, Reisfeld R. 1984. Biosynthetic studies of proteoglycans in human melanoma cells with a monoclonal antibody to a core glycoprotein of chondroitin sulfate proteoglycans. J Biol Chem 259:12733–12741.

214. Ross AH, Cossu G, Herlyn M, Bell JR, Steplewski Z, Koprowski H. 1983. Isolation and chemical characterization of a melanoma-associated proteoglycan antigen. Arch Biochem Biophys 225:370–383.

215. Stallcup WB, Dahlin-Huppe K. 2001. Chondroitin sulfate and cytoplasmic domain-dependent membrane targeting of the NG2 proteoglycan promotes retraction fiber formation and cell polarization. J Cell Sci 114:2315–2325.

216. Garrigues HJ, Lark MW, Lara S, Hellström I, Hellström KE, Wight TN. 1986. The melanoma proteoglycan: restricted expression on microspikes, a specific microdomain of the cell surface. J Cell Biol 103:1699–1710.

217. Tillet E, Ruggiero F, Nishiyama A, Stallcup WB. 1997. The Membrane-spanning Proteoglycan NG2 Binds to Collagens V and VI through the Central Nonglobular Domain of Its Core Protein. J Biol Chem 272:10769–10776.

218. Burg MA, Nishiyama A, Stallcup WB. 1997. A central segment of the NG2 proteoglycan is critical for the ability of glioma cells to bind and migrate toward type VI collagen. Exp Cell Res 235:254–264.

219. Goretzki L, Burg MA, Grako KA, Stallcup WB. 1999. High-affinity Binding of Basic Fibroblast Growth Factor and Platelet-derived Growth Factor-AA to the Core Protein of the NG2 Proteoglycan. J Biol Chem 274:16831–16837.

220. Wen Y, Makagiansar IT, Fukushi J, Liu F-T, Fukuda MN, Stallcup WB. 2006. Molecular basis of interaction between NG2 proteoglycan and galectin-3. J Cell Biochem 98:115–127.

221. Tucker KD, Wilkins TD. 1991. Toxin A of *Clostridium difficile* binds to the human carbohydrate antigens I, X, and Y. Infect Immun 59:73–78.

222. Christensen NR, Čalyševa J, Fernandes EFA, Lüchow S, Clemmensen LS, Haugaard-Kedström LM, Strømgaard K. 2019. PDZ Domains as Drug Targets. Adv Ther 2:1800143.

223. Ren X, Hurley JH. 2011. Proline-Rich Regions and Motifs in Trafficking: From ESCRT Interaction to Viral Exploitation. Traffic 12:1282–1290.

224. Makagiansar IT, Williams S, Mustelin T, Stallcup WB. 2007. Differential phosphorylation of NG2 proteoglycan by ERK and PKCα helps balance cell proliferation and migration. J Cell Biol 178:155–165.

225. Stegmüller J, Schneider S, Hellwig A, Garwood J, Trotter J. 2002. AN2, the mouse homologue of NG2, is a surface antigen on glial precursor cells implicated in control of cell migration. J Neurocytol 31:497 ppl= – 505.

226. Williamson MP. 1994. The structure and function of proline-rich regions in proteins. Biochem J 297:249.

227. Erlendsson S, Thorsen TS, Vauquelin G, Ammendrup-Johnsen I, Wirth V, Martinez KL, Teilum K, Gether U, Madsen KL. 2019. Mechanisms of PDZ domain scaffold assembly illuminated by use of supported cell membrane sheets. eLife 8:e39180.

228. Shen B, Delaney MK, Du X. 2012. Inside-out, outside-in, and inside-outside-in: G protein signaling in integrin-mediated cell adhesion, spreading, and retraction. Curr Opin Cell Biol 24:600–606.

229. Couchman JR. 2010. Transmembrane signaling proteoglycans. Annu Rev Cell Dev Biol 26:89–114.

230. Rolih V, Barutello G, Iussich S, De Maria R, Quaglino E, Buracco P, Cavallo F, Riccardo F. 2017. CSPG4: a prototype oncoantigen for translational immunotherapy studies. J Transl Med 15:151.

231. Yang J, Price MA, Neudauer CL, Wilson C, Ferrone S, Xia H, Iida J, Simpson MA, McCarthy JB. 2004. Melanoma chondroitin sulfate proteoglycan enhances FAK and ERK activation by distinct mechanisms. J Cell Biol 165:881–891.

232. Iida J, Wilhelmson KL, Ng J, Lee P, Morrison C, Tam E, Overall CM, McCarthy JB. 2007. Cell surface chondroitin sulfate glycosaminoglycan in melanoma: role in the activation of pro-MMP-2 (pro-gelatinase A). Biochem J 403:553–563.

233. Joo NE, Miao D, Bermúdez M, Stallcup WB, Kapila YL. 2014. Shedding of NG2 by MMP-13 attenuates anoikis. DNA Cell Biol 33:854–862.

234. Iida J, Pei D, Kang T, Simpson MA, Herlyn M, Furcht LT, McCarthy JB. 2001. Melanoma chondroitin sulfate proteoglycan regulates matrix metalloproteinase-dependent human melanoma invasion into type I collagen. J Biol Chem 276:18786–18794.

235. Asher RA, Morgenstern DA, Properzi F, Nishiyama A, Levine JM, Fawcett JW. 2005. Two separate metalloproteinase activities are responsible for the shedding and processing of the NG2 proteoglycan in vitro. Mol Cell Neurosci 29:82–96.

236. Larsen PH, Wells JE, Stallcup WB, Opdenakker G, Yong VW. 2003. Matrix metalloproteinase-9 facilitates remyelination in part by processing the inhibitory NG2 proteoglycan. J Neurosci 23:11127–11135.

237. Sardone F, Santi S, Tagliavini F, Traina F, Merlini L, Squarzoni S, Cescon M, Wagener R, Maraldi NM, Bonaldo P, Faldini C, Sabatelli P. 2016. Collagen VI–NG2 axis in human tendon fibroblasts under conditions mimicking injury response. Matrix Biol 55:90–105.

238. Nishiyama A, Lin XH, Stallcup WB. 1995. Generation of truncated forms of the NG2 proteoglycan by cell surface proteolysis. Mol Biol Cell 6:1819–1832.

239. Nishihara T, Remacle AG, Angert M, Shubayev I, Shiryaev SA, Liu H, Dolkas J, Chernov AV, Strongin AY, Shubayev VI. 2015. Matrix Metalloproteinase-14 Both Sheds Cell Surface Neuronal Glial Antigen 2 (NG2) Proteoglycan on Macrophages and Governs the Response to Peripheral Nerve Injury. J Biol Chem 290:3693–3707.

240. Sakry D, Neitz A, Singh J, Frischknecht R, Marongiu D, Binamé F, Perera SS, Endres K, Lutz B, Radyushkin K. 2014. Oligodendrocyte precursor cells modulate the neuronal network by activity-dependent ectodomain cleavage of glial NG2. PLoS Biol 12:e1001993.

241. Morandi F, Corrias MV, Levreri I, Scaruffi P, Raffaghello L, Carlini B, Bocca P, Prigione I, Stigliani S, Amoroso L. 2011. Serum levels of cytoplasmic melanoma-associated antigen at diagnosis may predict clinical relapse in neuroblastoma patients. Cancer Immunol Immunother 60:1485–1495.

242. Schenkelaars Q, Fierro-Constain L, Renard E, Hill AL, Borchiellini C. 2015. Insights into Frizzled evolution and new perspectives. Evol Dev 17:160–169.

243. Bhanot P, Brink M, Samos CH, Hsieh J-C, Wang Y, Macke JP, Andrew D, Nathans J, Nusse R. 1996. A new member of the frizzled family from Drosophila functions as a Wingless receptor. Nature 382:225–230.

244. Wang Y, Macke JP, Abella BS, Andreasson K, Worley P, Gilbert DJ, Copeland NG, Jenkins NA, Nathans J. 1996. A Large Family of Putative Transmembrane Receptors Homologous to the Product of the Drosophila Tissue Polarity Gene frizzled(∗). J Biol Chem 271:4468–4476.

245. Dann CE, Hsieh J-C, Rattner A, Sharma D, Nathans J, Leahy DJ. 2001. Insights into Wnt binding and signalling from the structures of two Frizzled cysteine-rich domains. Nature 412:86–90.

246. Cong F, Schweizer L, Varmus H. 2004. Wnt signals across the plasma membrane to activate the β-catenin pathway by forming oligomers containing its receptors, Frizzled and LRP.

247. Wong H-C, Bourdelas A, Krauss A, Lee H-J, Shao Y, Wu D, Mlodzik M, Shi D-L, Zheng J. 2003. Direct binding of the PDZ domain of Dishevelled to a conserved internal sequence in the C-terminal region of Frizzled. Mol Cell 12:1251–1260.

248. Hsieh J-C, Rattner A, Smallwood PM, Nathans J. 1999. Biochemical characterization of Wnt-Frizzled interactions using a soluble, biologically active vertebrate Wnt protein. Proc Natl Acad Sci 96:3546–3551.

249. Rulifson EJ, Wu C-H, Nusse R. 2000. Pathway specificity by the bifunctional receptor frizzled is determined by affinity for wingless. Mol Cell 6:117–126.

250. Punchihewa C, Ferreira AM, Cassell R, Rodrigues P, Fujii N. 2009. Sequence requirement and subtype specificity in the high-affinity interaction between human frizzled and dishevelled proteins. Protein Sci 18:994–1002.

251. Schulte G, Bryja V. 2007. The Frizzled family of unconventional G-protein-coupled receptors. Trends Pharmacol Sci 28:518–525.

252. Witte F, Dokas J, Neuendorf F, Mundlos S, Stricker S. 2009. Comprehensive expression analysis of all Wnt genes and their major secreted antagonists during mouse limb development and cartilage differentiation. Gene Expr Patterns 9:215–223.

253. Weeraratna AT, Jiang Y, Hostetter G, Rosenblatt K, Duray P, Bittner M, Trent JM. 2002. Wnt5a signaling directly affects cell motility and invasion of metastatic melanoma. Cancer Cell 1:279–288.

254. Vinson CR, Adler PN. 1987. Directional non-cell autonomy and the transmission of polarity information by the frizzled gene of Drosophila. Nature 329:549–551.

255. Veeman MT, Axelrod JD, Moon RT. 2003. A second canon: functions and mechanisms of β-catenin-independent Wnt signaling. Dev Cell 5:367–377.

256. Nusse R, Varmus HE. 1992. Wnt genes. Cell 69:1073–1087.

257. Nusse R, Varmus HE. 1982. Many tumors induced by the mouse mammary tumor virus contain a provirus integrated in the same region of the host genome. Cell 31:99–109.

258. Korinek V, Barker N, Moerer P, van Donselaar E, Huls G, Peters PJ, Clevers H. 1998. Depletion of epithelial stem-cell compartments in the small intestine of mice lacking Tcf-4. Nat Genet 19:379–383.

259. Barker N, Van Es JH, Kuipers J, Kujala P, Van Den Born M, Cozijnsen M, Haegebarth A, Korving J, Begthel H, Peters PJ. 2007. Identification of stem cells in small intestine and colon by marker gene Lgr5. Nature 449:1003–1007.

260. Elmentaite R, Kumasaka N, Roberts K, Fleming A, Dann E, King HW, Kleshchevnikov V, Dabrowska M, Pritchard S, Bolt L, Vieira SF, Mamanova L, Huang N, Perrone F, Goh Kai'En I, Lisgo SN, Katan M, Leonard S, Oliver TRW, Hook CE, Nayak K, Campos LS, Domínguez Conde C, Stephenson E, Engelbert J, Botting RA, Polanski K, van Dongen S, Patel M, Morgan MD, Marioni JC, Bayraktar OA, Meyer KB, He X, Barker RA, Uhlig HH, Mahbubani KT, Saeb-Parsy K, Zilbauer M, Clatworthy MR, Haniffa M, James KR, Teichmann SA. 2021. Cells of the human intestinal tract mapped across space and time. Nature 597:250–255.

261. Xie L, Fletcher RB, Bhatia D, Shah D, Phipps J, Deshmukh S, Zhang H, Ye J, Lee S, Le L, Newman M, Chen H, Sura A, Gupta S, Sanman LE, Yang F, Meng W, Baribault H, Vanhove GF, Yeh W-C, Li Y, Lu C. 2022. Robust Colonic Epithelial Regeneration and Amelioration of Colitis via FZD-Specific Activation of Wnt Signaling. Cell Mol Gastroenterol Hepatol 14:435–464.

262. Flanagan DJ, Phesse TJ, Barker N, Schwab RHM, Amin N, Malaterre J, Stange DE, Nowell CJ, Currie SA, Saw JTS, Beuchert E, Ramsay RG, Sansom OJ, Ernst M, Clevers H, Vincan E. 2015. Frizzled7 Functions as a Wnt Receptor in Intestinal Epithelial Lgr5+ Stem Cells. Stem Cell Rep 4:759–767.

263. Behrens J, Von Kries JP, Kühl M, Bruhn L, Wedlich D, Grosschedl R, Birchmeier W. 1996. Functional interaction of β-catenin with the transcription factor LEF-1. Nature 382:638–642.

264. Daniels DL, Weis WI. 2005. β-catenin directly displaces Groucho/TLE repressors from Tcf/Lef in Wnt-mediated transcription activation. Nat Struct Mol Biol 12:364–371.

265. Behrens J, Jerchow B-A, Würtele M, Grimm J, Asbrand C, Wirtz R, Kühl M, Wedlich D, Birchmeier W. 1998. Functional interaction of an axin homolog, conductin, with β-catenin, APC, and GSK3β. Science 280:596–599.

266. Molenaar M, Van De Wetering M, Oosterwegel M, Peterson-Maduro J, Godsave S, Korinek V, Roose J, Destrée O, Clevers H. 1996. XTcf-3 transcription factor mediates β-catenin-induced axis formation in Xenopus embryos. Cell 86:391–399.

267. Ozawa M, Baribault H, Kemler R. 1989. The cytoplasmic domain of the cell adhesion molecule uvomorulin associates with three independent proteins structurally related in different species. EMBO J 8:1711–1717.

268. Rubinfeld B, Albert I, Porfiri E, Fiol C, Munemitsu S, Polakis P. 1996. Binding of GSK3β to the APC-β-catenin complex and regulation of complex assembly. Science 272:1023–1026.

269. Aberle H, Bauer A, Stappert J, Kispert A, Kemler R. 1997. β-catenin is a target for the ubiquitin–proteasome pathway. EMBO J 16:3797–3804.

270. Munemitsu S, Albert I, Souza B, Rubinfeld B, Polakis P. 1995. Regulation of intracellular beta-catenin levels by the adenomatous polyposis coli (APC) tumor-suppressor protein. Proc Natl Acad Sci 92:3046–3050.

271. Orford K, Crockett C, Jensen JP, Weissman AM, Byers SW. 1997. Serine phosphorylation-regulated ubiquitination and degradation of β-catenin. J Biol Chem 272:24735–24738.

272. Janda CY, Waghray D, Levin AM, Thomas C, Garcia KC. 2012. Structural Basis of Wnt Recognition by Frizzled. Science 337:59–64.

273. Brown SD, Twells RC, Hey PJ, Cox RD, Levy ER, Soderman AR, Metzker ML, Caskey CT, Todd JA, Hess JF. 1998. Isolation and characterization of LRP6, a novel member of the low density lipoprotein receptor gene family. Biochem Biophys Res Commun 248:879–888.

274. Hey PJ, Twells RC, Phillips MS, Nakagawa Y, Brown SD, Kawaguchi Y, Cox R, Xie G, Dugan V, Hammond H. 1998. Cloning of a novel member of the low-density lipoprotein receptor family. Gene 216:103–111.

275. Kim D-H, Inagaki Y, Suzuki T, Ioka RX, Yoshioka SZ, Magoori K, Kang M-J, Cho Y, Nakano AZ, Liu Q. 1998. A new low density lipoprotein receptor related protein, LRP5, is expressed in hepatocytes and adrenal cortex, and recognizes apolipoprotein E. J Biochem (Tokyo) 124:1072–1076.

276. Kelly OG, Pinson KI, Skarnes WC. 2004. The Wnt co-receptors Lrp5 and Lrp6 are essential for gastrulation in mice.

277. Tamai K, Semenov M, Kato Y, Spokony R, Liu C, Katsuyama Y, Hess F, Saint-Jeannet J-P, He X. 2000. LDL-receptor-related proteins in Wnt signal transduction. Nature 407:530–535.

278. Wehrli M, Dougan ST, Caldwell K, O'Keefe L, Schwartz S, Vaizel-Ohayon D, Schejter E, Tomlinson A, DiNardo S. 2000. arrow encodes an LDL-receptor-related protein essential for Wingless signalling. Nature 407:527–530.

279. Zeng X, Huang H, Tamai K, Zhang X, Harada Y, Yokota C, Almeida K, Wang J, Doble B, Woodgett J. 2008. Initiation of Wnt signaling: control of Wnt coreceptor Lrp6 phosphorylation/activation via frizzled, dishevelled and axin functions.

280. Zeng X, Tamai K, Doble B, Li S, Huang H, Habas R, Okamura H, Woodgett J, He X. 2005. A dual-kinase mechanism for Wnt co-receptor phosphorylation and activation. Nature 438:873–877.

281. Bilic J, Huang Y-L, Davidson G, Zimmermann T, Cruciat C-M, Bienz M, Niehrs C. 2007. Wnt induces LRP6 signalosomes and promotes dishevelled-dependent LRP6 phosphorylation. Science 316:1619–1622.

282. Chen P, Tao L, Liu Z, Dong M, Jin R. 2019. Structural insight into Wnt signaling inhibition by *Clostridium difficile* toxin B. FEBS J 286:874–881.

283. Yamamoto H, Komekado H, Kikuchi A. 2006. Caveolin Is Necessary for Wnt-3a-Dependent Internalization of LRP6 and Accumulation of β-Catenin. Dev Cell 11:213–223.

284. Agajanian MJ, Walker MP, Axtman AD, Ruela-de-Sousa RR, Serafin DS, Rabinowitz AD, Graham DM, Ryan MB, Tamir T, Nakamichi Y, Gammons MV, Bennett JM, Couñago RM, Drewry DH, Elkins JM, Gileadi C, Gileadi O, Godoi PH, Kapadia N, Müller S, Santiago AS, Sorrell FJ, Wells CI, Fedorov O, Willson TM, Zuercher WJ, Major MB. 2019. WNT Activates the AAK1 Kinase to Promote Clathrin-Mediated Endocytosis of LRP6 and Establish a Negative Feedback Loop. Cell Rep 26:79-93.e8.

285. Yu A, Rual J-F, Tamai K, Harada Y, Vidal M, He X, Kirchhausen T. 2007. Association of Dishevelled with the Clathrin AP-2 Adaptor Is Required for Frizzled Endocytosis and Planar Cell Polarity Signaling. Dev Cell 12:129–141.

286. Papatheodorou P, Zamboglou C, Genisyuerek S, Guttenberg G, Aktories K. 2010. Clostridial glucosylating toxins enter cells via clathrin-mediated endocytosis. PloS One 5:e10673.

287. Takai Y, Miyoshi J, Ikeda W, Ogita H. 2008. Nectins and nectin-like molecules: roles in contact inhibition of cell movement and proliferation. 8. Nat Rev Mol Cell Biol 9:603–615.

288. Takai Y, Irie K, Shimizu K, Sakisaka T, Ikeda W. 2003. Nectins and nectin-like molecules: Roles in cell adhesion, migration, and polarization. Cancer Sci 94:655–667.

289. Harrison OJ, Vendome J, Brasch J, Jin X, Hong S, Katsamba PS, Ahlsen G, Troyanovsky RB, Troyanovsky SM, Honig B, Shapiro L. 2012. Nectin ectodomain structures reveal a canonical adhesive interface. 9. Nat Struct Mol Biol 19:906–915.

290. Kanzaki N, Ogita H, Komura H, Ozaki M, Sakamoto Y, Majima T, Ijuin T, Takenawa T, Takai Y. 2008. Involvement of the nectin-afadin complex in PDGF-induced cell survival. J Cell Sci 121:2008 LP – 2017.

291. Mandai K, Nakanishi H, Satoh A, Obaishi H, Wada M, Nishioka H, Itoh M, Mizoguchi A, Aoki T, Fujimoto T, Matsuda Y, Tsukita S, Takai Y. 1997. Afadin: A novel actin filament-binding protein with one PDZ domain localized at cadherin-based cell-to-cell adherens junction. J Cell Biol 139:517–528.

292. Takahashi K, Nakanishi H, Miyahara M, Mandai K, Satoh K, Satoh A, Nishioka H, Aoki J, Nomoto A, Mizoguchi A, Takai Y. 1999. Nectin/PRR: an immunoglobulin-like cell adhesion molecule recruited to cadherin-based adherens junctions through interaction with Afadin, a PDZ domain-containing protein. J Cell Biol 145:539–549.

293. Takekuni K, Ikeda W, Fujito T, Morimoto K, Takeuchi M, Monden M, Takai Y. 2003. Direct Binding of Cell Polarity Protein PAR-3 to Cell-Cell Adhesion Molecule Nectin at Neuroepithelial Cells of Developing Mouse. J Biol Chem 278:5497–5500.

294. Ohno S. 2001. Intercellular junctions and cellular polarity: the PAR–aPKC complex, a conserved core cassette playing fundamental roles in cell polarity. Curr Opin Cell Biol 13:641–648.

295. Fukuda T, Kominami K, Wang S, Togashi H, Hirata K, Mizoguchi A, Rikitake Y, Takai Y. 2014. Aberrant cochlear hair cell attachments caused by Nectin-3 deficiency result in hair bundle abnormalities. Development 141:399–409.

296. Togashi H, Kominami K, Waseda M, Komura H, Miyoshi J, Takeichi M, Takai Y. 2011. Nectins Establish a Checkerboard-Like Cellular Pattern in the Auditory Epithelium. Science 333:1144–1147.

297. Inagaki M, Irie K, Ishizaki H, Tanaka-Okamoto M, Morimoto K, Inoue E, Ohtsuka T, Miyoshi J, Takai Y. 2005. Roles of cell-adhesion molecules nectin 1 and nectin 3 in ciliary body development. Development 132:1525–1537.

298. Nakata H, Wakayama T, Takai Y, Iseki S. 2015. Quantitative analysis of the cellular composition in seminiferous tubules in normal and genetically modified infertile mice. J Histochem Cytochem 63:99–113.

299. Tanaka-Okamoto M, Hori K, Ishizaki H, Itoh Y, Onishi S, Yonemura S, Takai Y, Miyoshi J. 2011. Involvement of afadin in barrier function and homeostasis of mouse intestinal epithelia. J Cell Sci 124:2231–2240.

300. Chumbler NM, Farrow MA, Lapierre LA, Franklin JL, Haslam D, Goldenring JR, Lacy DB. 2012. *Clostridium difficile* Toxin B Causes Epithelial Cell Necrosis through an Autoprocessing-Independent Mechanism. PLOS Pathog 8:e1003072.

301. Farrow MA, Chumbler NM, Lapierre LA, Franklin JL, Rutherford SA, Goldenring JR, Lacy DB. 2013. *Clostridium difficile* toxin B-induced necrosis is mediated by the host epithelial cell NADPH oxidase complex. Proc Natl Acad Sci 110:18674–18679.

302. Chumbler NM, Farrow MA, Lapierre LA, Franklin JL, Lacy DB. 2016. *Clostridium difficile* Toxins TcdA and TcdB Cause Colonic Tissue Damage by Distinct Mechanisms. Infect Immun 84:2871–2877.

303. van der Wath RC, Gardiner BS, Burgess AW, Smith DW. 2013. Cell organisation in the colonic crypt: a theoretical comparison of the pedigree and niche concepts. PloS One 8:e73204.

304. Kozar S, Morrissey E, Nicholson AM, van der Heijden M, Zecchini HI, Kemp R, Tavaré S, Vermeulen L, Winton DJ. 2013. Continuous Clonal Labeling Reveals Small Numbers of Functional Stem Cells in Intestinal Crypts and Adenomas. Cell Stem Cell 13:626–633.

305. Kim J, Kim Y, Pai H. 2016. Clinical characteristics and treatment outcomes of *Clostridium difficile* infections by PCR ribotype 017 and 018 strains. PloS One 11:e0168849.

306. Shin B-M, Kuak EY, Yoo SJ, Shin WC, Yoo HM. 2008. Emerging toxin A– B+ variant strain of *Clostridium difficile* responsible for pseudomembranous colitis at a tertiary care hospital in Korea. Diagn Microbiol Infect Dis 60:333–337.

307. Autenrieth DM, Baumgart DC. 2012. Toxic megacolon. Inflamm Bowel Dis 18:584–591.

308. Lim SK, Stuart RL, Mackin KE, Carter GP, Kotsanas D, Francis MJ, Easton M, Dimovski K, Elliott B, Riley TV. 2014. Emergence of a ribotype 244 strain of *Clostridium difficile* associated with severe disease and related to the epidemic ribotype 027 strain. Clin Infect Dis 58:1723–1730.

309. Stabler RA, Dawson LF, Valiente E, Cairns MD, Martin MJ, Donahue EH, Riley TV, Songer JG, Kuijper EJ, Dingle KE. 2012. Macro and micro diversity of *Clostridium difficile* isolates from diverse sources and geographical locations. PloS One 7:e31559.

310. Hung Y-P, Lin H-J, Tsai B-Y, Liu H-C, Liu H-C, Lee J-C, Wu Y-H, Wilcox MH, Fawley WN, Hsueh P-R. 2014. *Clostridium difficile* ribotype 126 in southern Taiwan: a cluster of three symptomatic cases. Anaerobe 30:188–192.

311. Walker AS, Eyre DW, Wyllie DH, Dingle KE, Griffiths D, Shine B, Oakley S, O'Connor L, Finney J, Vaughan A. 2013. Relationship between bacterial strain type, host biomarkers, and mortality in *Clostridium difficile* infection. Clin Infect Dis 56:1589–1600.

312. Lewis BB, Carter RA, Ling L, Leiner I, Taur Y, Kamboj M, Dubberke ER, Xavier J, Pamer EG. 2017. Pathogenicity locus, core genome, and accessory gene contributions to *Clostridium difficile* virulence. MBio 8:e00885-17.

313. Costa AM, Leite M, Seruca R, Figueiredo C. 2013. Adherens junctions as targets of microorganisms: a focus on *Helicobacter pylori*. FEBS Lett 587:259–265.

314. Guttman JA, Finlay BB. 2009. Tight junctions as targets of infectious agents. Biochim Biophys Acta BBA-Biomembr 1788:832–841.

315. Nusrat A, von Eichel-Streiber C, Turner JR, Verkade P, Madara JL, Parkos CA. 2001. *Clostridium difficile* toxins disrupt epithelial barrier function by altering membrane microdomain localization of tight junction proteins. Infect Immun 69:1329–1336.

316. Hartsock A, Nelson WJ. 2008. Adherens and tight junctions: Structure, function and connections to the actin cytoskeleton. Biochim Biophys Acta BBA - Biomembr 1778:660–669.

317. Fehon RG, McClatchey AI, Bretscher A. 2010. Organizing the cell cortex: the role of ERM proteins. 4. Nat Rev Mol Cell Biol 11:276–287.

318. Jank T, Giesemann T, Aktories K. 2007. Rho-glucosylating *Clostridium difficile* toxins A and B: new insights into structure and function. Glycobiology 17:15R-22R.

319. Aspenström P, Fransson Å, Saras J. 2004. Rho GTPases have diverse effects on the organization of the actin filament system. Biochem J 377:327–337.

320. Holcombe RF, Marsh JL, Waterman ML, Lin F, Milovanovic T, Truong T. 2002. Expression of Wnt ligands and Frizzled receptors in colonic mucosa and in colon carcinoma. Mol Pathol 55:220–226.

321. Gujral TS, Chan M, Peshkin L, Sorger PK, Kirschner MW, MacBeath G. 2014. A Noncanonical Frizzled2 Pathway Regulates Epithelial-Mesenchymal Transition and Metastasis. Cell 159:844–856.

322. Gregorieff A, Pinto D, Begthel H, Destrée O, Kielman M, Clevers H. 2005. Expression pattern of Wnt signaling components in the adult intestine. Gastroenterology 129:626–638.

323. Gupta P, Zhang Z, Sugiman-Marangos SN, Tam J, Raman S, Julien J-P, Kroh HK, Lacy DB, Murgolo N, Bekkari K. 2017. Functional defects in *Clostridium difficile* TcdB toxin uptake identify CSPG4 receptor binding determinants. J Biol Chem jbc-M117.

324. Yang Y-A, Lee S, Zhao J, Thompson AJ, McBride R, Tsogtbaatar B, Paulson JC, Nussinov R, Deng L, Song J. 2018. In vivo tropism of *Salmonella* Typhi toxin to cells expressing a multiantennal glycan receptor. 2. Nat Microbiol 3:155–163.

325. Chen S, Barbieri JT. 2006. Unique Substrate Recognition by Botulinum Neurotoxins Serotypes A and E. J Biol Chem 281:10906–10911.

326. Perelman SS, James DB, Boguslawski KM, Nelson CW, Ilmain JK, Zwack EE, Prescott RA, Mohamed A, Tam K, Chan R. 2021. Genetic variation of staphylococcal LukAB toxin determines receptor tropism. Nat Microbiol 6:731–745.

327. Janezic S, Zidaric V, Pardon B, Indra A, Kokotovic B, Blanco JL, Seyboldt C, Diaz CR, Poxton IR, Perreten V, Drigo I, Jiraskova A, Ocepek M, Weese JS, Songer JG, Wilcox MH, Rupnik M. 2014. International *Clostridium difficile* animal strain collection and large diversity of animal associated strains. BMC Microbiol 14:173.

328. Chandrasekaran R, Kenworthy AK, Lacy DB. 2016. *Clostridium difficile* Toxin A Undergoes Clathrin-Independent, PACSIN2-Dependent Endocytosis. PLOS Pathog 12:e1006070.

329. Loo T, Patchett ML, Norris GE, Lott JS. 2002. Using secretion to solve a solubility problem: high-yield expression in *Escherichia coli* and purification of the bacterial glycoamidase PNGase F. Protein Expr Purif 24:90–98.

330. Scheuermann TH, Padrick SB, Gardner KH, Brautigam CA. 2016. On the acquisition and analysis of microscale thermophoresis data. Anal Biochem 496:79–93.

331. Lyon SA, Hutton ML, Rood JI, Cheung JK, Lyras D. 2016. CdtR Regulates TcdA and TcdB Production in *Clostridium difficile*. PLoS Pathog 12:e1005758.

332. Theriot CM, Koumpouras CC, Carlson PE, Bergin II, Aronoff DM, Young VB. 2011. Cefoperazone-treated mice as an experimental platform to assess differential virulence of *Clostridium difficile* strains. Gut Microbes 2:326–334.

333. Jardé T, Evans RJ, McQuillan KL, Parry L, Feng GJ, Alvares B, Clarke AR, Dale TC. 2013. In vivo and in vitro models for the therapeutic targeting of Wnt signaling using a Tet-OΔN89β-catenin system. 7. Oncogene 32:883–893.

334. Nefzger CM, Jardé T, Rossello FJ, Horvay K, Knaupp AS, Powell DR, Chen J, Abud HE, Polo JM. 2016. A Versatile Strategy for Isolating a Highly Enriched Population of Intestinal Stem Cells. Stem Cell Rep 6:321–329.

335. Jardé T, Kerr G, Akhtar R, Abud HE. 2018. Modelling Intestinal Carcinogenesis Using In Vitro Organoid Cultures. Methods Mol Biol Clifton NJ 1725:41–52.

336. Horvay K, Jardé T, Casagranda F, Perreau VM, Haigh K, Nefzger CM, Akhtar R, Gridley T, Berx G, Haigh JJ, Barker N, Polo JM, Hime GR, Abud HE. 2015. Snai1 regulates cell lineage allocation and stem cell maintenance in the mouse intestinal epithelium. EMBO J 34:1319–1335.

337. Jolley KA, Maiden MCJ. 2010. BIGSdb: Scalable analysis of bacterial genome variation at the population level. BMC Bioinformatics 11:595.

338. Stothard P. 2000. The sequence manipulation suite: JavaScript programs for analyzing and formatting protein and DNA sequences. BioTechniques 28:1102,1104.

339. Bodenhofer U, Bonatesta E, Horejš-Kainrath C, Hochreiter S. 2015. msa: an R package for multiple sequence alignment. Bioinformatics 31:3997–3999.

340. Zhou Z, Alikhan N-F, Sergeant MJ, Luhmann N, Vaz C, Francisco AP, Carriço JA, Achtman M. 2018. GrapeTree: visualization of core genomic relationships among 100,000 bacterial pathogens. Genome Res 28:1395–1404.

341. Letunic I, Bork P. 2019. Interactive Tree Of Life (iTOL) v4: recent updates and new developments. Nucleic Acids Res https://doi.org/10.1093/nar/gkz239.

342. Gp C, D L, Dl A, Ke M, Pm H, Jr O, Ji R. 2007. Binary toxin production in *Clostridium difficile* is regulated by CdtR, a LytTR family response regulator. J Bacteriol 189.

343. Stabler RA, He M, Dawson L, Martin M, Valiente E, Corton C, Lawley TD, Sebaihia M, Quail MA, Rose G. 2009. Comparative genome and phenotypic analysis of *Clostridium difficile* 027 strains provides insight into the evolution of a hypervirulent bacterium. Genome Biol 10:R102.

344. Carter GP, Douce GR, Govind R, Howarth PM, Mackin KE, Spencer J, Buckley AM, Antunes A, Kotsanas D, Jenkin GA, Dupuy B, Rood JI, Lyras D. 2011. The anti-sigma factor TcdC modulates hypervirulence in an epidemic BI/NAP1/027 clinical isolate of *Clostridium difficile*. PLoS Pathog 7:e1002317.

345. Richards M, Knox J, Elliott B, Mackin K, Lyras D, Waring LJ, Riley TV. 2011. Severe infection with *Clostridium difficile* PCR ribotype 027 acquired in Melbourne, Australia. Med J Aust 194:369–371.

346. Torres JF, Lönnroth I. 1988. Purification and characterisation of two forms of toxin B produced by *Clostridium difficile*. FEBS Lett 233:417–420.

347. Wüst J, Sullivan NM, Hardegger U, Wilkins TD. 1982. Investigation of an outbreak of antibiotic-associated colitis by various typing methods. J Clin Microbiol 16:1096–1101.

348. Wüst J, Hardegger U. 1983. Transferable resistance to clindamycin, erythromycin, and tetracycline in *Clostridium difficile*. Antimicrob Agents Chemother 23:784–786.

349. Squire MM, Carter GP, Mackin KE, Chakravorty A, Norén T, Elliott B, Lyras D, Riley TV. 2013. Novel Molecular Type of *Clostridium difficile* in Neonatal Pigs, Western Australia. Emerg Infect Dis J 19.

350. Guh AY, Mu Y, Winston LG, Johnston H, Olson D, Farley MM, Wilson LE, Holzbauer SM, Phipps EC, Dumyati GK, Beldavs ZG, Kainer MA, Karlsson M, Gerding DN, McDonald LC. 2020. Trends in U.S. Burden of *Clostridioides difficile* Infection and Outcomes. N Engl J Med 382:1320–1330.

351. Takai Y, Nakanishi H. 2003. Nectin and afadin: novel organizers of intercellular junctions. J Cell Sci 116:17–27.

352. Adams A, Wayne Vogl A. 2017. High Resolution Localization of Rab5, EEA1, and Nectin-3 to Tubulobulbar Complexes in the Rat Testis. Anat Rec 300:1160–1170.

353. Mühlebach MD, Mateo M, Sinn PL, Prüfer S, Uhlig KM, Leonard VHJ, Navaratnarajah CK, Frenzke M, Wong XX, Sawatsky B, Ramachandran S, McCray PB, Cichutek K, von Messling V, Lopez M, Cattaneo R. 2011. Adherens junction protein nectin-4 is the epithelial receptor for measles virus. 7378. Nature 480:530–533.

354. Noyce RS, Bondre DG, Ha MN, Lin L-T, Sisson G, Tsao M-S, Richardson CD. 2011. Tumor Cell Marker PVRL4 (Nectin 4) Is an Epithelial Cell Receptor for Measles Virus. PLOS Pathog 7:e1002240.

355. Krummenacher C, Baribaud I, Eisenberg RJ, Cohen GH. 2003. Cellular Localization of Nectin-1 and Glycoprotein D during Herpes Simplex Virus Infection. J Virol 77:8985–8999.

356. Delpeut S, Noyce RS, Richardson CD. 2014. The Tumor-Associated Marker, PVRL4 (Nectin-4), Is the Epithelial Receptor for Morbilliviruses. 6. Viruses 6:2268–2286.

357. Mendelsohn CL, Wimmer E, Racaniello VR. 1989. Cellular receptor for poliovirus: Molecular cloning, nucleotide sequence, and expression of a new member of the immunoglobulin superfamily. Cell 56:855–865.

358. Mahi NA, Najafabadi MF, Pilarczyk M, Kouril M, Medvedovic M. 2019. GREIN: An Interactive Web Platform for Re-analyzing GEO RNA-seq Data. 1. Sci Rep 9:7580.

359. Otte J-M, Rosenberg IM, Podolsky DK. 2003. Intestinal myofibroblasts in innate immune responses of the intestine. Gastroenterology 124:1866–1878.

360. Hsia L, Ashley N, Ouaret D, Wang LM, Wilding J, Bodmer WF. 2016. Myofibroblasts are distinguished from activated skin fibroblasts by the expression of AOC3 and other associated markers. Proc Natl Acad Sci 113:E2162–E2171.

361. Simmons JG, Pucilowska JB, Keku TO, Lund PK. 2002. IGF-I and TGF-beta1 have distinct effects on phenotype and proliferation of intestinal fibroblasts. Am J Physiol Gastrointest Liver Physiol 283:G809-18.

362. Sato T, Fujita N, Yamada A, Ooshio T, Okamoto R, Irie K, Takai Y. 2006. Regulation of the Assembly and Adhesion Activity of E-cadherin by Nectin and Afadin for the Formation of Adherens Junctions in Madin-Darby Canine Kidney Cells. J Biol Chem 281:5288–5299.

363. Involvement of afadin in barrier function and homeostasis of mouse intestinal epithelia | Journal of Cell Science | The Company of Biologists. https://journals.biologists.com/jcs/article/124/13/2231/31844/Involvement-of-afadin-in-barrier-function-and. Retrieved 21 October 2022.

364. Crawley SW, Mooseker MS, Tyska MJ. 2014. Shaping the intestinal brush border. J Cell Biol 207:441–451.

365. Kinchen J, Chen HH, Parikh K, Antanaviciute A, Jagielowicz M, Fawkner-Corbett D, Ashley N, Cubitt L, Mellado-Gomez E, Attar M, Sharma E, Wills Q, Bowden R, Richter FC, Ahern D, Puri KD, Henault J, Gervais F, Koohy H, Simmons A. 2018. Structural Remodeling of the Human Colonic Mesenchyme in Inflammatory Bowel Disease. Cell 175:372-386.e17.

366. Stauffer W, Sheng H, Lim HN. 2018. EzColocalization: An ImageJ plugin for visualizing and measuring colocalization in cells and organisms. 1. Sci Rep 8:15764.

367. Dawson C. 2022. ggprism: A "ggplot2" Extension Inspired by "GraphPad Prism" (1.0.4).

368. Wickham H, Chang W, Henry L, Pedersen TL, Takahashi K, Wilke C, Woo K, Yutani H, Dunnington D, RStudio. 2022. ggplot2: Create Elegant Data Visualisations Using the Grammar of Graphics (3.4.0).

369. Clarke E, Sherrill-Mix S. 2017. ggbeeswarm: Categorical Scatter (Violin Point) Plots (0.6.0).

370. R Core Team. 2022. R: A language and environment for statistical computing (4.2.0). R Foundation for Statistical Computing, Vienna, Austria.

371. Tham DKL, Moukhles H. 2017. Determining cell-surface expression and endocytic rate of proteins in primary astrocyte cultures using biotinylation. JoVE J Vis Exp e55974.

372. Nigro A, Finardi A, Ferraro MM, Manno DE, Quattrini A, Furlan R, Romano A. 2021. Selective loss of microvesicles is a major issue of the differential centrifugation isolation protocols. Sci Rep 11:3589.

373. Ramesh P, Kirov AB, Huels DJ, Medema JP. 2019. Isolation, Propagation, and Clonogenicity of Intestinal Stem Cells BT - Stem Cell Niche: Methods and Protocols, p. 61–73. *In* Turksen, K (ed.), . Springer New York, New York, NY.

374. Polański K, Young MD, Miao Z, Meyer KB, Teichmann SA, Park J-E. 2020. BBKNN: fast batch alignment of single cell transcriptomes. Bioinformatics 36:964–965.

375. Virshup I, Rybakov S, Theis FJ, Angerer P, Wolf FA. 2021. anndata: Annotated data. bioRxiv 2021.12.16.473007.

376. Reback J, McKinney W, jbrockmendel, Bossche JV den, Augspurger T, Cloud P, gfyoung, Sinhrks, Hawkins S, Klein A, Roeschke M, Tratner J, She C, Petersen T, Ayd W, MomIsBestFriend, Garcia M, Schendel J, Hayden A, Jancauskas V, Saxton D, McMaster A, Battiston P, Seabold S, chris-b1, h-vetinari, Hoyer S, Dong K, Overmeire W, Winkel M. 2020. pandas-dev/pandas: Pandas 1.1.2 https://doi.org/10.5281/ZENODO.4019559.

377. McKinney W. 2010. Data Structures for Statistical Computing in Python, p. 56–61. *In* van der Walt, S, Millman, J (eds.), Proceedings of the 9th Python in Science Conference.

378. Harris CR, Millman KJ, van der Walt SJ, Gommers R, Virtanen P, Cournapeau D, Wieser E, Taylor J, Berg S, Smith NJ, Kern R, Picus M, Hoyer S, van Kerkwijk MH, Brett M, Haldane A, del Río JF, Wiebe M, Peterson P, Gérard-Marchant P, Sheppard K, Reddy T, Weckesser W, Abbasi H, Gohlke C, Oliphant TE. 2020. Array programming with NumPy. Nature 585:357–362.

379. Niell N, Larriba MJ, Ferrer-Mayorga G, Sánchez-Pérez I, Cantero R, Real FX, del Peso L, Muñoz A, González-Sancho JM. 2018. The human PKP2/plakophilin-2 gene is induced by Wnt/β-catenin in normal and colon cancer-associated fibroblasts. Int J Cancer 142:792–804.

380. Stirling DR, Swain-Bowden MJ, Lucas AM, Carpenter AE, Cimini BA, Goodman A. 2021. CellProfiler 4: improvements in speed, utility and usability. BMC Bioinformatics 22:433.

381. Dao D, Fraser AN, Hung J, Ljosa V, Singh S, Carpenter AE. 2016. CellProfiler Analyst: interactive data exploration, analysis and classification of large biological image sets. Bioinforma Oxf Engl 32:3210–3212.

382. Pachitariu M, Stringer C. 2022. Cellpose 2.0: how to train your own model. Nat Methods 1–8.

383. Campeau E, Ruhl VE, Rodier F, Smith CL, Rahmberg BL, Fuss JO, Campisi J, Yaswen P, Cooper PK, Kaufman PD. 2009. A versatile viral system for expression and depletion of proteins in mammalian cells. PloS One 4:e6529.

384. Nam H, Benezra R. 2009. High levels of Id1 expression define B1 type adult neural stem cells. Cell Stem Cell 5:515–526.

385. Greco A, Ho JGS, Lin S-J, Palcic MM, Rupnik M, Ng KKS. 2006. Carbohydrate recognition by *Clostridium difficile* toxin A. Nat Struct Mol Biol 13:460–461.

386. Tao L, Tian S, Zhang J, Liu Z, Robinson-McCarthy L, Miyashita S-I, Breault DT, Gerhard R, Oottamasathien S, Whelan SPJ, Dong M. 2019. Sulfated glycosaminoglycans and low-density lipoprotein receptor contribute to *Clostridium difficile* toxin A entry into cells. Nat Microbiol 4:1760–1769.

387. Pothoulakis C, Gilbert RJ, Cladaras C, Castagliuolo I, Semenza G, Hitti Y, Montcrief JS, Linevsky J, Kelly CP, Nikulasson S, Desai HP, Wilkins TD, LaMont JT. 1996. Rabbit sucrase-isomaltase contains a functional intestinal receptor for *Clostridium difficile* toxin A. J Clin Invest 98:641–649.

388. Na X, Kim H, Moyer MP, Pothoulakis C, LaMont JT. 2008. gp96 Is a Human Colonocyte Plasma Membrane Binding Protein for *Clostridium difficile* Toxin A. Infect Immun 76:2862–2871.

389. Schöttelndreier D, Langejürgen A, Lindner R, Genth H. 2020. Low Density Lipoprotein Receptor-Related Protein-1 (LRP1) Is Involved in the Uptake of *Clostridioides difficile* Toxin A and Serves as an Internalizing Receptor. Front Cell Infect Microbiol 10:565465.

390. Grant BD, Donaldson JG. 2009. Pathways and mechanisms of endocytic recycling. 9. Nat Rev Mol Cell Biol 10:597–608.

391. Hamza T, Zhang Z, Melnyk RA, Feng H. 2016. Defective mutations within the translocation domain of *Clostridium difficile* toxin B impair disease pathogenesis. Pathog Dis 74:ftv098.

392. Lanis JM, Hightower LD, Shen A, Ballard JD. 2012. TcdB from hypervirulent *Clostridium difficile* exhibits increased efficiency of autoprocessing. Mol Microbiol 84:66–76.

393. Ozaki-Kuroda K, Nakanishi H, Ohta H, Tanaka H, Kurihara H, Mueller S, Irie K, Ikeda W, Sakai T, Wimmer E, Nishimune Y, Takai Y. 2002. Nectin Couples Cell-Cell Adhesion and the Actin Scaffold at Heterotypic Testicular Junctions. Curr Biol 12:1145–1150.

394. Wang X-D, Su Y-A, Wagner KV, Avrabos C, Scharf SH, Hartmann J, Wolf M, Liebl C, Kühne C, Wurst W, Holsboer F, Eder M, Deussing JM, Müller MB, Schmidt MV. 2013. Nectin-3 links CRHR1 signaling to stress-induced memory deficits and spine loss. 6. Nat Neurosci 16:706–713.

395. Mizoguchi A, Nakanishi H, Kimura K, Matsubara K, Ozaki-Kuroda K, Katata T, Honda T, Kiyohara Y, Heo K, Higashi M, Tsutsumi T, Sonoda S, Ide C, Takai Y. 2002. Nectin : an adhesion molecule involved in formation of synapses. J Cell Biol 156:555–565.

396. Nance J, Zallen JA. 2011. Elaborating polarity: PAR proteins and the cytoskeleton. Dev Camb Engl 138:799–809.

397. Similar and Distinct Properties of MUPP1 and Patj, Two Homologous PDZ Domain-Containing Tight-Junction Proteins | Molecular and Cellular Biology. https://journals.asm.org/doi/full/10.1128/MCB.01505-08. Retrieved 8 November 2022.

398. Fujiwara Y, Goda N, Tamashiro T, Narita H, Satomura K, Tenno T, Nakagawa A, Oda M, Suzuki M, Sakisaka T, Takai Y, Hiroaki H. 2015. Crystal structure of afadin PDZ domain–nectin-3 complex shows the structural plasticity of the ligand-binding site. Protein Sci 24:376–385.

399. Kawagishi R, Tahara M, Morishige K, Sakata M, Tasaka K, Ikeda W, Morimoto K, Takai Y, Murata Y. 2005. Expression of nectin-2 in mouse granulosa cells. Eur J Obstet Gynecol Reprod Biol 121:71–76.

400. Crawley SW, Shifrin DA, Grega-Larson NE, McConnell RE, Benesh AE, Mao S, Zheng Y, Zheng QY, Nam KT, Millis BA, Kachar B, Tyska MJ. 2014. Intestinal Brush Border Assembly Driven by Protocadherin-Based Intermicrovillar Adhesion. Cell 157:433–446.

401. Pinette JA, Mao S, Millis BA, Krystofiak ES, Faust JJ, Tyska MJ. 2019. Brush border protocadherin CDHR2 promotes the elongation and maximized packing of microvilli in vivo. Mol Biol Cell 30:108–118.

402. Negussie AB, Dell AC, Davis BA, Geibel JP. 2022. Colonic Fluid and Electrolyte Transport 2022: An Update. 10. Cells 11:1712.

403. Muhl L, Genové G, Leptidis S, Liu J, He L, Mocci G, Sun Y, Gustafsson S, Buyandelger B, Chivukula IV, Segerstolpe Å, Raschperger E, Hansson EM, Björkegren JLM, Peng X-R, Vanlandewijck M, Lendahl U, Betsholtz C. 2020. Single-cell analysis uncovers fibroblast heterogeneity and criteria for fibroblast and mural cell identification and discrimination. 1. Nat Commun 11:3953.

404. Hao Y, Hao S, Andersen-Nissen E, Mauck WM, Zheng S, Butler A, Lee MJ, Wilk AJ, Darby C, Zager M, Hoffman P, Stoeckius M, Papalexi E, Mimitou EP, Jain J, Srivastava A, Stuart T, Fleming LM, Yeung B, Rogers AJ, McElrath JM, Blish CA, Gottardo R, Smibert P, Satija R. 2021. Integrated analysis of multimodal single-cell data. Cell 184:3573-3587.e29.

405. Huang J, Kelly CP, Bakirtzi K, Villafuerte Gálvez JA, Lyras D, Mileto SJ, Larcombe S, Xu H, Yang X, Shields KS, Zhu W, Zhang Y, Goldsmith JD, Patel IJ, Hansen J, Huang M, Yla-Herttuala S, Moss AC, Paredes-Sabja D, Pothoulakis C, Shah YM, Wang J, Chen X. 2019. *Clostridium difficile* toxins induce VEGF-A and vascular permeability to promote disease pathogenesis. 2. Nat Microbiol 4:269–279.

406. Siebert JR, Conta Steencken A, Osterhout DJ. 2014. Chondroitin Sulfate Proteoglycans in the Nervous System: Inhibitors to Repair. BioMed Res Int 2014:845323.

407. Wilcox MH, Gerding DN, Poxton IR, Kelly C, Nathan R, Birch T, Cornely OA, Rahav G, Bouza E, Lee C. 2017. Bezlotoxumab for prevention of recurrent *Clostridium difficile* infection. N Engl J Med 376:305–317.

Appendix

List of Publications

Peritore-Galve, F. C., Shupe, J. A., Cave, R. J., Childress, K. O., Washington, M. K., Kuehne, S. A., & Lacy, D. B. (2022). Glucosyltransferase-dependent and independent effects of *Clostridioides difficile* toxins during infection. **PLoS Pathogens**. https://doi.org/10.1371/journal.ppat.1010323

Markham, N.O., Bloch, S.C., Shupe, J.A., Laubacher, E.N., Thomas, A.K., Kroh, H.K., Childress, K.O., Peritore-Galve, F.C., Washington, M.K., Coffey, R.J. and Lacy, D.B. (2021) Murine intrarectal instillation of purified recombinant *Clostridioides difficile* toxins enables mechanistic studies of pathogenesis. **Infection and Immunity**. https://doi.org/10.1128/IAI.00543-20

Mileto S.J.*, Jardé T.*, Childress K.O.*, Jensen J.L., Rogers A.P., Kerr G., Hutton M.L., Sheedlo M.J., Bloch S.C., Shupe J.A., Horvay K., Flores T., Engel R., Wilkins S., McMurrick P.J., Lacy D.B., Abud H.E., Lyras D. (2020) *Clostridioides difficile* infection damages colonic stem cells via TcdB, impairing epithelial repair and recovery from disease. **Proceedings of the National Academy of Sciences**. DOI: 10.1073/pnas.1915255117. ***Co-first authors***

List of Manuscripts Under Review

Childress K.O., Cencer C.S., Tyska M.J., Lacy D.B. Nectin-3 and Shed Forms of CSPG4 Can Serve as Epithelial Cell Receptors for *Clostridioides difficile* TcdB. *In revision*